SAPIENZA
UNIVERSITÀ DI ROMA

PhD Course in Biochemistry

XXXVII Cycle (Academic Years 2021-2024)

Investigating the Ferroportin-Ferroxidase System

PhD student

Matteo Amadei

Tutor

Prof. Maria Carmela Bonaccorsi di Patti

Coordinator

Prof. Marialuisa Mangoni

Copertina: Alberto Burri, *Iron sp*, 1961.

Ringraziamenti

Ringrazio innanzitutto la Professoressa Maria Carmela Bonaccorsi, che mi ha guidato e ispirato durante questi lunghi anni, insegnandomi tutto ciò che so.
Ringrazio poi la mia collega e compagna Flavia, una persona davvero speciale con cui ho condiviso le gioie e le difficoltà di questo percorso, rendendolo unico e indimenticabile.
Un grazie di cuore va ad Antonella, Claudio, Anna, Alessia, Simone, Irene, Federica e a tutti i ragazzi del CU020, con cui ho trascorso lunghe giornate in laboratorio, fatte di esperimenti, confronti e risate.
Un ringraziamento speciale va anche ai miei colleghi e amici Andrea e Dario, che sono stati sempre al mio fianco.
Per ultima, ma in realtà per prima, ringrazio tutta la mia famiglia, e in particolare mia madre e mio padre, senza i quali nulla avrei potuto.

Summary

1. INTRODUCTION 1

1.1 Human Iron Metabolism 1

1.1.1 Dietary Iron Absorption 3

1.1.3 Intracellular Iron Trafficking and Storage 5

1.1.4 Iron Recycling 9

1.1.5 Regulation of Iron Homeostasis 11

1.2 The Ferroportin-Ferroxidase System 14

1.2.1 Ferroportin (FPN): The Iron Exporter 15

1.2.1.1 FPN Function and Physiology 15

1.2.1.2 FPN structure and mechanism 17

1.2.1.3 FPN Regulation 27

1.2.2 The Ferroxidases: Ceruloplasmin (CP) and Hephaestin (HEPH) 33

1.2.3 Pathologies associated to FPN-Ferroxidase system 42

2. AIM OF THE THESIS 48

3. MATERIALS AND METHODS 51

3.1 *Pichia pastoris* strains and cell lines 51

3.2 Vectors and Constructs 51

3.3 Recombinant FPN Expression and Purification 53

3.4 Recombinant HEPH expression and purification 54

3.5 Recombinant CP expression and purification 56

3.6 CP purification from human plasma 56

3.7 Fluorescence Spectroscopy 57

3.8 CP and HEPH activity assays 58

3.9 Immunofluorescence and Proximity Ligation Assay (PLA) 58

3.10 FPN-CP pull-down assay and Size Exclusion Chromatography (SEC) 60

3.11 FPN-HEPH crosslinking and Size Exclusion Chromatography (SEC) . 61

4. RESULTS AND DISCUSSION 62

4.1 Genetic Incorporation of Dansylalanine in Human Ferroportin to Probe the Alternating Access Mechanism of Iron Transport 62

4.1.1 Selection of Reporter Residues and Incorporation of Dansylalanine (DA) into FPN 64

4.1.2 Fluorescence Spectroscopy of FPN DA 67

4.1.3. Cobalt Titration of FPN DA 69

4.1.4 Discussion 74

4.2 The Different Affinity of the Two Metal-Binding Sites of Human Ferroportin Drives Outward Directionality of Transport 74

4.2.1 Results 76

4.2.2 Discussion 82

4.3 Production and Characterization of CP mutants 88

4.3.1 Characterization of CP mutants N244S and G876A 88

4.3.2 Characterization of CP residues potentially involved in iron channelling 90
4.3.3 Discussion 95

4.4 Hephaestin expression and purification 97
4.3.1 Hephaestin production and purification screening in different expression systems 97
4.3.2 Discussion 111

4.5 Functional Characterization of HEPH Cancer-Related Variants 112
4.5.1 Results and Discussion 113

4.6 Ferroportin-Ferroxidase Interaction 116
4.6.1 Proximity Ligation Assay enables FPN-CP complex *in situ* detection 116
4.6.2 FPN-CP interaction assays on purified proteins 120
4.6.3 AlphaFold prediction of FPN-CP complex 125
4.6.4 FPN-HEPH interaction assays on purified proteins 127
4.6.5 Discussion 131

5. CONCLUSIONS 134

6. PUBLICATIONS 139

7. BIBLIOGRAPHY 140

1. INTRODUCTION

Iron is one of the most abundant elements on Earth, and since the dawn of life, it has been intimately linked to biological processes. Its dual nature, which allows it to easily accept and donate electrons by cycling between its Fe^{2+} and Fe^{3+} oxidation states, makes it essential for fundamental processes in nearly all life forms. Iron is crucial for several key biological functions, including electron transport, DNA synthesis, and in multicellular eukaryotes, oxygen transport/storage and drug detoxification. However, this same dual nature makes iron highly toxic when present in excess in biological systems. To manage this, organisms have evolved sophisticated mechanisms for its safe handling. In humans, three proteins are critical for maintaining iron homeostasis: ferroportin, ceruloplasmin, and hephaestin, which together form the ferroportin-ferroxidase system.

1.1 Human Iron Metabolism

Iron is the cofactor of about 2% of human proteins, which mediate life-essential functions such as ATP generation, nucleic acid synthesis and repair, and oxygen transport (Galy et al., 2024). Human iron metabolism consists of a finely regulated balance between iron absorption, utilization, recycling, and loss that ensures enough iron is available to meet physiological needs without causing toxicity. The adult human body contains approximately 3 to 5 grams

of iron, distributed across several compartments. About 70% of total body iron is found in erythrocytes and erythroid precursors, bound to hemoglobin for oxygen transport. Another 10% is present in the myoglobin of skeletal and cardiac muscles and other cellular types. The remaining pool is stored mainly in the liver, which acts as a reservoir of iron to be used when required (Abbaspour et al., 2014; Galy et al., 2024).

Less than 2 mg of iron is absorbed daily from dietary sources, and a comparable amount is lost. So, to meet the erythropoiesis requirement, the body must efficiently recycle iron (approximately 25 mg daily), mostly from senescent erythrocytes through macrophage-mediated erythrophagocytosis, particularly in the spleen and liver. This recycled iron is delivered to the bone marrow, where it is taken up by erythroid precursors for hemoglobin synthesis. (Katsarou & Pantopoulos, 2020; Muckenthaler et al., 2017).

Excess iron is taken up by the liver, which stores excess iron and regulates systemic iron levels via the hormone hepcidin. Together, these processes ensure an appropriate supply of iron to tissues for metabolic needs avoiding its toxic accumulation. Disruptions in this balance can lead to severe iron-related disorders, making a deep understanding of iron metabolism essential for developing therapeutic strategies.

1.1.1 Dietary Iron Absorption

Duodenal enterocytes absorb iron in the small intestine. Dietary iron is available in two forms: non-heme iron, which is mainly in the ferric state (Fe^{3+}), and heme iron, derived from hemoglobin and myoglobin in animal products(Gulec et al., 2014). Non-heme iron must first be converted to the ferrous form (Fe^{2+}) to be absorbed. Fe^{3+} reduction is mediated by enterocyte apical ferrireductases such as duodenal cytochrome b (DCYTb), an ascorbate-dependent reductase (also known as CYBRD1) (Lane et al., 2015). The ferrous iron is now bioavailable and can be transported into enterocytes by the divalent metal transporter 1 (DMT1), which mediates the symport of H+ along with various divalent metals, thanks to the proton gradient generated by sodium hydrogen (Na+/H+) exchanger 3 (NHE3) (Shawki et al., 2015, 2016).

Heme iron is absorbed more efficiently than inorganic iron but the molecules and mechanism mediating its uptake remain poorly understood (Hooda et al., 2014; Katsarou et al., 2020). Initially identified heme carrier protein 1 (HCP1) is now considered to carry mostly folate (Hentze et al., 2010), other transporters may be candidates such as HRG-1 which mediates haem efflux from the macrophage phagolysosome although it is expressed at a moderate level in the intestine (Galy et al., 2024). Inside the enterocyte, heme is degraded by heme-oxygenases, which liberate ferrous iron from the porphyrin ring. This iron then enters the same intracellular pool as non-heme iron, following the same fate (Katsarou et al., 2020).

Once inside the enterocyte, iron, which can be stored in ferritin, is more likely transported across the basolateral membrane into the bloodstream. The export of iron from enterocytes is mediated by Ferroportin (FPN), the only known

iron exporter in humans (Bonaccorsi di Patti et al., 2018). To ensure safe transport in the blood, ferrous export by FPN is coupled with its re-oxidation to ferric iron (Fe^{3+}) by the ferroxidase Hephaestin (Vashchenko & MacGillivray, 2013). This process prevents ROS generation due to Fe^{2+} autoxidation through Fenton reaction and allows iron to bind to Transferrin (Tf), which can only bind iron in its ferric form.

1.1.2 Systemic Iron Transport and Cellular Uptake

Tf serves as the primary systemic iron transporter, delivering the metal obtained from dietary absorption, recycled by macrophages, or mobilized from liver storage to all cells, including erythroblasts in the bone marrow. Tf is a glycoprotein with two high-affinity binding sites for ferric iron (Fe^{3+}), primarily synthesized by hepatocytes (Yu et al., 2020; Gkouvatsos et al., 2012). During the delivery process, Tf tightly binds plasma iron in a soluble, non-reactive form, which is essential for preventing the formation of reactive oxygen species (ROS) and limiting iron availability to extracellular pathogens. Tf-bound iron (holo-Tf) enters cells through receptor-mediated endocytosis mediated by Transferrin receptor 1 (TfR1). TfR1, which is widely expressed on the surface of many cell types, is a single-pass glycoprotein that forms homodimers, each monomer binds one Tf molecule (Aisen, 2004). The binding of holo-Tf to TfR1 triggers clathrin-mediated endocytosis, resulting in the formation of an endosome containing the Tf-TfR1 complex (Galy et al., 2024). Tf binds iron tightly but reversibly; at the neutral pH of the blood, Tf exhibits a high affinity for iron, which significantly decreases in the acidic environment

of the endosome. The endosomal lumen is acidified by H+/ATPase pumps, which lower the pH, inducing the release of Fe^{3+} from transferrin (Cheng et al., 2004). The released ferric iron (Fe^{3+}) is then reduced to ferrous iron (Fe^{2+}) by the endosomal ferrireductase STEAP3 (Sendamarai et al., 2008). Once reduced, Fe^{2+} can be transported across the endosomal membrane into the cytosol via DMT1 (Galy et al., 2024). Following iron release and reduction, the apo-Tf (iron-free transferrin) and TfR1 are recycled back to the cell surface. Tf recycling is crucial as Tf binds about 3 mg of iron, while the production of new erythrocytes requires 25-30 mg, to sustain erythropoiesis Tf undergoes 10 turnovers daily (Abbaspour et al., 2014). TfR1 serves as a receptor for ferritin as well (see below), and several pathogens also use this receptor to enter cells. Together with its homologue TFR2, TFR1 is involved in cellular signalling processes and interacts with hereditary hemochromatosis protein (HFE) in hepatocytes to modulate transcription of the *HAMP* gene, which encodes for hepcidin, the FPN inhibiting hormone that will be presented below.

1.1.3 Intracellular Iron Trafficking and Storage

Once in the cytoplasm, iron enters the labile iron pool (LIP), a dynamic reservoir of bioavailable iron that cells can draw from for various metabolic needs. From the LIP, iron is trafficked to specific intracellular (or extracellular) destinations depending on the cell's requirements. The iron trafficking mechanisms in cells are complex and not fully understood yet.

A significant portion of this iron is transported to the mitochondria matrix, where it is used for synthesis of heme and iron-sulfur clusters (Fe-S), which

are essential prosthetic groups in proteins involved in oxygen, oxidative phosphorylation, and other critical cellular processes.

To enter the mitochondrial matrix iron must be transported across the outer mitochondrial membrane, this process may be mediated by DMT1 (Natascha A. Wolff et al., 2018) followed by import across the inner mitochondrial membrane through mitoferrin-1 in erythroid cells or mitoferrin-2 in non-erythroid-cells. Recent evidence supports the "kiss-and-run" hypothesis, particularly in erythroid cells, where the demand for iron is extraordinarily high for hemoglobin synthesis. According to this model, iron is directly transferred from Tf-containing endosomes and ferritin-containing lysosomes (see below) to mitochondria, bypassing iron release in cytosolic LIP (Aronova et al., 2021; Hamdi et al., 2016).

In addition to those synthesized in the mitochondrion, iron is incorporated into a plethora of cytosolic and nuclear apoproteins using Fe^{2+} ions coming from LIP as cofactors. The cell must carefully manage the excess of the LIP to prevent toxicity. In the cytosol, LIP iron is chaperoned by poly(rC)-binding proteins (PCBPs, PCBP1 and PCBP2). Initially known for their ability to regulate transcription and RNA metabolism by binding to cytosine-rich DNA or RNA sequences, PCBPs also function as Fe^{2+} chaperones, promoting iron incorporation into apoproteins while limiting its dangerous reactivity (Philpott et al., 2020). PCBP1 and PCBP2 bind three Fe^{2+} ions with low micromolar affinity, with glutathione (GSH) required for stable metal coordination. The binding of PCBPs to iron promotes its interaction with targets, enabling the metalation of a large set of apoproteins (mono and di-iron proteins and extra-mitochondrial Fe–S proteins). PCBPs are also responsible for delivering iron to ferritin for iron storage or to FPN for iron export (see below). Additionally,

PCBP2 interacts with DMT1 and heme oxygenases (HMOX) (Yanatori et al., 2014) mediating iron uptake, as well as with the iron exporter FPN, for iron export (Yanatori et al., 2016). PCBPs therefore escort iron from the moment it enters the cytosol, mediating its trafficking to intracellular stores (ferritin), to apoproteins requiring the metal and facilitating its export from the cell.

The excess of iron that cannot be managed by PCBPs or readily engaged in biological processes must leave the LIP and be stored or exported.

In cells, iron is stored in cytosolic ferritin nanocages. Ferritin (FT) is a large, hollow protein complex sequestering up to 4500 iron atoms in a safe, non-reactive ferric state (Arosio et al., 2015). It is a heteropolymer composed of 24 subunits of H (heavy) and L (light) chains that self-assemble in a shell-like structure. The H subunit contains a di-iron center that catalyzes the conversion of Fe^{2+} from the LIP (delivered by PCBPs) to Fe^{3+}, the L subunit provides a nucleation site that facilitates the mineralization of the metal (Koorts et al., 2007). FT acts as a buffer for intracellular iron, encapsulating it in a safe form when in excess and releasing it when needed through a process called ferritinophagy that is triggered by liquid-like ferritin condensation. Iron depletion activates the nuclear co-activator receptor 4 (NCOA4) that binds FT. FT-NCOA4 particles undergo liquid-liquid phase separation, and the resulting condensates are then recognized by the autophagy adaptor Tax1 binding protein 1 (TAX1BP1), which recruits autophagy machinery and is degraded in lysosomes. Iron released from FT is reduced by ferrireductases and exported from lysosomes to the cytosol, where it becomes part of LIP for reuse, or can be directly transferred to mitochondria through the ‘kiss and run’ mechanism mentioned before (Galy et al., 2024).

Mitochondrial ferritin, a specialized form of ferritin found within mitochondria, also plays a crucial role in protecting against iron-induced oxidative damage, particularly within the context of high metabolic activity and oxygen consumption in these organelles.

Iron can also be exported from LIP outside the cell. Iron export into plasma takes place, especially in enterocytes, which mediate dietary iron absorption, in macrophages that recycle iron from senescent erythrocytes, and in iron-storing hepatocytes. The major iron exit route is the FPN-ferroxidase system, which was mentioned before and will be treated extensively in the following sections. FPN not only is the unique iron exporter known in humans (and in all mammals) but the system is also at the core of systemic iron regulation. Indeed, FPN is the target of the main systemic iron regulator molecule, the liver hormone hepcidin.

Although the FPN-ferroxidase system is the key of the entire systemic homeostasis of iron, it is not the only way for iron to exit the cell. Iron can be secreted from cells via ferritin secretory autophagy or endosomal microautophagy. In certain conditions, cells also release ferritin-containing exosomes, facilitating iron transport between neighbouring cells. Furthermore, heme iron can be exported from cells through specialized transporters.

1.1.4 Iron Recycling

Iron recycling is a critical aspect of iron homeostasis, ensuring that the body efficiently reuses iron from senescent erythrocytes to meet erythropoiesis needs. Indeed, iron intestinal absorption accounts only for a small amount of iron (2 mg daily) compared to the 20-25 mg acquired by developing erythrocytes every day. This recycling process is primarily carried out by macrophages in the reticuloendothelial system, particularly in the spleen, liver, and bone marrow. These macrophages phagocytize senescent or damaged erythrocytes in a process known as erythrophagocytosis (de Back et al., 2014).

Within macrophages, phagosomes containing engulfed erythrocytes fuse with lysosomal vesicles forming erythrophagolysosomes. Here hemoglobin of red blood cells is degraded, and the released heme is exported to the cytosol by heme transporter HRG 1(White et al., 2013). In the cytosolic compartment, heme is further broken down by heme oxygenase-1 (HMOX1) to produce biliverdin, carbon monoxide, and ferrous iron. HMOX1 directly interacts with PCPB2 which chaperones the iron upon its release (Galy et al., 2024). Iron can then be stored temporarily in ferritin or exported into the bloodstream via the FPN-ferroxidase pathway (Zhuzhen Zhang et al., 2012). This exported iron re-enters the circulation bound to TF, contributing to the iron pool available for erythropoiesis in the bone marrow and completing its recycling.

The efficiency of iron recycling is underscored by the fact that the amount of metal released daily by macrophages accounts for most of the need for erythropoiesis.

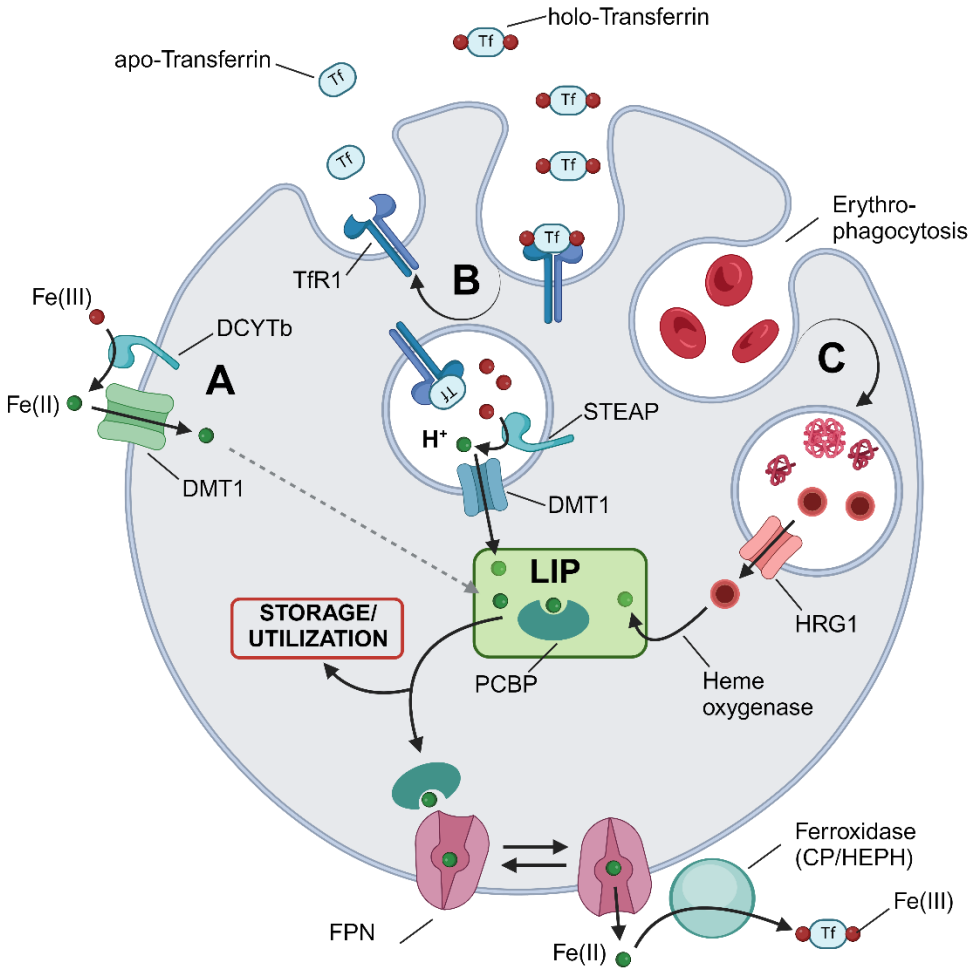

Figure 1. Main iron import and export cellular pathways. The three primary import mechanisms include: iron uptake through DMT1 in enterocytes (A); iron acquisition via TF/Tfr1 clathrin-dependent endocytosis in various cell types (B); and iron absorption via erythrophagocytosis in macrophages (C). In contrast, the sole major export pathway is mediated by the FPN-ferroxidase system.

1.1.5 Regulation of Iron Homeostasis

The regulation of iron homeostasis consists of a complex interplay between systemic and cellular mechanisms that ensure iron is absorbed, stored, and recycled according to the body's needs while avoiding its intrinsic toxicity.

At the cellular level, iron homeostasis is primarily regulated by the Iron Regulatory Protein/Iron-Responsive Element (IRP/IRE) system. IRPs function as iron cellular level sensors. Under conditions of normal levels, IRP1 (also known as aconitase) is bound to a 4Fe-4S cluster and exploits its enzymatic activity, during iron starvation IRP1 is found in its apo-state and functions as a post-transcriptional regulator (Hognon et al., 2021). IRP2 lacks aconitase activity and is instead regulated by iron- and oxygen-dependent interaction with leucine-rich repeat5 F-box protein (FBXL5), which regulates IRP2 proteasomal degradation in an iron level-dependent manner (Hui Wang et al., 2020). When IRPs are active (low cellular iron level) they bind with high-affinity IRE cis-regulatory elements, that are present on 5' and 3' UTRs of mRNA encoding key proteins involved in iron metabolism. When IREs are located in the 5' UTR of the *FTL*, *FTH1,* and *SLC40A1* mRNAs (encoding for FT light chain, FT heavy chain, and FPN respectively) IRPs inhibit their translation (Muckenthaler et al., 1998). Conversely, IRPs interaction with IREs in the 3' UTR of *TFRC* mRNA (encoding for TfR1) protects the transcript from endoribonuclease-mediated degradation (Yoshinaga et al., 2017). The net effect of these regulations is the increase of cytosolic iron bioavailability, lowering iron storage and export, and increasing its acquisition via TfR1, when cellular iron levels are low. As iron levels rise, IRPs lose their affinity for IREs, allowing for the translation of FT and FPN while promoting the degradation of

TfR1 mRNA, thus decreasing iron uptake and increasing storage and export (Galy et al., 2024).

Beyond the central role of the IRP/IRE system in regulating intracellular iron levels, additional regulatory mechanisms respond to changes in the cell redox state and oxygen availability. These mechanisms are primarily mediated by the transcription factors NRF2 and HIF, which bind AREs (Antioxidant Response Elements) and HREs (Hypoxia Response Elements) respectively.

In conditions of oxidative stress, iron homeostasis is closely linked to the antioxidant response, as free iron accumulation can catalyze the formation of reactive oxygen species (ROS) through Fenton chemistry. NRF2 is a key transcription factor in this response, controlling the expression of genes involved in antioxidant defence and iron management. Under normal conditions, NRF2 is bound to KEAP1, which targets it for degradation via the ubiquitin-proteasome pathway. However, during oxidative stress, cysteine residues in KEAP1 are modified, preventing the binding of NRF2 and allowing its translocation into the nucleus. Here, NRF2 activates the expression of ARE containing genes, some of which are directly involved in iron homeostasis like genes that encode for HMOX1, and FPN. NRF2 also regulates both the synthesis and degradation of FT, controlling the size of the LIP. Thus, preventing excessive free iron accumulation, and reducing the risk of oxidative damage (Cuadrado et al., 2019; Galy et al., 2024).

The hypoxic response is another additional mechanism that regulates iron homeostasis, particularly important when oxygen is scarce, such as during anemia (often due to iron deficiency) or high-altitude exposure. HIF transcription factors, which are regulated by both oxygen and iron levels, play a central role in this process. Under normoxic conditions, prolyl hydroxylases

(PHDs) hydroxylate HIFs, marking them for degradation via the ubiquitin-proteasome pathway. PHDs need both molecular oxygen and iron to function, thus during hypoxia or iron deficiency, HIFs are stabilized, and can accumulate and translocate to the nucleus, where they activate the expression of genes involved in iron uptake and erythropoiesis. HIFs control the transcription of genes that encode for TF and TfR1, increasing iron transport and uptake, DMT1, regulating intestinal iron absorption, and HMOX1, which facilitates heme degradation and iron recycling required by erythropoiesis (Gassmann et al., 2015; Haase, 2017).

Systemically, iron homeostasis is controlled only by the hepcidin-FPN axis. Hepcidin is a peptide hormone produced by the liver in response to increased body iron levels, inflammation, or decreased erythropoietic activity. Hepcidin binds to FPN on the surface of enterocytes, macrophages, and hepatocytes, triggering its inhibition, internalization, and degradation. This process effectively reduces dietary iron absorption and the release of recycled iron into the bloodstream, thereby lowering plasma iron levels. The regulation of hepcidin itself is influenced by several factors, including iron levels sensed by transferrin receptor 2 (TfR2) and hemojuvelin (HJV), as well as inflammatory cytokines like interleukin-6 (IL-6) and signals from bone morphogenetic proteins (BMPs) (Katsarou et al., 2020; Muckenthaler et al., 2017).

FPN systemic and cellular regulation will be discussed in detail in section 1.2.

1.2 The Ferroportin-Ferroxidase System

Iron homeostasis in humans is a complex process involving multiple intricate mechanisms that operate at both the cellular and systemic levels. Within the cell, various transcriptional and post-transcriptional processes regulate the iron uptake and mobilization from its cytosolic storage. These mechanisms play a crucial role in maintaining iron balance at the cellular level but it is the FPN-hepcidin axis that serves as the central hub for homeostatic regulation. This axis governs the distribution of iron throughout the body, by regulation of the efflux of iron from cells. This process is mediated by a complex interplay of proteins that facilitate the transport of iron from the cytoplasm to transferrin. The main characters of this process are FPN, already presented as the sole iron exporter that mediates the export of the metal, and two ferroxidase proteins of the multicopper oxidase (MCO) family: Ceruloplasmin (CP) and Hephaestin (HEPH). A third less characterized member of the family is zyklopen. These ferroxidases act on the extracellular side of differential cell types, promoting the FPN export of iron and aiding in its loading onto TF. In essence, FPN, CP (or HEPH) collaborate as part of a finely tunable export system referred to as the FPN-ferroxidase system. This system ensures safe handling and precise control over the distribution of iron in the human body.

1.2.1 Ferroportin (FPN): The Iron Exporter

The key component of this system is FPN, which transports iron from the cytosol to the extracellular space. FPN is the only known iron exporter in human and mammalian cells. It belongs to the Major Facilitator Superfamily (MFS) of transporters and is encoded by the SLC40A1 gene located on chromosome 2 (2q32). The gene consists of 8 exons of 3330 base pairs and its mRNA translates into a 571 amino acid transmembrane protein (Musci et al., 2014). FPN sequence is conserved in all mammals and has orthologs in plants and worms, but has no relationship with other mammalian transporters (Drakesmith et al., 2015). The transporter instead shares some similarities with bacterial iron transporters.

1.2.1.1 FPN Function and Physiology

FPN was first identified in 2000 by three different groups, which described, in mice and zebrafish models, a novel cDNA encoded in cells of organs and tissues known to be involved in iron adsorption and turnover. Its expression at both mRNA and protein levels is increased under conditions of increased iron absorption and its mRNA contains an iron-responsive element (IRE) at 5' UTR. When *Xenopus* oocytes are transfected with FPN cDNA the resulting protein stimulates iron efflux (Abboud & Haile, 2000; Donovan et al., 2000; McKie et al., 2000).

The relevant role of FPN was later defined in the following studies. In 2001 FPN mutation in humans was first linked to iron homeostasis dysregulation

and hemochromatosis (Montosi et al., 2001). In the same year, the first *in vivo* experiments using FPN-deleted transgenic mice showed that this protein is required for proper embryonic development, iron absorption, and homeostasis in adult individuals. Disruption of both copies of the FPN sequence (FPN null/null mice) is lethal. Mice did not complete embryonic development probably due to inefficient iron transport by epithelial cells of the extraembryonic visceral endoderm (exVE), where FPN expression level in wild type mice is high to guarantee iron transfer between placenta and embryo. When FPN conditional disruption was performed, inactivating FPN in all tissues except exVE and placenta, mice completed embryonic development but after birth, when the only route of ingress for iron became the duodenum, rapidly became anemic and runted with marked iron accumulation in enterocytes, hepatocytes, splenic and liver macrophages, indicating a key role for FPN in those cell types. Adult mice in which FPN was inducibly and exclusively deleted in intestinal cells also rapidly showed severe iron deficiency that was rescued by parenteral iron administration, demonstrating that FPN is essential for intestinal absorption of dietary iron. These findings represented the first evidence of the importance of FPN in the absorption of iron by the exVE and the intestine, the severity of the symptoms observed in the absence of this protein indicated the importance if not the uniqueness of the FPN role in the export of iron from cells (Donovan et al., 2005).

Moreover, further research showed that FPN is necessary for the efficient mobilization of stored iron in macrophages and hepatocytes. Mice lacking FPN in these cells become anemic more quickly than controls when given an iron-deficient diet (Zhang et al., 2011; Zhang et al., 2012). Milder mutations have been used to demonstrate that FPN is required for the development of the neural tube and forebrain in mice (Mao et al., 2010). Overall, it appears that

FPN is the only protein mediating iron export in human cells (Drakesmith et al., 2015). Indeed, since FPN discovery only a few other iron exit routes were identified which play a minor role.

FPN is primarily expressed on the basolateral cell surface of enterocytes, macrophages, and hepatocytes which are sites for iron absorption, recycling, and storage respectively. FPN also serves in placental syncytiotrophoblasts, astrocytes, and microglial cells in the central nervous system (Jormakka, 2023; Drakesmith et al., 2015).

1.2.1.2 FPN structure and mechanism

Research has provided a good understanding of how FPN is regulated (see below), but until 2020 there had been limited characterization of its biochemical features.

Solving the FPN structure was the main challenge in the field until Billesbølle and colleagues finally released the first structure of the human transporter solved by cryo-EM (Billesbølle et al., 2020), followed by other groups (Pan et al., 2020; Elena Farah Lehmann et al., 2023). Before that, different studies investigated FPN topology and architecture using epitope tagging (Liu et al., 2005), solving the structure of a bacterial homologoue (BbFPN) (Taniguchi et al., 2015), predicting FPN structure by homology-modelling or threading, and deriving important structural insights from patients with iron disorders (Bonaccorsi Di Patti et al., 2014; Le Gac et al., 2013; Tortosa et al., 2017; Wallace et al., 2010). Liu et al first defined the intra- and extracellular location of several FPN loops, proposing a 12 TM helices architecture (Liu et al., 2005) and defined localization of both N- and C-termini. Although this last aspect

has remained controversial, it is now generally accepted that both N- and C-term are located intracellularly, as confirmed more recently by another study (Rishi et al., 2020). Several models were proposed based on different approaches that all conformed to a 12 TM architecture suggestive that FPN belonged to the Major Facilitator Superfamily (MFS) of secondary transporters (Bonaccorsi Di Patti et al., 2014; Le Gac et al., 2013; Wallace et al., 2010). All those studies helped to map and derive a comprehensive structure-function analysis of FPN pathogenic mutations (reported in Fig. 1).

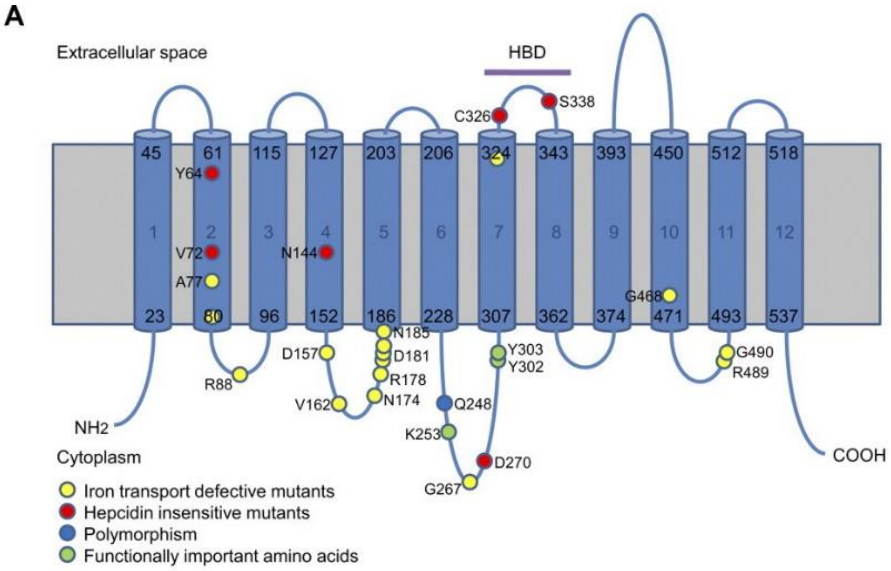

Figure 2. FPN topology, known pathogenic mutations are mapped. Modified from (Wallace et al., 2010).

Since 2020 different human and mammalian FPN structures have been released thanks to the emerging technique of cryo-EM (Billesbølle et al., 2020; Lehmann et al., 2023; Pan et al., 2020). These structures confirmed the previous models: FPN adopts a classic MFS fold, with N- and C-domains composed of TM 1-6 and TM 7-12, respectively (Bonaccorsi Di Patti et al., 2014; Le Gac et al., 2013; Tortosa et al., 2017; Wallace et al., 2010).

MFS members adopt at least three conformational states during their transport cycle: inward-open, occluded, and outward-open during a process known as "alternating access" (Drew et al., 2021; Quistgaard et al., 2016).

The structure of BbFPN from the bacterium *Bdellovibrio bacteriovorus* was solved both in inward- and outward-open conformation, clearly confirming that this protein adopts this mechanism as well (Taniguchi et al., 2015). Instead, all available structures of mammalian FPN (Hs, *Homo sapiens*; Ts, *Tarsius syrichta*) captured the transporter only in the outward-open conformation, except one which shows a partial occlusion (Elena Farah Lehmann et al., 2023), suggesting that the outward-open state may represent the resting state of the transporter.

Several residues form an "intracellular gate" that stabilizes the outward open conformation and closes the central cavity on the intracellular side. This gate is formed by two clusters of mixed ionic and hydrogen-bond interactions that make N- and C- domains interact on the cytosolic side, thus the protein internal cavity results to be accessible only from the extracellular side (outward-open). In HsFPN the first cluster involves a bonding network between residues R489 and E486 in TM11 (C-domain) with R88 in TM3 and D157 in TM4 (N-domain). This network is conserved in TsFPN as well, here only the two Arg and Glu residues participate. This group of interacting charged aa is known as motif-A, a common feature in the MFS family which is believed to have a role

in the gating of these transporters (Pan et al., 2020; Quistgaard et al., 2016). The second cluster is formed by an extended network of interactions between TM5 in the N domain and TM10 in the C domain of FPN, which involves 9 different residues (Fig. 3). A similar network involving the same corresponding residues is conserved in the BbFPN outward open structure (Taniguchi et al., 2015), which highlights the importance of these residues in intracellular gate formation.

Notably, the importance of some of the residues in intracellular gating was already known well before the structure of FPN was discovered. Indeed, mutation of several residues of this interaction network leads to FPN loss of function in ferroportin disease (Billesbølle et al., 2020; Guellec et al., 2019; Tortosa et al., 2017), presumably altering the equilibrium between FPN conformations, impairing the inward-open to outward-open transition, and leading to decreased ability to translocate iron.

All FPN structures feature a key structural characteristic: TM7 is divided into halves (TM7a and TM7b) by a short non-helical segment of six residues. This unique feature among the MFS family gives this helix increased flexibility, especially for TM7b and the non-helix region, which is likely required in the transport cycle. This region indeed accommodates two key residues for metal binding, and hepcidin-mediated regulation (D325 and C326). Molecular dynamic simulations showed that TM7b is highly dynamic, while the presence of Fe^{2+} stabilizes it (Billesbølle et al., 2020).

As already mentioned, an inward-open structure is currently unavailable for mammalian FPN. This conformation, which would help to answer many questions regarding the translocation mechanism, can only be inferred by its bacterial homolog BbFPN (Taniguchi et al., 2015) and the HsFPN homology models.

Recently, another structure of HsFPN has been released in which the closing of the central cavity has been observed both in the presence and absence of vamifeport, an inhibitor that has been developed for the treatment of beta thalassemia (Manolova et al., 2020). In this structure, residues on TM7b (including T333 and T334) move towards the TM1 and TM1-TM2 connecting loop, increasing interactions between N- and C- domains on the extracellular side. In addition, the lower part of the TM7b helix unfolds, extending the TM7 loop, which mediates additional contacts to TM1 and TM5 to occlude the center of the transporter, while the intracellular side of the protein is unchanged. Therefore, the structure can be considered as a "partially occluded" conformation of the transporter.

This structure is stabilized by a sybody that binds both the N- and C-terminal domains on the extracellular side, sealing the cleft between them. Thus, there is a certain degree of ambiguity concerning its functional relevance. According to the authors, it is currently not possible to establish how faithfully this structure can represent an HsFPN transport cycle intermediate. On the other hand, this structure seems to adopt an intermediate orientation between the outward- and inward-open conformations observed in the closely related homolog BbFPN (Jormakka, 2023; Pan et al., 2020).

Moreover, a similar closure mechanism of the extracellular entrance mediated by TM7 is also found in other members of the MFS (Lehmann et al., 2023). These observations provide reliability to the occluded state identified. In the absence of structures representing other occluded and inward-open conformations, this represents the unique structural proof of the mammalian FPN alternate access mechanism.

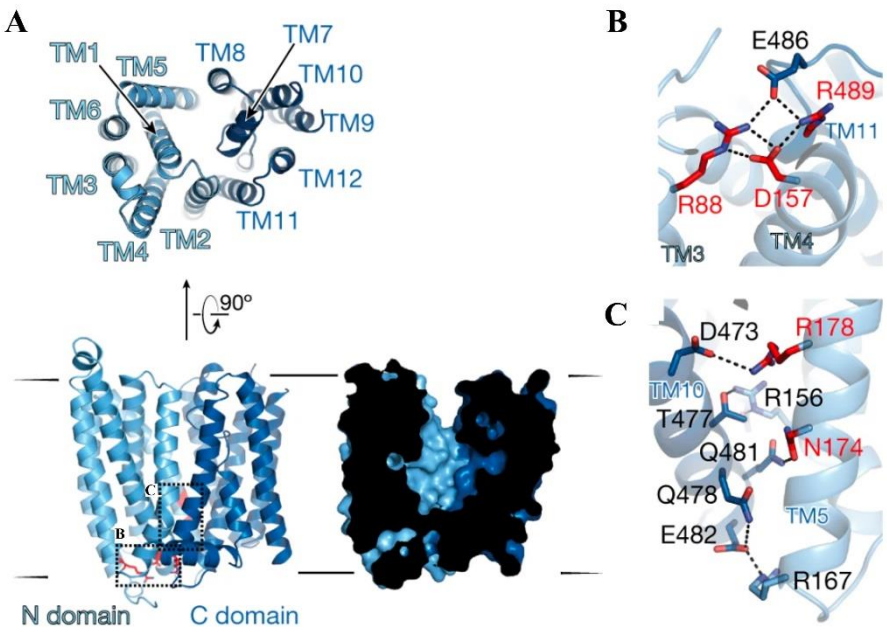

Figure 3. A) Ribbon diagram of HsFPN showing the 12 transmembrane helices, with the N and C domains shaded in different tones of blue. Cut-away surface view (right) illustrates the outward-open conformation. B-C) Close-up detail of residues of the intracellular gate stabilizing the outward-open state. Residues marked in red correspond to loss-of-function mutations linked to ferroportin disease in humans. Modified from Billesbølle et al., 2020.

Another significant structural feature of FPN regards metal binding. In these structural studies (Billesbølle et al., 2020; Pan et al., 2020; Billesbølle et al., 2020) FPN was solved both in apo- and holo-state and Co^{2+} was employed as an iron-mimicking metal, which has been widely used in FPN biology, given its similarities with Fe^{2+} but at the same time its greater stability.

Differently from other members of the MSF family, and to what emerged in previous studies on BbFPN, mammalian FPN has two metal-binding sites. In

both HsFPN and TsFPN, two Co^{2+} atoms were identified bound to the N- and C- domain, and coordination sites were named S1 and S2 respectively (Billesbølle et al., 2020; Pan et al., 2020). These two sites are found to be 15 Å apart, both accessible from the extracellular side in the outward-open conformation, with S1 closer to the cytosolic side. Site S1 consists of TM1 residues D39 and H43 while C326 and H507 (H508 in TsFPN (Pan et al., 2020)) coordinate the metal in the S2 site (Fig. 4).

Iron is typically coordinated in an octahedral geometry with ligands provided by four or more residues, which is crucial for the selectivity between metals. In FPN, however, the metal is coordinated by only two residues in both sites (Jormakka, 2023). This feature could be due to the outward open conformation in which the structures were solved, this state should represent the conformation in which the metal is released into the extracellular environment. Therefore, it is possible that in the inward-open and occluded conformations, other residues are part of the two binding sites, for example, residue D181 has been shown to have a role in iron binding and transport (Bonaccorsi Di Patti et al., 2014).

On the other hand, the scarcity of residues around the coordination shell of S1 and S2 would explain the promiscuity for the binding and transport of different divalent metals that has been observed (see below). The high dynamicity of these sites was also shown by the binding of hepcidin at the S2 site, which has a central role in hormone binding. The presence of the hormone alters the coordination of this site, with two more residues adding to the coordination shell: D325 and T320 form water-mediated contact with Co^{2+} and the C-terminus of hepcidin directly interacts with the metal. Given that what we have up to now represents a snapshot of the conformation in theory with less affinity to the metal, the S1 and S2 sites are likely much more complex with several

additional residues, some of which could act as a link between one site and the other.

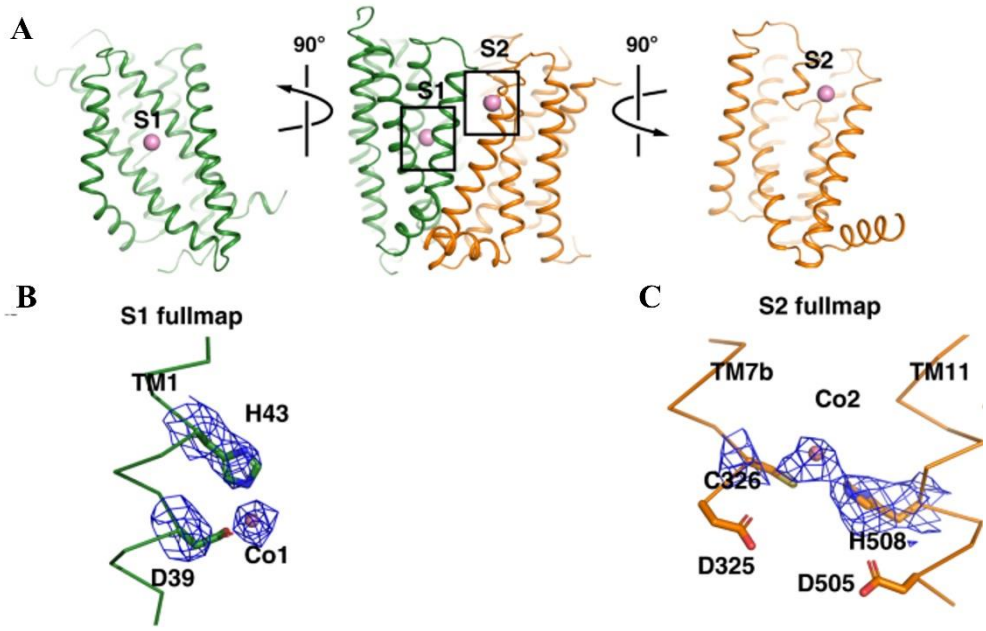

Figure 4. Cartoon representation of TsFPN is shown in three orientations with the locations of S1 and S2 marked by the bound Co^{2+} (colored in pink). B) Detail of S1 site. C) Detail of S2 site. Modified from Pan et al., 2020.

The existence of two binding sites raises several questions, complicating the understanding of the transport mechanism that FPN operates. Which of the two sites is crucial for iron binding and transport? Why is there a need for two binding sites for the same ion?

Site-directed mutagenesis and functional studies indicate that S1 is primarily required for iron transport, while S2 may have a more regulatory role,

mediating hepcidin binding (Bonaccorsi Di Patti et al., 2014; Billesbølle et al., 2020).

Conversely, other studies suggest that S2 is more crucial than the S1 site for metal ion binding and transport (Shen et al., 2023; Pan et al., 2020).

Despite structural data identifying two metal binding sites, the few available Co^{2+} binding data consider only one binding site. Both bacterial FPN and mammalian TsFPN show a similar low affinity for Co^{2+} (Kd 195 μM and 183 μM, respectively), and it is not clear to which binding site this affinity should be attributed. In TsFPN, mutations affecting S1 resulted in increased Kd (267 μM) while for the S2 the affinity resulted unchanged (Pan et al., 2020).

While the D39A mutation (S1 site) abolishes iron transport (M Bonaccorsi Di Patti et al., 2014), molecular dynamics simulations show that Fe^{2+} spontaneously binds to the S2 site, only occasionally contacting D39 of S1 (Billesbølle et al., 2020). The binding studies also do not fit with data obtained by transport assays which attribute a substantially lower Km to FPN (in the low micromolar range) for Co^{2+} and Fe^{2+} (Pan et al., 2020; Billesbølle et al., 2020) and do not help to figure out the possible relationship between the two sites, which is currently unclear.

It is also interesting to note that in a more recent structure of BbFPN, a second binding site has been identified in which a Ni-EDTA complex is present close to the loop between TM7a and 7b coordinated by H261 of BbFPN, which corresponds to D325 in the human protein (Deshpande et al., 2018). Although the exact location and coordination of the ion binding sites differ in mammalian FPN and BbFPN, both have two metal ion binding sites, a feature that may have some evolutionary implications in this type of protein.

Metal(s) transport by mammalian and bacterial FPN has been studied employing different techniques based on cellular metal efflux assays in *Xenopus laevis* oocytes and mammalian cells (Deshpande et al., 2018; Manolova et al., 2020; Mitchell et al., 2014) and in proteoliposome metal import assays (Shen et al., 2023; Pan et al., 2020; Li et al., 2020; Billesbølle et al., 2020). For mammalian FPN the Km for iron was found to be in the low micromolar range, and slightly higher for cobalt (Pan et al., 2020; Billesbølle et al., 2020).

At the moment, there is not much consensus on the type of transport mediated by FPN, the nature of the other ions involved, and the factors driving the conformational change from outward to inward-facing. Some groups have shown a certain pH-gradient dependence on the transport (Mitchell et al., 2014; Jormakka, 2023), and different models have proposed FPN as a Fe^{2+}/2H+ antiporter (Pan et al., 2020) or a Fe^{2+}/H^{+} symporter (Li et al., 2020). But transport activity has been observed to occur also at a neutral and positive pH gradient (Jormakka, 2023).

Other transport studies have provided evidence of the involvement of Ca^{2+} ions in FPN-mediated iron efflux, and a Ca^{2+} binding site has been identified in which residues D39, Q99, N212, and E219 are involved (Deshpande et al., 2018; Shen et al., 2023). However, there is no agreement on the role of Ca^{2+}. Some groups suggested it as a positive modulator of Fe transport (Billesbølle et al., 2020; Deshpande et al., 2018) others proposed FPN as a Ca^{2+} uniporter, with Fe^{2+} as a negative modulator of this process (Shen et al., 2023).While a Fe^{2+}/Ca^{2+} antiport mechanism is considered an attractive hypothesis (Jormakka, 2023), the physiological significance of Ca^{2+} transport by FPN is still unclear and needs further investigations (Pasquadibisceglie et al., 2023).

Recent data suggest that Ca^{2+} may also play a role in trafficking/subcellular localization of FPN (Rosenblum et al., 2024).

In addition to calcium, several studies have shown a certain promiscuity of FPN for the binding and transport of several divalent ions such as Zn^{2+}, Ni^{2+}, Sr^{2+}, and Mn^{2+} (Deshpande et al., 2018; Mitchell et al., 2014). Whether this transport occurs in cells and its physiological role is unclear.

1.2.1.3 FPN Regulation

Due to its crucial role, FPN must be tightly regulated to guarantee adequate iron levels in the human body and cells. FPN levels rely on a complex regulation network based on several systemic and cellular factors responsive to iron cellular and systemic levels, hypoxia, and inflammation at different layers as transcriptional, post-transcriptional, and post-translational level in a cell-specific modality (Drakesmith et al., 2015; Jormakka, 2023).

- **Transcriptional regulation**

  FPN transcription is regulated by AREs (Antioxidant Response Elements) and HREs (Hypoxia Response Elements). AREs-mediated regulation is predominant in macrophages while HREs in enterocytes. ARE elements upstream FPN transcription initiation site are recognized by transcription factors BACH1 and NRF2 and act as FPN transcriptional repressors or activators, respectively. High levels of heme and oxidative stress lead to BACH1 degradation, enabling FPN upregulation by NRF2, with a similar effect on heme oxygenase and ferritin, in a coordinated cellular response (Marro et al., 2010; Drakesmith et al., 2015).

HREs can be bound by HIFs in hypoxia response, HIFs degradation is triggered by iron-dependent hydroxylation of proline residues, so HIFs serve also as iron sensors. In enterocytes, iron deficiency response is mediated by HIF2alpha which upregulates the expression of FPN together with iron apical membrane importers Dcytb and DMT1 (Shah et al., 2009; Taylor et al., 2011), promoting intestinal iron uptake. HIF2alpha is the primary factor responsible for regulating erythropoietin transcription, suggesting its potential role as a mediator between iron availability and erythropoiesis during the hypoxic response (Drakesmith et al., 2015).

- **Post-transcriptional regulation**

  FPN mRNA 5' UTR possesses IRE (Iron Response Element). Under iron deficiency conditions IRPs (Iron Response Protein) bind IRE downregulating FPN translation. Upon the iron cellular level increase, the metal inactivates IRP resulting in the derepression of FPN mRNA translation. The IRE/IRP mechanism regulates iron levels in most cells while taking on relevance in macrophages, where after erythrophagocytosis, iron levels increase following the release of the metal from the heme group mediated by heme oxygenase (activated by NRF2) (Drakesmith et al., 2015), supporting systemic iron recycling. In enterocytes, the IRE/IRP system is bypassed by FPN transcripts lacking the 5' IRE (Zhang et al., 2009).

  FPN mRNA 3' UTR serves as a target for different miRNA induced by cellular iron deficiency: miR-485-3p (Sangokoya et al., 2013), miR17-5p (Kong et al., 2019) miR20a and miR20b (Jiang et al., 2019) that have been shown to increase cellular iron content by downregulating FPN translation.

Hepcidin Regulation

All the regulatory mechanisms described so far regulate FPN levels at the cellular scale, providing for intracellular iron homeostasis. However, the only FPN systemic regulator is hepcidin. Hepcidin is a small (25 aa) hormone peptide, featuring a β-hairpin structure stabilized by four disulfide bonds. Hepcidin is primarily synthesized and secreted by hepatocytes in response to various physiological signals, including systemic iron levels, inflammation, and hypoxia. Hepcidin is the main negative regulator of FPN, which is its only known receptor.

Hepcidin binding to FPN triggers two different downregulation mechanisms. The first regulatory effect identified is hepcidin-induced internalization and degradation (Nemeth et al., 2004; Nemeth & Ganz, 2006). The hormone binding promotes the ubiquitination of some Lys residues in the third intracellular loop of FPN, mediated by the rapid ring finger protein 217 (RNF217). Ubiquitination induces FPN internalization and consequent degradation via lysosomal or proteasomal pathways leading to a slow and permanent downregulation of iron efflux (L. Jiang et al., 2021; Nemeth & Ganz, 2006; Qiao et al., 2012).

Later an alternative mechanism was proposed which instead is rapid and reversible: hepcidin directly inhibits FPN, acting as a molecular cork that locks the transporter in the outward-open conformation, obstructing the central cavity and preventing iron efflux in the plasma (Aschemeyer et al., 2018). This mechanism should also provide an FPN downregulation in those cell types where ubiquitination machinery is absent (like erythrocytes).

The recent structural characterization of the FPN-hepcidin complex has provided deeper insights into the regulatory mechanism mediated by hepcidin (Billesbølle et al., 2020).

The structure of the FPN-Co^{2+}-hepcidin complex shows the hormone binding to the central cavity of the transporter. Hepcidin interacts with several residues within the FPN cavity through extensive polar and hydrophobic contacts. Among these N144, C326, Y333, Y501, D504, and H507 seem to be crucial, given that mutations on these residues are associated with FPN gain-of-function in hereditary hemochromatosis (Billesbølle et al., 2020). A surprising detail revealed by the structure is that the hepcidin C-terminus binds FPN residues C326 and H507 of the S2 binding site bridged by a Co^{2+} ion. When hepcidin binds indeed, S2 rearranges to include the hepcidin C-terminus in the Co^{2+} coordination shell, together with the backbone carbonyl of T320, and water molecule stabilized by D325 (Fig. 5) (Billesbølle et al., 2020).
The presence of Fe^{2+} increased the affinity of FPN for hepcidin ~80-fold, while disruption of the S2 site results in a weaker binding by hepcidin even in the presence of the metal. Molecular dynamic simulation showed how binding of divalent metals to the S2 domain stabilizes the dynamic TM7b helix into a conformation that promotes hepcidin binding (Billesbølle et al., 2020).
Also, the presence of hepcidin decreases Co^{2+} transport directly when measured in FPN proteoliposomes (Billesbølle et al., 2020), corroborating the direct inhibition model (Aschemeyer et al., 2018).

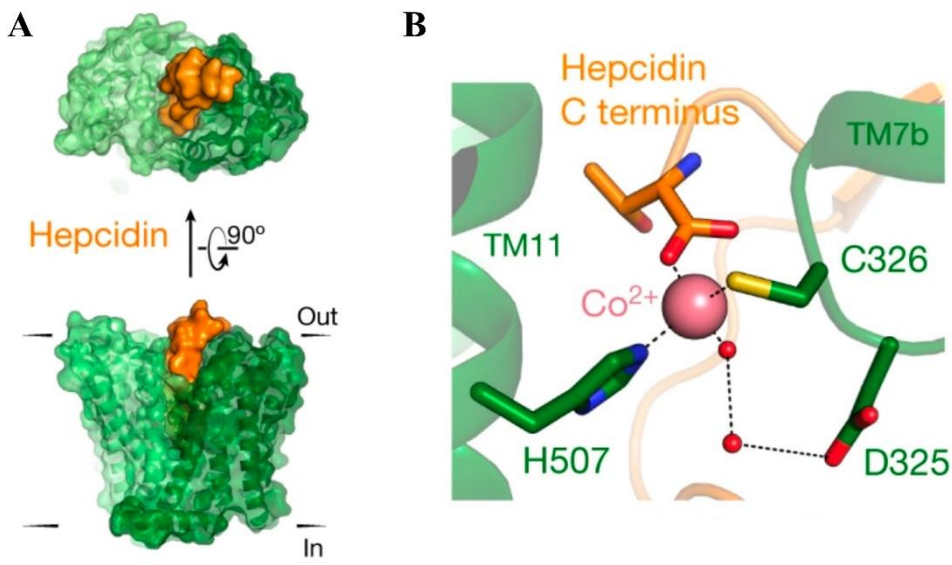

Figure 5. A) Surface representation of the HsFPN–Co^{2+}–hepcidin complex. B) Close-up of S2 domain metal-binding site in the presence of hepcidin. The residues H507, C326, and the C-terminus of hepcidin directly coordinate Co^{2+}, while the residue D325 participates in the binding site through two water molecules, shown as red spheres. Modified from Billesbølle et al., 2020.

This feature underlies the hepcidin selective recognition, ensuring that hepcidin binds and inhibits only the active, iron-loaded form of FPN, thus regulating its activity in a localized, homeostatic manner. This process may intersect with the FPN regulation by CP and HEPH ferroxidases (see below) and explain the increased FPN degradation when those enzymes are missing (Fuqua et al., 2018).

When plasma iron levels are elevated, a larger proportion of FPN becomes metal-bound, exceeding the capacity of ferroxidases to facilitate metal release.

The accumulation of FPN-Fe^{2+} complexes on the membrane would initiate hepcidin recognition and downregulation of the transporter.

Regulation by Ferroxidases

FPN is further regulated during iron release by the ferroxidases CP and HEPH. As mentioned before ferroxidases support iron release, enhancing the rate of iron efflux. Furthermore, it has been demonstrated that the ferroxidase activity of CP is required to stabilize cell surface FPN and that FPN is rapidly internalized and degraded in the absence of CP (De Domenico et al., 2007). The ferroxidase/FPN connection is strengthened by the finding that also HEPH stabilizes FPN (Ji et al., 2018). Moreover, it has been reported that CP can partially prevent the internalization of FPN mediated by hepcidin and that in the presence of ferroxidase activity, FPN is less sensitive to hepcidin in human brain microvascular endothelial cells (McCarthy et al., 2014; 2013).

The mechanisms underlying this regulation remain to be fully understood. Recent pieces of evidence suggest that HEPH co-localizes and physically interacts with FPN (Dlouhy et al., 2019; Han et al., 2007; Baringer et al., 2023), and this ability is likely conserved in CP as well. In this context, it is plausible to speculate on a competitive binding mechanism between hepcidin and ferroxidases, where the binding of one may prevent the interaction of the other with FPN.

1.2.2 The Ferroxidases: Ceruloplasmin (CP) and Hephaestin (HEPH)

Since the discovery of FPN, the importance of ferroxidases in regulating proper iron efflux has been well established. Ceruloplasmin (CP) and Hephaestin (HEPH) are two critical proteins that play essential roles in maintaining mammalian iron homeostasis. Both catalyze the oxidation of Fe^{2+} to Fe^{3+}, a crucial step in iron metabolism. This ferroxidase activity is essential for safe iron export from the cell: the metal is translocated across the plasma membrane by the membrane transporter FPN, as Fe^{2+}, while transferrin, the main protein responsible for iron transport in the blood, can only bind Fe^{3+}. CP and HEPH act as an intermediary between these two transport systems, promptly converting Fe^{2+} exported from the cell into a form suitable for binding to apo-Tf, in a manner that prevents tissue damage. Fe^{2+} does not require a catalyst for oxidation to Fe^{3+}, a transformation that occurs rapidly and spontaneously at physiological pH via the Fenton reaction. However, this reaction would generate a series of highly damaging reactive oxygen species for biological macromolecules. Ferroxidases prevent the spontaneous oxidation of Fe^{2+} by reducing oxygen to water with the electrons taken from the metal, thus safely mediating iron loading onto Tf.

Although CP and HEPH share structural and functional similarities, they exhibit distinct differences in tissue distribution and regulation.

CP and HEPH are large, multi-domain glycoprotein enzymes conserved across all vertebrates, belonging to the multicopper oxidase (MCO) family; together with the less characterized Zyklopen (ZP) (Helman et al., 2021) they form the group of Multi-Copper-Ferroxidase (MCFs) in humans. These enzymes are characterized by the presence of multiple copper atoms with distinct structural

and functional properties, which safely couple the oxidation of substrates to the controlled reduction of oxygen to water without the release of potentially toxic intermediates.

CP is the better studied MCF. First identified by Holmberg and Laurell in 1948, its name comes from its intensely blue color. CP has multiple functions, but in humans, its primary role is as a "ferroxidase", capable of catalyzing the oxidation of Fe^{2+} to Fe^{3+}(Bonaccorsi di Patti et al., 2018).

In mammals, CP exists in two isoforms: a soluble form found in plasma and a membrane-associated form anchored via a glycosylphosphatidylinositol (GPI) anchor. The CP-GPI isoform arises from alternative splicing of exons 19 and 20, where the last five residues of the soluble form C-terminus are replaced by 30 amino acids linked to the GPI anchor (Patel et al., 2000). Plasma-soluble CP is primarily synthesized by hepatocytes in the liver and directly secreted into the bloodstream. CP-GPI is anchored to the plasma membrane of various cell types that are not in contact with systemic circulation, underscoring the functional significance of this protein. This isoform has been identified in macrophages, astrocytes, leptomeningeal cells, and the retina, and is also expressed in Sertoli cells, and other cell types outside the CNS. Ceruloplasmin primarily functions as a ferroxidase, aiding in iron release from macrophages and hepatocytes, thereby promoting metal recycling and mobilization from liver stores.

Hephaestin (HEPH) was first identified in the sex-linked anemia (*sla*) mouse model (Vulpe et al., 1999). In this kind of anemia, an accumulation of iron is observed in the intestinal epithelium: the enterocytes are capable of absorbing the Fe introduced with the diet but not of exporting it into the blood. Indeed,

this ferroxidase plays a pivotal role in intestinal iron absorption, mediating dietary iron efflux into plasma from enterocytes basolateral membrane together with FPN. In addition to its role in the small intestine, HEPH has been detected in other tissues, including the heart, brain, pancreas, and lungs (Helman et al., 2023)

HEPH shares 50% identity and 68% similarity with the sequence of CP and a similar size of 130 kDa, but unlike the latter HEPH is tethered to the cellular membrane by a transmembrane domain at the C-terminal. Its N-terminal domain has a predicted architecture very similar to CP and resides on the extracellular side where it can aid FPN in the iron export. This structural difference between CP and HEPH reflects their distinct physiological roles, with HEPH adapted for localized ferroxidase activity in the gut and CP functioning more broadly across tissues, while the CP-GPI version ensures the presence of CP in tissues isolated from the systemic circulation or in cells with high iron efflux, such as macrophages.

Our understanding of the structure, function, and biosynthesis of mammalian MCFs is primarily based on the detailed characterization of CP.

Human CP has a molecular weight of 132 ± 4 kDa, with approximately 12 kDa contributed by oligosaccharide chains. It is encoded by the CP gene, a 65 kb sequence organized into 20 exons that undergo alternative splicing, located on the short arm of chromosome 3 (3q23-q24). The single polypeptide chain of human CP, comprising 1,046 amino acid residues, folds to form six cupredoxin domains. These domains associate with each other through hydrophobic interactions between domains 1-2, 3-4, and 5-6, and polar interactions between

domains 2, 3, 4, and 5, adopting a pseudo-ternary symmetry. Five loops connect these six domains, each sharing the initial motif CX(R/K).

CP has three Cu binding sites known as type 1 (T1) located in domains 2, 4, and 6, while the other three Cu atoms form together the so-called trinuclear cluster (TNC) which is found at the interface between domains 1 and 6. This cluster is essential not only for enzymatic activity but also for maintaining the protein's structure, stabilizing the globular form of CP by linking its N-terminal and C-terminal domains (Zaitseva et al., 1996).

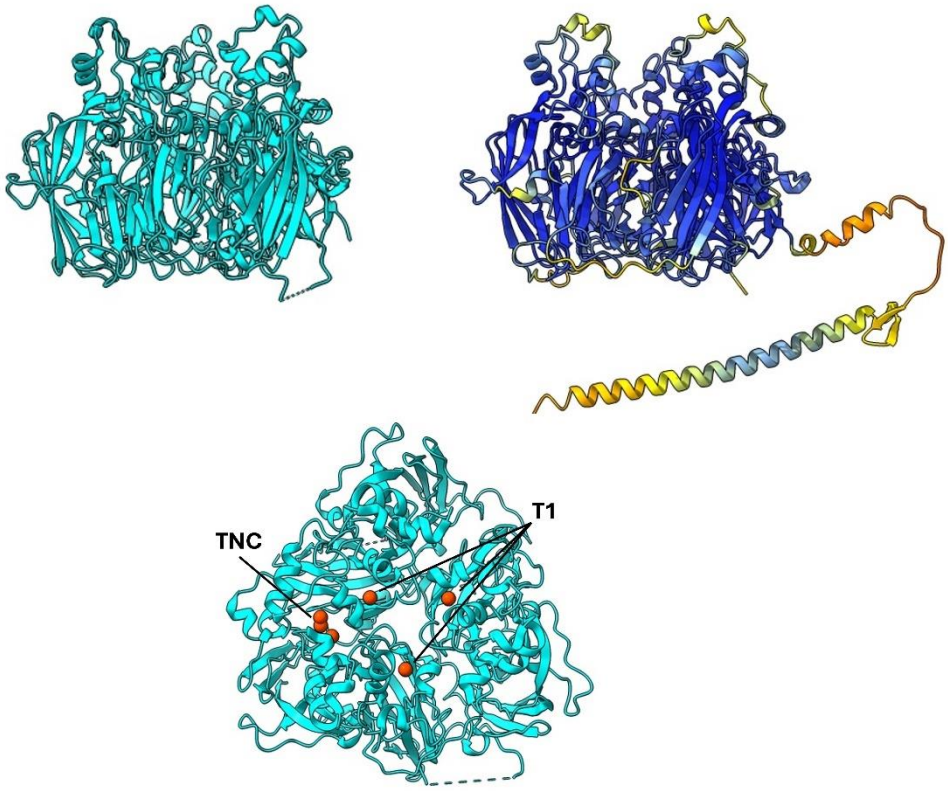

Figure 6. Crystallographic 3D structure of CP (PDB: 4ENZ, top left) and the 3D model of HEPH predicted by AlphaFold, colored by pLDDT score (top right). A detailed top view of CP TNC and T1 copper centers (bottom).

The T1 sites in domains 4 and 6 can exist in both reduced and oxidized states, the copper atoms of these two sites are coordinated by two histidine residues and one cysteine in the equatorial position and a methionine residue in the axial position, giving a trigonal pyramid arrangement. The third T1 site (in domain 2) is atypical, the methionine is replaced by a non-coordinating leucine residue. This T1 appears stable in its reduced state and cannot be oxidized without compromising the structural integrity of the protein, suggesting that this site is likely not involved in catalysis (Machonkin et al., 1998).

In addition to copper-binding sites essential for mediating electron transport and oxygen reduction, CP features binding sites for various substrates, including Fe^{2+}, for which the enzyme exhibits high specificity. Based on the crystal structure solved at approximately 3 Å in the presence of Fe atoms (Lindley et al., 1997), two Fe^{2+} binding sites with different affinities have been identified in the protein: one in domain 6, formed by residues D1025, E935, H940, and E272 from domain 2; and another in domain 4, where iron is similarly coordinated by residues E971, D684, E597, and H602. Additionally, two water molecules likely participate in forming these sites, which are surrounded by a negatively charged amino acid-rich region on the surface, possibly guiding the positively charged Fe^{2+} toward them.

The Fe^{2+} binding sites are located near the T1 copper sites in domains 4 and 6, approximately 9 Å below them. This positioning further supports the role of the T1 sites in domains 4 and 6 as primary electron acceptors, which acquire electrons directly from the substrate.

In contrast, the corresponding residues in domain 2 differ, and Fe binding is not expected, confirming that the T1 site in this domain is not directly involved in the protein's ferroxidase activity (Machonkin et al., 1998).

Upon binding, ferrous iron transfers an electron to the closest T1 copper site, this is coupled with the transfer of the oxidized iron to an adjacent site that holds ferric iron (Helman et al., 2023). Several pathways have been proposed for electron transfer from Fe^{2+} to the T1 copper center in domain 6, with the most energetically efficient involving residue E272, which is directly linked via a hydrogen bond to H1026, coordinating the copper atom at the T1 site of domain 6 (Quintanar et al., 2007). From T1 Cu electrons can flow via a branched His-Cys-His pathway that connects the T1 site Cys ligand to two histidine ligands to the TNC, where molecular oxygen binds. The TNC site can then sequentially transfer a total of four electrons, originally donated from different ferrous iron atoms, to dioxygen to form water.

Although the 3D structure of HEPH is still not available, comparative studies and molecular modeling predict a structure that closely aligns with the known structure of CP (Syed et al., 2002; Chen et al., 2010) as confirmed by AlphaFold modeling (Fig. 6). Apart from the C-terminal transmembrane region, which is not shared between the two proteins, the HEPH ectodomain possesses 6 cupredoxin domains binding 6 Cu atoms, of which three are present at T1 sites distributed in domains 2, 4, and 6 while the other three go to form the TNC at the interface between domain 6 and domain 1, exactly as for CP. The predicted model also showed the conservation of cysteine residues involved in disulfide bridge formation and the two binding sites for Fe^{2+} that are composed of the canonical set of ligands (three acidic residues plus a His residue): specifically residues D616, H621, S703, D996 of HEPH domain 4

correspond respectively to E597, H602, D684, E971 of CP while for domain 6 HEPH residues E960, H965, D1050, E300 correspond to E935, H940, D1025, E272 of the CP. Site-directed mutagenesis confirmed that residues E960 and H965 in domain 6 are critical for iron binding and ferroxidase activity (Vashchenko et al., 2012).

Differently from CP, HEPH T1 in domain 2 has a ‘classical’ coordination arrangement with an apical methionine, and this domain is predicted to have an additional low-affinity Fe binding site (Vashchenko et al., 2012; Zaitsev et al., 2019).

The biosynthesis of CP follows the classical secretory pathway for extracellular proteins; its co-translational translocation, directed by its signal peptide, targets the protein to the endoplasmic reticulum (ER), where the initial steps of N-glycosylation occur. CP has seven potential glycosylation sites in its amino acid sequence. Studies on CP purified from plasma have confirmed that residues N119, N339, N378, and N743 are modified by the addition of bi- and tri-antennary oligosaccharide chains, while N208, N569, and N907, located in β-strands within hydrophobic regions, are not glycosylated (Baerenfaenger et al., 2019; Takahashi et al., 1984).

After reaching the Trans-Golgi Network via the secretory pathway, apo-ceruloplasmin is loaded with copper in a process mediated by ATP7B, a P-type ATPase pump that receives cytosolic copper from the chaperone Atox1. Atox1 binds the metal and transfers it to ATP7B, which transports it into the Golgi lumen using ATP hydrolysis. The molecular details underlying copper incorporation by CP remain unknown. The CP metalation process is considered "all or nothing," as partially saturated forms of copper have never been identified (Hellman et al., 2002).

The structural integrity of the five loops connecting the globular domains of CP is crucial for proper metal loading by apo-CP; despite their low sequence homology, these loops all start with a CX(R/K) motif, stabilized by disulfide bridges formed by cysteine residues. These loops are similarly arranged at the protein's base. Mutations in cysteine, arginine, or lysine residues render CP inactive, preventing it from acquiring copper from ATP7B, trapping it in the Golgi, or secreting it as apo-CP. One hypothesis suggests that these inter-domain loops are necessary for proper interaction between apo-CP and the short loops connecting the transmembrane domain with the luminal domain of ATP7B, from which Cu is released (Maio et al., 2010).

The biosynthetic pathways for HEPH and ZP are likely to be similar to those of CP, but they have not been studied in detail (Chen et al., 2006, 2010).

Despite the detailed structural characterization of CP, many of its functions remain unclear, with the protein having been attributed various roles over time (Bielli et al., 2002). In addition to Fe^{2+}, CP can oxidize a wide range of organic substrates, including biogenic amines such as hormones (adrenaline, noradrenaline) and neurotransmitters (serotonin and dopamine), xenobiotics, and LDL. Other proposed roles include copper detoxification and transport in the blood, modulation of NO release, and antioxidant activities such as glutathione peroxidase-like activity (Musci et al., 2014).

Given the variety of roles CP can play, which vary depending on the different protein partners it interacts with (Vasilyev, 2019) and the tissues in which it is expressed, CP has been described as a "moonlighting protein" (Bielli et al., 2002), and its primary function has been the subject of debate.

Nevertheless, several lines of evidence indicate that CP's primary activity is as a ferroxidase: Fe^{2+} is indeed the substrate with the highest Vmax and the lowest Km (Osaki, 1966). Additionally, genetic defects leading to a deficiency of the protein in plasma (a condition known as aceruloplasminemia) present phenotypes primarily attributable to iron metabolism dysfunction and its accumulation in tissues, suggesting that CP's most important function is to mediate metal export from the cell (Miyajima, 2015). CP has two Km values for Fe^{2+}: 0.6 μM and 50 μM, corresponding to high- and low-affinity sites in domains 6 and 4 (Musci et al., 2014), respectively. Studies on kinetics of recombinant HEPH have shown how the affinities of the two sites for iron are close to those of CP with two Km equal to 3.5 μM and ≈ 107 μM (Vashchenko et al., 2012; 2013) indicating how the catalytic mechanism and the biological function of the two proteins are completely comparable. Also, Km for some organic substrates (such as p-phenylendiamine) are quite similar to those measured for CP, but HEPH seems to have specificity for a smaller group of organic substrates being for example incapable to oxidize biogenic amines such as adrenaline and dopamine (Vashchenko and MacGillivray, 2012). More recently the kinetic constants were revised measuring CP ferroxidase activity under more physiologically relevant conditions, providing Km ≈ 15 μM (Wong et al., 2014).

1.2.3 Pathologies associated to FPN-Ferroxidase system

The importance of the ceruloplasmin-ferroportin system is highlighted by the severe consequences caused by mutations in these two proteins. Disruption of this system leads to the development of serious conditions characterized by imbalances in iron metabolism at cellular, tissue, and systemic levels. Diseases associated with alterations in these two proteins are known as aceruloplasminemia (ACP) and ferroportin disease (FD), depending on whether the mutation affects CP or FPN, respectively.

ACP is a rare autosomal recessive disorder caused by mutations (over 40 identified so far) in the gene encoding CP (Fig. 7). While heterozygous individuals usually do not develop clinical symptoms and do not exhibit disruptions in iron homeostasis, homozygous individuals experience a range of defects related to iron accumulation in various organs and tissues, including the brain, retina, liver, and pancreas. Indeed, aceruloplasminemia is the unique iron-overload syndrome in which both systemic and brain metabolism are affected.

ACP iron overload affects different tissues leads to the development of a wide range of pathologies such as anemia, diabetes mellitus, retinal degeneration, and progressive neurological symptoms, including involuntary movements caused by extrapyramidal system dysfunction, ataxia, parkinsonism, and dementia (Miyajima, 2015).

Clinically, patients with ACP present with microcytic anemia, low plasma CP levels, low transferrin saturation, and elevated serum ferritin levels. ACP has a late onset, making early diagnosis and effective treatment difficult. Among the

various disorders caused by this condition, the most significant effects of the lack of functional CP are seen in the brain, where iron accumulation primarily affects the basal ganglia, striatum, thalamus, and dentate nucleus. Aceruloplasminemia is classified within a group of neurological disorders known as NBIA (neurodegeneration with brain iron accumulation), which distinguishes it from other iron metabolism-related diseases.

Given the strong functional connection between FPN and CP (De Domenico et al., 2007; McCarthy et al., 2013; 2014), the current model proposes that iron accumulation in ACP arises from impairment in the rate of iron efflux from storage sites (Piperno et al., 2018). Lack of functional CP disrupts the iron export machinery leading to FPN internalization and degradation with consequent reduction of FPN-mediated efflux of the metal that cause iron overload. Its intracellular accumulation prevents iron from being utilized for erythropoiesis (leading to iron-restricted erythropoiesis and anemia), and at the same time leads to increased oxidative stress due to Fenton reactions with cellular damage and death and consequent organ damage.

In the central nervous system (CNS), oligodendrocytes and astrocytes are the primary cell types responsible for iron storage and distribution (Piperno et al., 2018), and they are the most affected by its accumulation. In this context, ACP indirectly affects neurons through multiple mechanisms. First, neurons become deprived of iron, as the metal is sequestered within glial cells (Suh et al., 2006; Kono, 2013). This deprivation is further exacerbated by the loss of functional astrocytes and glial cells, which are essential for providing neurons with the necessary metabolic support (Suh et al., 2006). Moreover, it has been proposed that as iron-overloaded glial cells undergo apoptosis/ferroptosis, they release large amounts of toxic ferrous iron into the surrounding environment. This free

iron promotes oxidative damage to neurons, further contributing to neurodegeneration (Piperno et al., 2018). Over time, the combination of iron starvation, lack of glial support, and the release of toxic iron species leads to progressive neuronal damage and cell death.

Many of the CP mutations responsible for this condition are unique and often specific to certain families, usually associated with consanguinity (Kono, 2013). The mutations that most significantly affect CP include frameshift and nonsense mutations, which generally lead to premature termination of translation. Missense mutations can be classified based on the type of structural and functional alterations they cause. Some mutations lead to the retention of CP in the endoplasmic reticulum (e.g., I9F, G176R, P177R, D58H, F198S, W264S, A331D, G606E, and G873E mutants), while others result in proper secretion but produce apo-CP, lacking copper atoms. This occurs with mutations in residues G631, Q692, and G969, which are located near the T1 copper-binding sites (Kono, 2013). Another group of mutations, such as Y356H and G876A, are thought to fail to stabilize FPN on the plasma membrane, leaving it unprotected from the action of hepcidin, which triggers the internalization and degradation of the transporter (Kono et al., 2010).

An interesting mutation, R701W, identified in a young patient with severe movement coordination deficits, shows a pathological phenotype even in heterozygous conditions. The dominance of the mutation appears to be due to the inability to establish proper interaction with the copper-loading system in the Golgi, functionally inactivating the ATP7B pump and causing structural alteration of the organelle, resulting in its dispersion into vesicles (Bonaccorsi di Patti et al., 2009; Kono, 2013).

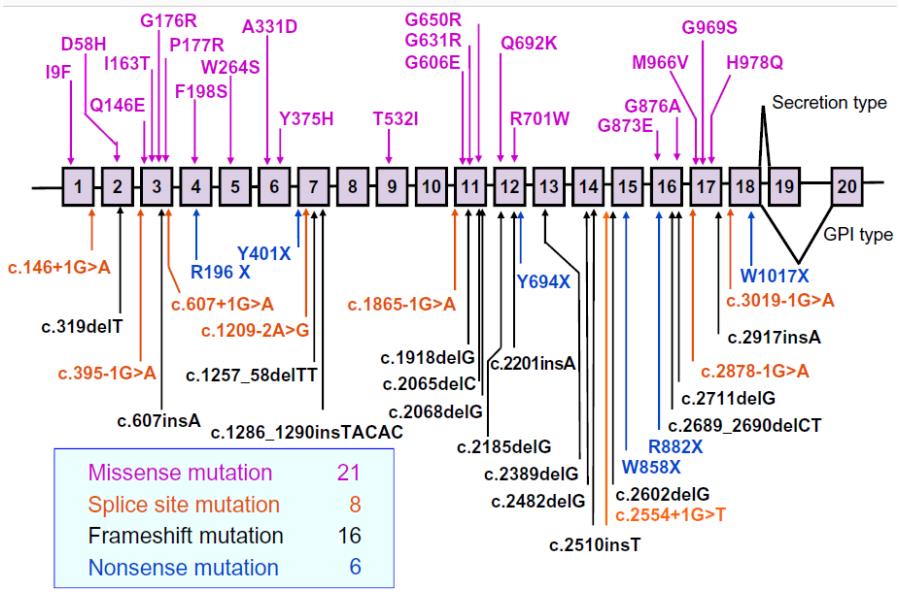

Figure 7. Genetic mutations characterized in patients with aceruloplasminemia and their family members (Kono, 2013).

FD also known as type 4 hemochromatosis (Montosi et al., 2001) is an autosomal dominant iron overload condition, caused by mutations in the *SLC40A1* gene. Sixty *SLC40A1* pathogenic variants have been described so far (Vlasveld et al., 2019), each associated with different clinical manifestations and varying severities of iron overload (Fig. 8). Since its discovery, FD has been divided into two different classes. The first class is the so-called "classical ferroportin disease" or Type 4 A hemochromatosis, it is caused by loss-of-function (LOF) mutations that reduce FPN expression on the cell surface, thereby decreasing its cellular iron efflux. This results in iron accumulation especially in macrophages and limited iron availability for erythropoiesis. Clinically, Type 4A is characterized by elevated serum ferritin levels and low or normal transferrin saturation (TSAT), along with reduced tolerance to phlebotomy. The second class is the "non-classical ferroportin disease" or Type 4B hemochromatosis, which instead is caused by gain-of-function (GOF) mutations, making FPN resistant to the down-regulatory effects of hepcidin, resulting in continuous cellular iron export, even with high levels of the hormone. This is characterized by iron accumulation in hepatocytes, elevated serum ferritin, and increased TSAT (Vlasveld et al., 2019). Most of the LOF mutations are found to be at the intracellular side and on the N-terminal half of FPN. In this region are located several residues important for the protein function. D39, H43, and D181 which are essential for iron transport and residues that take part in the intracellular gate that stabilizes the outward-open conformation of the transporter are all found in this region and are targets of LOF mutations (Bonaccorsi di Patti et al., 2018; Vlasveld et al., 2019). When tested in cells, most LOF variants are observed to be mislocalized with decreased expression on the membrane.

Conversely, GOF mutations affect residues on the extracellular side of the protein. Variants such as Y64N, C36Y, C326S, Y501C, D504N, and H507R retain full iron export capacity in functional assays but are resistant to downregulation by hepcidin. This resistance may be due to the loss of residues that are critical for hepcidin binding, as seen in mutations involving residues 326, 501, and 504, or because these mutations prevent proper ubiquitination of FPN upon hepcidin binding, as in the case of Y64N.

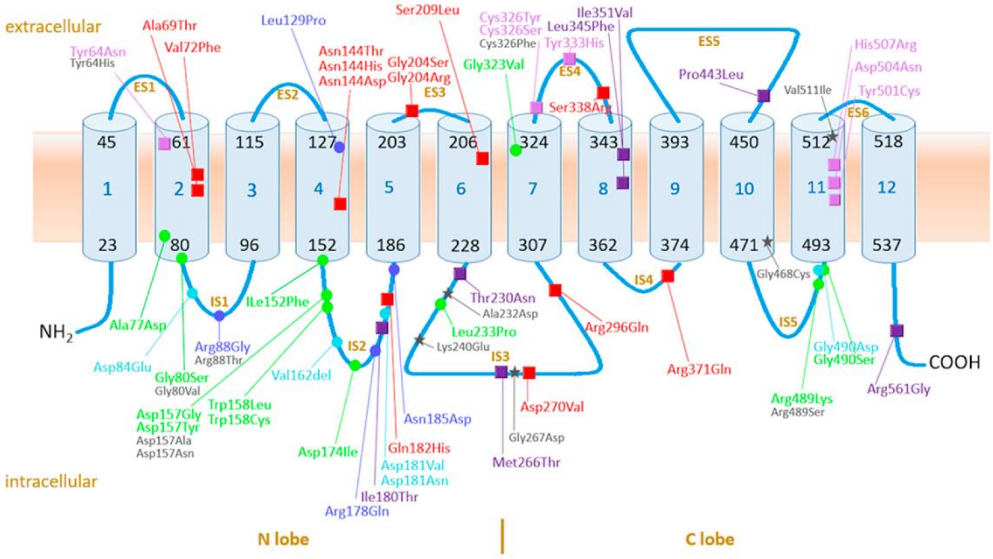

Figure 8. The two-dimensional (2D) structure of FPN. All the variants are shown as hepcidin-resistant (pink), hepcidin-sensitive or neutral (purple) and hepcidin conflicting/uncertain/unknown (red) GOF variants (squares). and hepcidin resistant (light blue), hepcidin sensitive (dark blue), and hepcidin conflicting-uncertain-unknown (green) LOF variants (dots), or non-classified variants (grey asterisk) (Vlasveld et al., 2019).

2. AIM OF THE THESIS

Iron homeostasis is critical for numerous physiological processes, and its dysregulation is associated with severe diseases. Central to systemic iron regulation is the ferroportin (FPN)-ferroxidase system, where FPN functions as the sole iron exporter, supported by ferroxidases such as ceruloplasmin (CP) and hephaestin (HEPH). However, the precise molecular mechanisms underlying this system, including the dynamics of iron transport and protein interactions, remain incompletely understood.

This thesis is divided into three sections, each addressing different unresolved aspects of this system. The first section focuses on the FPN transporter. FPN, like other members of the Major Facilitator Superfamily (MFS), is thought to mediate iron translocation through the alternating access mechanism. However, conflicting models of this mechanism have been proposed by different research groups, and the absence of a reliable system to study alternating access has limited our understanding of how FPN operates.

The first goal of this section is to establish an experimental system for systematically investigating the conformational changes that underlie iron translocation in FPN. This will be achieved through an innovative approach for such experimental challenges, based on the site-specific incorporation of unnatural amino acids. By expanding the genetic code of *Pichia pastoris*, the possibility of introducing the unnatural amino acid dansylalanine at selected positions within the protein is explored. The dansyl group is a well-known fluorophore highly sensitive to its microenvironment, making it particularly suited for probing conformational changes in proteins. The aim is to assess the

feasibility of this system, focusing on the efficiency of incorporating the fluorescent amino acid into FPN and validating the ability of dansyl-labeled FPN to detect conformational changes induced by metal binding. Once this experimental system is established, it can be used to thoroughly investigate the translocation mechanism mediated by FPN.

The second goal of this section is to characterize the two metal-binding sites identified in the 3D structures of FPN, a unique feature within the MFS family, yet overlooked by most of the proposed models for FPN's mechanism. Through mutagenesis, the role of these two sites in metal binding and their relative affinity for iron will be defined using fluorescence spectroscopy. A detailed understanding of the involvement of these two sites will be essential for proposing an updated model of FPN iron translocation mechanism. In parallel with this analysis, the study will also include specific FPN mutants known to destabilize the intracellular gate. The impact of these mutations on iron binding will be assessed to provide a more comprehensive understanding of how these structural alterations affect the protein's function.

The second section of this thesis focuses on the ferroxidases CP and HEPH. The absence of a reliable protocol for the expression and purification of recombinant CP has long hindered the biochemical characterization of pathological mutants of this protein and has limited the exploration of specific residues through structure-based mutagenesis. Thanks to a strategy recently developed by our laboratory for the production of recombinant CP, this section will present the functional characterization of two mutants of this protein, whose pathogenicity remains unclear. Additionally, the role of residues potentially involved in channeling iron into the catalytic core of CP will be investigated. These two examples will be employed to demonstrate the

potential of obtaining high-quality recombinant CP for unlocking the in-depth analysis of residues whose roles are yet to be defined.

Concerning HEPH, only a few papers have reported its purification, and these studies have consistently achieved this by removing the transmembrane region of the protein. The goal is to develop an expression and purification protocol that allows the production of full-length HEPH. Reaching this goal is crucial for solving the 3D structure of the protein, which has not yet been elucidated. Following the successful production of HEPH, the ferroxidase activity of two cancer-related variants will also be characterized, as their functionality and involvement in tumorigenesis have not yet been investigated at the molecular level.

The third part of this thesis aims to investigate the interaction between FPN and ferroxidases. While the FPN-HEPH interaction in cells has been recently demonstrated, only indirect evidence suggests an interaction with CP. Therefore, the existence of a FPN-CP complex will be investigated through the application of the Proximity Ligation Assay (PLA), a recently developed technology that enables the detection of weak and transient protein-protein interactions directly in cells. This assay will finally provide a definitive answer to the long-standing question of whether these two proteins interact. Additionally, this objective will involve integrating these results with assays on purified proteins to understand the role of hepcidin in competing with CP for this interaction.

3. MATERIALS AND METHODS

3.1 *Pichia pastoris* strains and cell lines

FPN wild type and mutants described in section 4.2 were expressed in *Pichia pastoris* GS115 (His^+) (Invitrogen), while FPN wild type described in section 4.5 was expressed in *Spodoptera frugiperda* (Sf9) cells. Dansylated (DA) FPN was expressed in *Pichia pastoris* JC300 (His^+, Arg^+, Ade^+). The JC300 strain (Lin Cereghino et al., 2001) was a generous gift of J. Cregg (Oregon Graduate Institute of Science and Technology, USA). Recombinant CP was expressed in the glycoengineered *Pichia pastoris* SuperMan5 (och1Δ1, GAP-mannosidaseHDEL, his4Δ1) strain (SM5) (Biogrammatics). HEPH expression was tested in *Pichia pastoris* SM5, Sf9 cells, and Expi293F cells, with Expi293F cells used for HEPH production. For immunofluorescence and proximity ligation assays, HEK293TT and U373GM cells were employed.

3.2 Vectors and Constructs

The pREAV vector carrying the tRNA/aaRS pair specific for dansylalanine (DA) was a generous gift from Prof. P.G. Schultz (The Scripps Research Institute). This vector allows expression of the DA-RS in *Pichia pastoris* under control of the methanol-inducible FLD1 promoter. The plasmid was linearized with AatII prior to transformation in *Pichia pastoris* JC300 cells by electroporation.

The cDNA of wild-type human FPN, Flag-tagged at the C-terminus, was cloned in pIB2 vector for constitutive expression under the control of the GAP promoter in *Pichia pastoris*. The pIB4 vector allows expression from the methanol-inducible AOX1 promoter and was used to construct the pADE vector by replacing the HIS4 auxotrophic marker with the *Pichia pastoris* ADE1 gene. Wild-type Flag-tagged FPN was cloned in EcoRI/KpnI in pADE. FPN mutants V46amber, Y54amber, V161amber, and Y331amber were obtained through site-directed mutagenesis using QuikChange II XL kit (Agilent) or by overlap extension PCR.

The plasmid for constitutive expression of the secreted isoform of human CP is described in Bonaccorsi Di Patti et al., 2021. CP mutants N244S, G876A, F298I-F659I-F1000I (Triple), Y290F-Y992F-E651A-E851A (4EY) were obtained by site-directed mutagenesis using QuikChange II XL kit (Agilent) or by overlap extension PCR.

All constructs were sequence-verified by automated DNA sequencing at GATC Biotech/Microsynth. Plasmids were linearized with StuI (pIB2) or EcoNI (pADE) prior to transformation in *Pichia pastoris* JC300/DA-RS cells by electroporation. Integration of all plasmids in the *Pichia pastoris* genome was confirmed by PCR on genomic DNA extracted from His^+ (GS115, SuperMan5) or Arg^+, Ade^+ (JC300) colonies.

Human HEPH full-length coding sequence was amplified by PCR (Phusion Flash) from pCMV6-Heph (Origene #215550) and cloned in different vectors: pOPINEneo-3C-TGP-His, pOPINEneo-TEV-TGP-His, pOPINEneo-TGP-2Strep-His, and pOPINEneo-link3C-TGP-His, for expression in Expi293F cells; pFB-CT-His-FLAG and pFB-CT-His-2Strep, for expression in Sf9 cells by ligation independent cloning (ClonExpress®II One-Step Cloning kit). All

vectors were provided by the Membrane Protein Lab, as well as the vector for FPN expression in Sf9 cells.

3.3 Recombinant FPN Expression and Purification

For medium-scale expression of FPN wild type and mutants employed in section 4.2, GS115 cells were grown in YPD (1 L) to OD600 8–10 and harvested by centrifugation at 4500 rpm for 10'. The cell pellet (10–15 mL) was resuspended in an equal volume of lysis buffer (25 mM MOPS, 150 mM NaCl, pH 7.4, complete protease inhibitor cocktail (Roche), 2 µg/mL leupeptin and pepstatin, 1 mM PMSF, 10 U/mL DNase, 2 µg/mL RNase) and lysed by the glass beads method. Cell membranes were collected by ultracentrifugation at 35,000 rpm (Beckman 70Ti rotor) for 50' and were washed with 25 mM MOPS, 300 mM NaCl, pH 7.4, and centrifuged at 35,000 rpm for 20'. Membrane proteins were extracted in 15 mL extraction buffer (25 mM MOPS, 150 mM NaCl, pH 7.4, 1% Triton X-100, 2 µg/mL leupeptin and pepstatin, 1 mM PMSF) for 1 h at room temperature, followed by centrifugation at 35,000 rpm for 20'. For medium-scale expression of dansylalanine (DA) FPN amber mutants, yeast cells were grown in YPD (1 L) to OD600 8–10, centrifuged, and induced in 200 mL BMMYH (0.67% yeast nitrogen base, 50 mM potassium phosphate buffer pH 6.8, 1% methanol, 50 µg/mL histidine) supplemented with 1 mM DA for 72–96 h, adding 1% methanol daily. Cell lysis and membrane protein extraction were performed as described above for wild-type FPN. FPN was purified by affinity chromatography on anti-Flag M2 agarose (Merck) or anti-Flag G1 agarose (GenScript). The resin (1 mL) was washed with 50–55 bed volumes of 25 mM MOPS, 300 mM NaCl, 0.01% DDM, pH 7.0, to OD280 < 0.03 to remove contaminants and exchange Triton X-100 with dodecylmaltoside (DDM). The elution step was performed with

MOPS/NaCl/DDM containing 0.1 mg/mL Flag peptide (3 mL), followed by 100 mM glycine, 150 mM NaCl, 0.01% DDM, pH 3.5 (6 mL). Millipore Ultra 30 K devices were used to concentrate purified FPN and exchange the protein with buffer when required. Protein content was measured with the microBCA assay (ThermoFisher). The monoclonal anti-human FPN antibodies, 31A5 (mouse-monoclonal) and 38G6 (human-monoclonal), used for Western blot were a generous gift of Dr. Tara Arvedson (Amgen).

3.4 Recombinant HEPH expression and purification

Expi293F cultures (2.5×10^6 cells/mL) were transfected by gently adding a transfection mixture consisting of plasmid DNA (1 μg/mL of culture) and PEI Max 40K diluted in Opti MEM medium (Gibco). After 8–10 h, cultures were supplemented with 5 mM valproic acid, 6.5 mM sodium propionate, 0.9% (w/v) glucose, and 50 μM $CuSO_4$, and placed in a shaking humidified 8% CO_2 incubator at 30°C and 80 rpm. Cells were harvested after 72 h by centrifugation and washed with cold PBS. The cell pellet was resuspended in base buffer (50 mM HEPES, 200 mM NaCl, 5% glycerol, 0.5 mM TCEP, pH 7.5) supplemented with protease inhibitors (complete Roche). For the expression test and the detergent screen, cell pellets coming from micro (2 mL) and small-scale (30 mL) cultures were disrupted by sonication. After clarification, the membranes were extracted with different detergents (see below) for 1 h at 4°C and employed for small-scale purification with Co^{2+} charged-TALON resin (Takara Bio).

The detergents (Anatrace) employed were: n-Dodecyl-β-D-maltoside (DDM); n-Dodecyl-β-D-maltoside + Cholesteryl Hemisuccinate (DDM+CHS); n-

Decyl-β-D-maltoside (DM); n-Decyl-β-D-maltoside + Cholesteryl Hemisuccinate (DM+CHS); Octyl-β-D-glucoside (OG); Lauryl Maltose Neopentyl Glycol (LMNG); Octyl Glucoside Neopentyl Glycol + Cholesteryl Hemisuccinate (OGNG+CHS); Lauryldimethylamine-N-oxide (LDAO); Octaethylene Glycol Monododecyl Ether (C12E8); Nonylphenyl-Polyethylene Glycol + Cholesteryl Hemisuccinate (C12E9+CHS); 5-Cyclohexylpentyl-β-D-maltoside (CYMAL-5); Fos-Choline-12 (FC-12).

For purification, pellets from large-scale cultures (1 L) were disrupted using a cell disruptor (CF 2 model, Constant Systems). Cell membranes were obtained by ultracentrifugation at 195,000 g. Membrane proteins were solubilized in base buffer containing 1% (w/v) N-dodecyl-β-D-maltopyranoside (DDM, Anatrace), 0.1% (w/v) cholesteryl hemisuccinate (CHS, Anatrace), for 1 h at 4°C, and then ultracentrifuged again. HEPH was purified from the resulting supernatant with Co^{2+} charged-TALON resin (Takara Bio). After extensive washing, the protein was eluted with base buffer containing 300 mM imidazole and 0.03% DDM, 0.003% CHS. Imidazole was removed with a desalting column (CentriPure100-Z25M, Emp Biotech), and the protein was incubated overnight with HRV 3C protease to remove the tag. After incubation with TALON resin, flow-through containing cleaved protein was collected, concentrated, and further purified by Size Exclusion Chromatography (SEC) on a Superdex G200 increase column (Cytiva). Protein purity was assessed by SDS-PAGE and concentration was determined by absorbance at 280 nm (ε280 200,000 $M^{-1}cm^{-1}$). The primary antibody for Western Blots was the mouse-monoclonal sc-365365 (Santa Cruz).

3.5 Recombinant CP expression and purification

Expression of CP and purification were performed as described in Bonaccorsi Di Patti et al., 2021. Briefly, expression of secreted CP was performed in MD medium buffered with 50 mM potassium phosphate at pH 6.8, supplemented with 100 µM $CuSO_4$. Cultures grown overnight at 28°C were filtered, diluted, and adjusted to pH 7.1 before being loaded onto a DEAE-Sepharose column equilibrated with buffer containing 25 mM MOPS, 30 mM NaCl, pH 7. After washing, the protein was eluted with 25 mM MOPS, 150 mM NaCl, pH 7. The eluate was diluted 1:3 and further purified with a sepharose resin derivatized with chloroethylamine (AE-Sepharose) equilibrated in 25 mM MOPS, 150 mM NaCl, pH 7. After a wash with the same buffer the protein was eluted with 25 mM MOPS, 500 mM NaCl, pH 7 and then concentrated using Millipore Ultra 30K devices.

3.6 CP purification from human plasma

Cp was purified by chromatography on AE-Sepharose from human plasma obtained from the Transfusion Center at Policlinico Umberto I (Rome). Briefly, 150 ml plasma was loaded on AE-Sepharose (10 ml) equilibrated in K-phosphate buffer 30 mM pH 7. The resin was washed with the same buffer (20 ml), followed by 10 column volumes of K-phosphate 80 mM pH 7 and 4 column volumes of K-phosphate 100 mM pH 7. The protein was eluted with 4 column volumes of K-phosphate 200 mM pH 7. Cp was diluted 1:4 and further

purified by chromatography on DE-52 cellulose to remove apo-protein. Holo-CP was eluted with a gradient 40-200 mM K-phosphate pH 7.

3.7 Fluorescence Spectroscopy

Fluorescence spectra were obtained using a Jobin Yvon Fluoromax-3 spectrofluorometer. Protein samples were diluted in 25 mM MOPS, 150 mM NaCl, 0.01% DDM, pH 7.0, and titrated with $CoCl_2$ (2–60 μM) for FPN DA mutants (section 4.1), while FPN wild type and mutants used in section 4.2 were titrated with $CoCl_2$ up to 9000 μM. For experiments described in section 4.1, the excitation wavelength was set at 340 nm and emission spectra were recorded between 400 and 650 nm at room temperature (slit width: 5 nm for both excitation and emission). For cobalt titration of FPN wild type (non-dansylated) and FPN mutants (section 4.2), excitation was set at 295 nm and emission spectra were recorded between 300 and 450 nm. Titration data were fitted to a one-site or two-site binding model using GraphPad Prism 8. When necessary, cobalt was removed by gel filtration using a PD10 prepacked column (Cytiva) equilibrated in 25 mM MOPS, 150 mM NaCl, 0.01% DDM, pH 7.0. In section 4.5, FPN Y54DA was titrated with $CoCl_2$ up to 100 and 4000 μM, and subsequently with plasma purified CP (0.32–3.8 μM). The excitation wavelength was set at 340 nm, and emission spectra were recorded between 400 and 650 nm.

3.8 CP and HEPH activity assays

CP ferroxidase activity was measured at 25°C in a buffer containing 25 mM MOPS, 150 mM NaCl, pH 7. Wild-type CP and mutants (0.25 μM) were added to a solution of 200 μM $Fe(NH_4)_2(SO_4)_2$ in a quartz cuvette (0.5 cm path length), and Fe^{2+} oxidation was monitored at 315 nm using a UV6000 spectrophotometer (Metash).

CP oxidase activity against o-dianisidine (oDA) was measured according to the protocol described by (H. P. Lehmann et al., 1974) oDA was diluted in 0.1 M sodium acetate, pH 5.5, to a concentration of 0.1 mg/mL and incubated with 0.25 μM CP (wild type and mutants) for 1 h at 37°C. The reaction was stopped by adding 4.5 M H_2SO_4, and the oxidized oDA was measured at 540 nm using a UV6000 spectrophotometer (Metash).

HEPH ferroxidase activity was measured at 25°C in a buffer containing 50 mM HEPES, 200 mM NaCl, 0.02% DDM, and 0.002% CHS, pH 7.5. Upon addition of 60–300 μM $FeSO_4$ to 0.3 μM HEPH, Fe^{2+} oxidation was monitored at 315 nm using a CLARIOstar Plus microplate spectrophotometer (BMG Labtech). Each measurement was repeated three times for error bar generation.

3.9 Immunofluorescence and Proximity Ligation Assay (PLA)

HEK293TT cells were cultured at 37°C under a 5% CO_2 atmosphere in DMEM supplemented with 10% fetal bovine serum. Cells were plated on poly-D-lysine-coated glass coverslips in 6-well plates and transiently co-transfected with pCMV-FPN-FLAG or pCMV-FPN-GFP and pCMV-CP-GPI using

calcium phosphate. After 48 h, coverslips were washed 3 times with cold PBS and incubated at 4°C for 1 h with anti-FPN (31A5, mouse-monoclonal, 1:1000) and anti-CP (DAKO, rabbit-polyclonal 1:1500), diluted in cold medium for surface labeling. After fixation with 4% PFA for 20', coverslips were used for immunofluorescence or PLA. For immunofluorescence, quenching and blocking were performed by incubating the cells in 1% BSA, 0.1% Triton X-100, and 50 mM glycine in PBS for 30' at room temperature. Alexa Fluor 488 or 594-conjugated secondary antibodies (1:300) were applied for 30' at room temperature. PLA was performed using the Duolink® In Situ Detection kit (Sigma-Aldrich). Negative controls were generated by incubating cells with either one or the other of the two primary antibodies or with none. The protocol was modified to detect plasma membrane complexes only. After primary antibody incubation and fixation, coverslips were incubated with Duolink Blocking Solution for 1 h at 37°C. Cells were then incubated with secondary antibodies conjugated with PLUS and MINUS probes for 1 h at 37°C. After two washes with buffer A, ligase solution was applied for 30' at 37°C. Following two more washes with buffer A, coverslips were incubated with polymerase solution for 100' at 37°C and subjected to a final wash with buffer B. PLA was also performed on U373MG cells following the same protocol. For both immunofluorescence and PLA, after staining nuclei with 1:1000 DAPI (Sigma-Aldrich), images were acquired using a Leica DM3000 microscope and Leica DFC320 digital camera.

3.10 FPN-CP pull-down assay and Size Exclusion Chromatography (SEC)

For the pull-down assay, recombinant Flag-tagged FPN (4 μM) was pre-incubated with 0, 4, and 20 μM hepcidin for 15' at 4°C in the presence of 10 μM $(NH_4)_2Fe(SO_4)_2$ in a buffer containing 25 mM MOPS, 150 mM NaCl, and 0.01% DDM, pH 7. After pre-incubation, 4 μM purified CP from plasma was added, and a negative control was prepared with CP in buffer without FPN. The samples were incubated for 30' at 4°C, under the same conditions as the previous incubation. Then, 30 μL of anti-Flag G1 agarose resin (GenScript) were added, and samples were incubated for 30' with gentle rotation at 4°C. After incubation, the resin was washed seven times with 1 mL of the same buffer. Bound proteins were eluted with an acidic buffer containing 100 mM glycine, 150 mM NaCl, 0.01% DDM, pH 3.5. Both input and elution fractions were analyzed by Western blotting.

For SEC, FPN and CP were mixed at a 1:1 ratio in a buffer containing 25 mM MOPS, 150 mM NaCl, 0.01% DDM, and 1 mM $CoCl_2$. After 30' at room temperature, the samples were loaded onto a Superdex 200 Increase 10/300 GL (Cytiva) column with a flow rate of 0.5 mL/min. The same procedure was used for the individual protein runs. Fractions of 0.5 mL were collected and analyzed by Western blotting.

3.11 FPN-HEPH crosslinking and Size Exclusion Chromatography (SEC)

For crosslinking, HEPH and FPN were mixed at a 1:1 ratio in a buffer containing 50 mM HEPES, 150 mM NaCl, 0.02% DDM, and 0.001% CHS, in the presence or absence of 1 mM $CoCl_2$. BS3 crosslinker (ThermoFisher) was added to a final concentration of 0.8 mM. Control samples were prepared under the same conditions but without BS3. The samples were incubated at room temperature for 30' and subsequently analyzed by SDS-PAGE.

For SEC, HEPH and FPN were mixed at a 1:2 ratio in the same buffer containing 1 mM $CoCl_2$. Two additional samples containing the individual proteins were prepared under the same conditions. After 30' at room temperature, the three samples were loaded onto a Superose 6 Increase 10/300 GL (Cytiva) column with a flow rate of 0.4 mL/min. Fractions of 0.2 mL were collected for all three runs and analyzed by SDS-PAGE.

4. RESULTS AND DISCUSSION

4.1 Genetic Incorporation of Dansylalanine in Human Ferroportin to Probe the Alternating Access Mechanism of Iron Transport

As described in the introduction section, FPN belongs to the Major Facilitator superfamily (Billesbølle et al., 2020; Gac et al., 2013; Wallace et al., 2010; Maria C. Bonaccorsi Di Patti et al., 2014). Proteins belonging to this widespread group typically display a 12 TM organization (the 'MFS fold') and are believed to act with an alternating access mechanism that involves extensive conformational changes to translocate their substrate across the membrane. These include at least three different conformations, namely inward-open, occluded, and outward-open. As mentioned before, an open question regards the molecular mechanism of iron translocation by FPN; in fact, conflicting data have been reported suggesting that FPN is a uniporter (Deshpande et al., 2018) a proton-coupled symporter (Li et al., 2020), or a proton-coupled antiporter (Pan et al., 2020; Shen et al., 2023).

The conformational states of membrane proteins can be probed directly using fluorescence-based techniques. Analysis of the fluorescence of naturally occurring and/or engineered tryptophan residues has been widely employed. Additionally, chemical reactions that target cysteine thiol groups have been used to covalently attach environment-sensitive probes to proteins. However, these approaches can be challenging because they require the generation of a

tryptophan- or cysteine-free background to achieve single-site labelling. Such limitations can be overcome by site-specific introduction of unnatural amino acids with unique functional groups that are not found in native proteins.

The *amber* codon suppression strategy has been used to achieve site-specific incorporation of non-canonical amino acids into FPN. *Amber* codon suppression relies on the ability of an engineered orthogonal aminoacyl-tRNA synthetase (aaRS) to charge its cognate tRNA with an unnatural amino acid and suppress a TAG *amber* stop codon placed within a coding sequence. This approach has been used to introduce genetically encoded unnatural amino acids to label target proteins selectively and site-specifically with different probes (Liu & Schultz, 2010; Wang, 2017).

Dansylalanine (DA) is an unnatural fluorescent amino acid that can be incorporated into polypeptide chains thanks to this strategy. The dansyl group of DA is an environment-sensitive fluorophore and this non-canonical amino acid has been used for the fluorescence spectroscopy analysis of protein unfolding (Jiangyun Wang et al., 2006). The fluorescence of the dansyl group originates from an intramolecular charge transfer excited state in which electron density is transferred from the NMe_2 group to the electron-accepting sulfonyl substituent of dansyl. Solvation and hydrogen bonding (together with the presence of nearby charged residues) affect emission maximum and quantum yield, making the dansyl group (and DA) useful to probe the polarity and dynamics of the local environment in proteins (Lakowicz, 2006). Given these features, we chose to employ DA incorporation into FPN to investigate the potential of the site-specific genetic incorporation approach for studying the conformational changes in FPN, predicted to take place during the transport of iron.

4.1.1 Selection of Reporter Residues and Incorporation of Dansylalanine (DA) into FPN

To identify regions of the protein predicted to undergo major conformational changes during the transport cycle, the structural models of human FPN in different conformations (Tortosa et al., 2017) were employed, since an inward-open structure of FPN is still not available. This preliminary analysis was performed with the purpose of selecting appropriate positions to place the unnatural amino acid DA. Of note, the outward-open structure of human FPN is fully consistent in the *in silico* model employed, thus validating the selection of specific residues to be mutated. On the extracellular side of the protein, in the inward-open conformation, residue Y331, located on TM7, is close to Y54 which is found in the loop connecting TM1 and TM2 (Fig. 9). When FPN switches to the outward-open conformation these two residues are predicted to move away from each other and residue Y54 is predicted to substantially increase its solvent exposure (Fig. 9). Therefore, positions 54 and 331 appeared to be suitable to act as sensors of the conformational transitions of FPN. A sequence of three consecutive valines is found on the intracellular side of the protein in the loop connecting TM4 and TM5. Deletion of one of these valine residues was one of the first loss-of-function FPN mutations identified, giving rise to hemochromatosis type 4A (Montosi et al., 2001). We therefore chose to mutate the central valine in the sequence, namely V161. Another valine, residue V46, was also chosen because it is located within TM1 in the channel through which iron is translocated. On the basis of the models, changes in solvent accessibility between inward-open and outward-open conformations of FPN are predicted to lead to decreased exposure of both these valine residues.

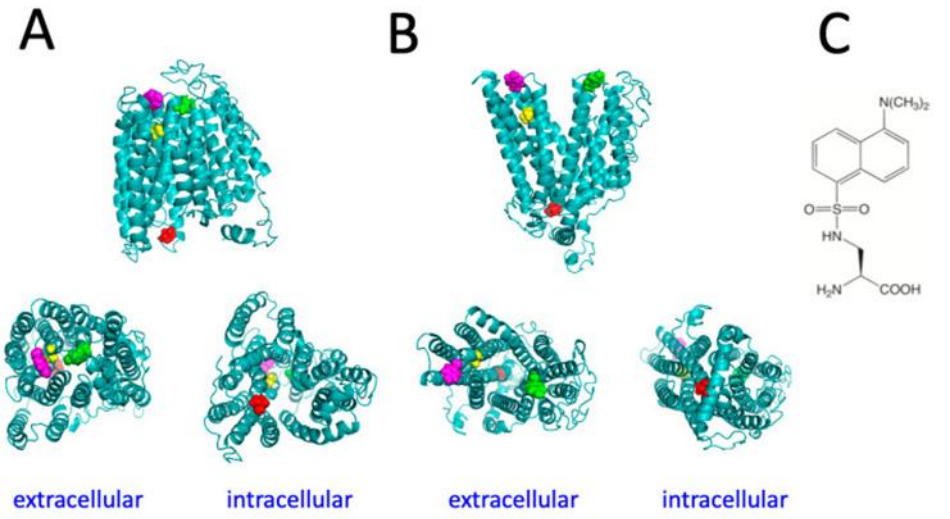

Figure 9. Structural models of the inward-facing conformation (A) and outward-facing conformation (B) of human FPN; side-view (upper panels), bottom-view (lower panels). Residues V46 (yellow), Y54 (magenta), V161 (red), and Y331 (green) are shown in spacefill representation; Structure of dansylalanine (C) .

FPN V46*amber*, Y54*amber*, V161*amber,* and Y331*amber* mutants were produced in order to exploit *amber* codon suppression in the yeast host *P. pastoris* to achieve the incorporation of DA into FPN. Mutations Y54F and Y331F were shown to have no impact on the iron transport ability of FPN (Bonaccorsi Di Patti et al., 2014), suggesting that amino acid changes in these positions are well-tolerated by the protein. *P. pastoris* strains expressing the tRNA/aaRS pair specific for DA and the FPN mutants under the control of methanol-inducible promoters were grown for 96 h in the presence of methanol with or without the unnatural amino acid. Western blot analysis evidenced the presence of full-length FPN (ca. 62 kDa), indicating that suppression of the *amber* stop codon is effective and appears to be quite specific since much lower

expression is found in cells grown in the absence of the unnatural amino acid (Fig. 10). Expression levels varied, with Y54*amber* and V161*amber* showing significantly higher expression compared to V46*amber* and Y331*amber*.

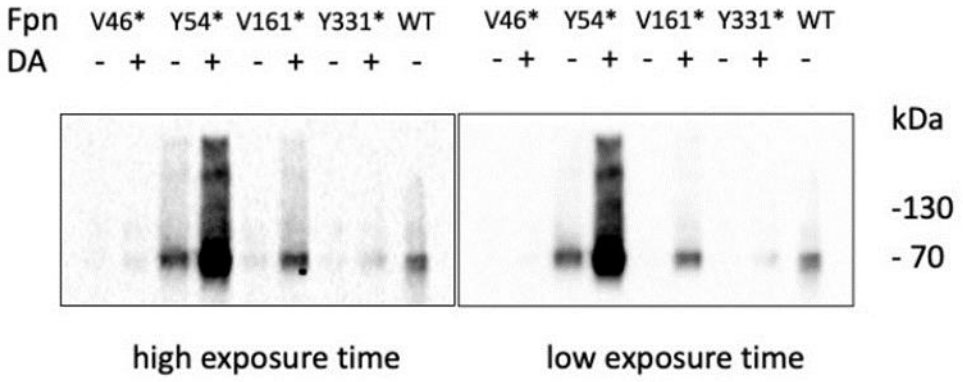

Figure 10. Expression of FPN *amber* mutants. Western blot analysis of FPN mutants ± DA.

Single-step purification of FPN from membrane extracts was performed by immunoaffinity anti-FLAG chromatography. The purity of the protein was assessed by SDS-PAGE and was similar for all mutants (data not shown). Yields of FPN DA mutants were ca. 0.2–0.3 mg per liter of culture, somewhat lower than those obtained for wild type FPN (ca. 0.5 mg per liter of culture). This result is in line with the consistently lower expression levels reported for other proteins incorporating genetically encoded unnatural amino acids compared to the wild type counterparts (Summerer et al., 2006; Young et al., 2009).

4.1.2 Fluorescence Spectroscopy of FPN DA

Fluorescence spectroscopy analysis of FPN was performed in order to evaluate the incorporation of the fluorescent probe. DA fluorophore is maximally excited at 340 nm and emits at about 550–570 nm in aqueous solution (Summerer et al., 2006). The emission peak is significantly blue-shifted when the dansyl group is in a hydrophobic milieu. The emission spectra of purified FPN V46DA, Y54DA, V161DA, and Y331DA show a significantly blue-shifted peak with different maxima depending on the local position of the fluorophore (Fig. 11). Human FPN wild type (non-dansylated) showed a weak emission close to 400 nm, possibly due to the 10 tryptophan residues present in the protein (Fig. 11, dashed line). This result confirms that the emission band in the 470–490 nm region can be attributed to the genetically incorporated non-canonical amino acid DA.

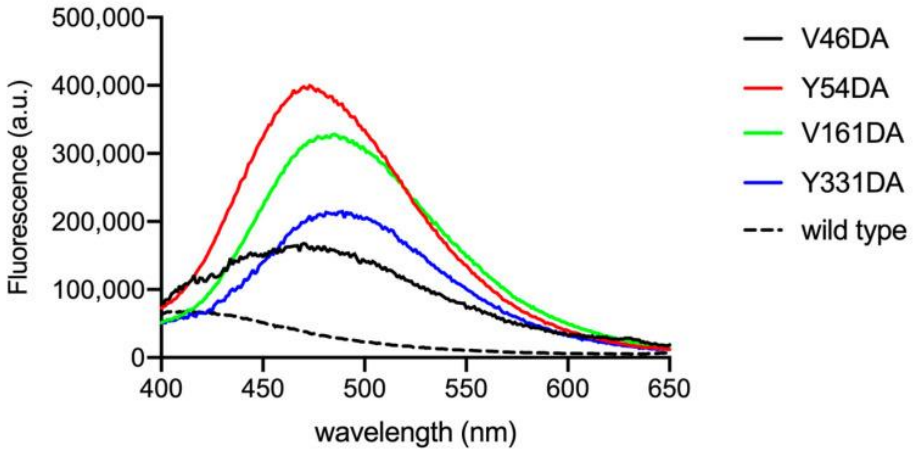

Figure 11. Fluorescence spectra of FPN V46DA, Y54DA, V161DA, and Y331DA. Emission spectra were recorded in MOPS 25 mM pH 7.0, NaCl 150 mM, DDM 0.01%. Excitation was at 340 nm; the spectra are normalized on protein content determined by BCA. The spectrum of non-dansylated FPN wild type is also shown.

Among the mutants, V46DA appears to be the variant with the most hydrophobic environment surrounding dansylalanine (λ_{max} 470 nm), followed by Y54DA (λ_{max} 473 nm), V161DA (λ_{max} 485 nm), and Y331DA (λ_{max} 489 nm) with a 19 nm shift between V46DA and Y331DA. Based on the spectral properties of the mutants and the position of dansylalanine in the protein structure, the interpretation of the resting state of FPN is not clear-cut. A conformation more closely resembling the outward-open state could be in line with the observed λ_{max} values which indicate that positions 161 and 331 (which are found on opposite sides of the membrane bilayer) are in the most polar environment. This assumption is supported by the analysis of two outward-open HsFPN structures (PDB 6W4S (Billesbølle et al., 2020) and 8C03

(Lehmann et al., 2023) which indicates that accessible surface area (ASA, calculated with PyMOL) is highest for Y331 (53–47 $Å^2$), followed by V161 (42–31 $Å^2$) and confirms that V46 is buried (ASA 10–9 $Å^2$). The calculated solvent-accessible area for Y54 yields two significantly different values (ASA 61 $Å^2$ for 6W4S or 27 $Å^2$ for 8C03) possibly due to slight changes in the position of TM2 and of the loop connecting TM3 and TM4 in the two structures, suggesting a certain degree of flexibility in this region. It should be pointed out that the two structures differ for the absence (6W4S) or presence (8C03) of the inhibitor vamifeport in the central cavity of FPN. The λ_{max} value for the Y54DA protein is consistent with a less polar environment compared to Y331DA and V161DA. Whether this is correlated to a more buried location of Y54 or to local higher hydrophobicity due to other factors, such as a lack of neighboring hydrogen bonding or charged residues, remains to be established.

4.1.3. Cobalt Titration of FPN DA

To evaluate whether dansylalanine can be useful to probe the conformational changes that FPN undergoes during metal translocation, all DA mutants (1 μM) were titrated with $CoCl_2$ (0–52 μM), which is more stable than Fe^{2+} and has been routinely employed as Fe substitute.

Fluorescence spectra (Fig. 12A) were collected immediately after metal addition, and fluorescence intensity values at λ_{max} for each mutant were then plotted as a function of the metal concentration (Fig. 12B). To better evaluate changes in the DA probe, spectra obtained for the wild type (non-dansylated) FPN (1 μM) at 340 nm excitation were subtracted from all spectra of the DA mutants.

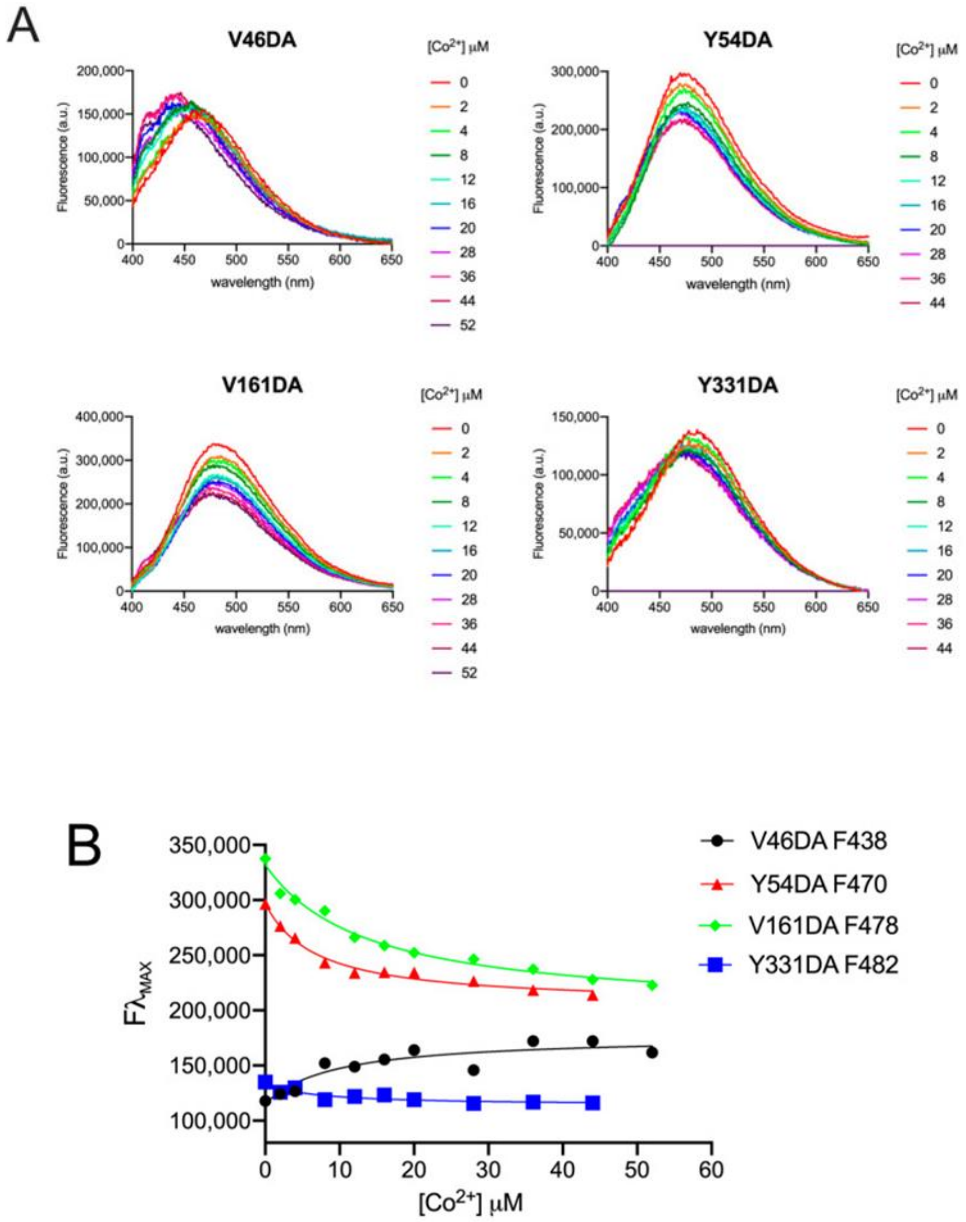

Figure 12. Fluorescence spectra of FPN V46DA, Y54DA, V161DA, and Y331DA titrated with cobalt. (A) Emission spectra of FPN 1 µM after addition of the indicated concentration of $CoCl_2$ were recorded in MOPS 25 mM pH 7.0, NaCl 150 mM, DDM 0.01%. Excitation was at 340 nm. The spectrum of FPN wild type was subtracted as baseline. (B) Fluorescence changes at λ_{max} for each FPN DA mutant. Data were fitted to a one-site binding model.

All mutants exhibited a similar affinity for Co^{2+} (K_D 6–14 μM). The K_D for FPN wild type was determined in the same conditions except that excitation was at 295 nm and the protein was 0.1 μM to avoid saturation of the fluorescence signal (data not shown). The K_D values are in line with K_M values in the low μM range reported for the transport activity of FPN reconstituted in liposomes and assayed with calcein (Li et al., 2020; Lehmann et al., 2023).

Following the addition of cobalt, Y54DA, V161DA exhibited a similar trend with a significant quenching of fluorescence and blue shifts of λ_{max}. Y331DA showed a comparable blue shift but reduced fluorescence quenching. V46DA, instead, exhibited an opposite behavior: increasing DA fluorescence during metal titration and blue shifting its λ_{max} by about 15 nm.

Size exclusion chromatography (SEC) on a PD10 desalting column was performed to remove $CoCl_2$ from samples in order to check the reversibility of the observed changes. Changes affecting λ_{max} appeared to be fully reversible, as demonstrated by the spectra measured after the removal of cobalt by SEC. Figure 13 shows the spectra for FPN Y54DA and V161DA; analogous results were obtained for V46DA and Y331DA.

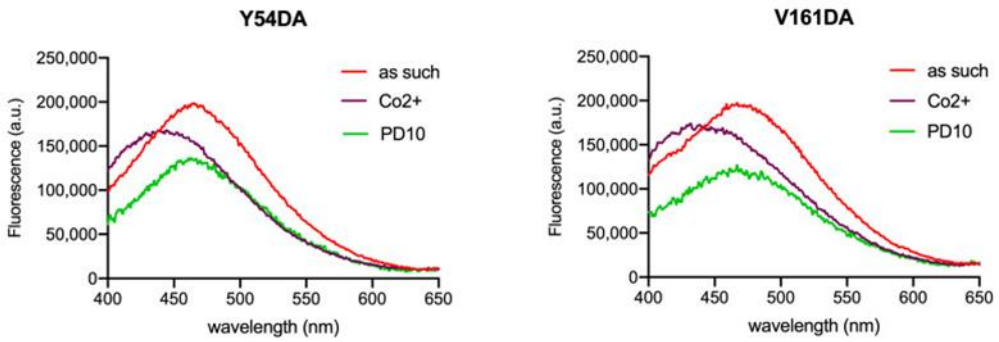

Figure 13. Fluorescence spectra of FPN Y54DA and V161DA after the removal of $CoCl_2$. Emission spectra of FPN 1 µM as such, after titration with cobalt (36/28 µM), and after gel-filtration (PD10) were recorded in MOPS 25 mM pH 7.0, NaCl 150 mM, DDM 0.01%. The PD10 spectrum is arbitrarily scaled to evidence the λ_{max} position. Excitation was at 340 nm.

In the 3D structure of FPN, two binding sites for cobalt have been identified: one formed by D39 and H43 and a second site that includes C326 and H507 (Billesbølle et al., 2020; Wilbon et al., 2023). V46 is close to the first cobalt binding site, and Y331 is relatively close to the second site, while Y54 and V161 are located in regions of the protein distant from the metal binding sites. Direct quenching of DA fluorescence by cobalt does not appear to be responsible for the observed changes, as titration of free DA with $CoCl_2$ induces no substantial spectral variation (Fig. 14). Thus, it can be assumed that conformational changes due to metal binding alter the polarity of the probe microenvironment, thus affecting emission λ_{max} and intensity. The λ_{max} blue shift indicates an increase in hydrophobicity. For V46DA, this also leads to an increase in fluorescence intensity, while for Y54DA, V161DA, and Y331DA a decrease is apparent. In the case of V46DA, it is tempting to speculate that cobalt binding may induce a local conformational change that diminishes quenching by neighboring W42. It is known that tryptophan is able to quench

fluorescence of (dimethylamino)naphthalene-based dyes (Pospíšil et al., 2014).

Inspection of the recently reported structure of FPN in occluded conformation (PDB 8C02, (Lehmann et al., 2023)) shows that the solvent accessible area is decreased mainly for Y331 (14 $Å^2$), followed by Y54 (38 $Å^2$), while V161 (41 $Å^2$) and V46 (9 $Å^2$) are only modestly affected. No experimentally determined 3D structure is available for human FPN in the inward-open conformation, so the local environment of specific sidechains can only be inferred from the model (Tortosa et al., 2017), which suggests that V161 and V46 increase their solvent accessibility, at variance with Y54 and Y331.

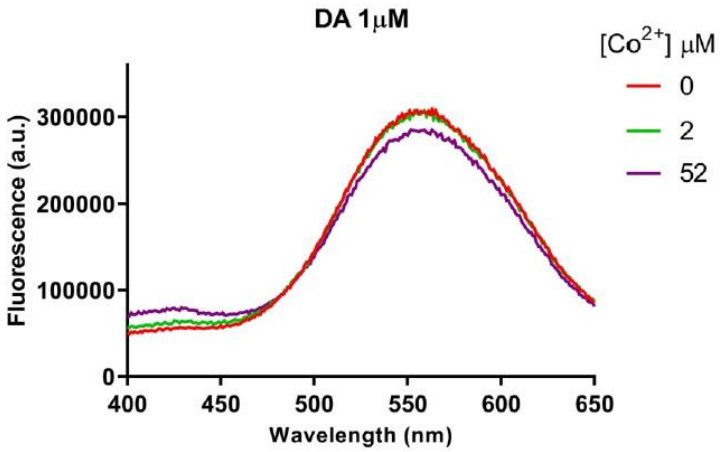

Figure 14. Fluorescence spectra of DA 1 μM titrated with cobalt. Emission spectra after the addition of the indicated concentration of CoCl2 were recorded in MOPS 25 mM pH 7.0, NaCl 150 mM, DDM 0.01%. Excitation was at 340 nm.

4.1.4 Discussion

Taken together, the observed spectral changes could be tentatively explained by a cobalt-induced transition from an outward-open to an occluded conformation, consistent with structure-based solvent accessibility information and the local rearrangement of hydrogen bonding networks/van der Waals interactions. A more compact occluded conformation would lead to decreased polarity in the microenvironment for all four positions of the DA probe. In conclusion, the genetic incorporation of DA in FPN has been achieved and the potential of this approach for the analysis of conformational transitions induced by the binding of cobalt has been investigated.

4.2 The Different Affinity of the Two Metal-Binding Sites of Human Ferroportin Drives Outward Directionality of Transport

The existence of two substrate-binding sites is a peculiarity of FPN compared to other MFS membrane transporters. To further investigate the metal-binding properties of FPN, the possibility that the two iron-binding sites have distinct affinities for the substrate has been explored. Also for these studies, cobalt was used as a substitute for ferrous iron due to its stability in the presence of oxygen. As a matter of fact, all the structures of mammalian FPN with bound metals have been obtained with cobalt and most in vitro transport assays have

been carried out with this metal (Billesbølle et al., 2020; Lehmann et al., 2023; Pan et al., 2020; Shen et al., 2023; Wilbon et al., 2023).

For these studies intrinsic tryptophan fluorescence spectroscopy has been used to assess the affinity for cobalt of human FPN wild type and a set of mutants (Fig. 15). The S1 site mutant D39A is unable to transport iron and it was shown to have impaired iron-binding capacity (Bonaccorsi Di Patti et al., 2014). On the other hand, substitution C326S at site S2 causes resistance to hepcidin without impairing the iron export capacity of FPN (Fernandes et al., 2009; Aschemeyer et al., 2018). Mutation D181V has been identified in hemochromatosis patients and it has been classified as loss of function since the protein is unable to transport iron and it has reduced iron-binding ability (Bonaccorsi Di Patti et al., 2014; Praschberger et al., 2014; Vlasveld et al., 2019). Other pathogenic loss of function mutants examined in this work include G80S, D157G and N174I which are part of a network of interactions thought to stabilize the outward-open conformation of FPN acting as an intracellular gate (Vlasveld et al., 2019; Guellec et al., 2019; Tortosa et al., 2017). This conformation has been proposed to represent the resting state of FPN in solution (Jormakka, 2023; Billesbølle et al., 2020). Therefore, it is possible that disruption of the intracellular gate could cause the protein to adopt a prevalent inward-open or occluded conformation, allowing access to these forms of FPN. Lastly, mutant D325A targets an aspartate residue preceding the coordinating C326 at site S2, and it has been shown to be involved in iron binding through a water-mediated contact (Billesbølle et al., 2020). Notably, the D325A mutant displays substantially decreased iron export capacity (Bonaccorsi Di Patti et al., 2014; Deshpande et al., 2018).

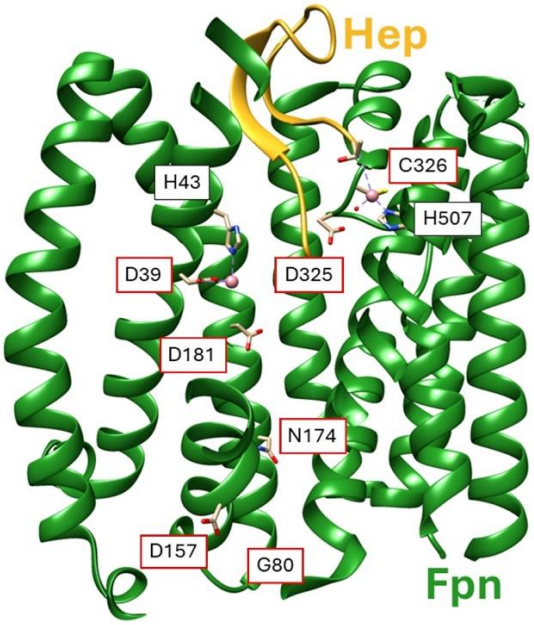

Figure 15. Metal binding sites of Fpn. Cross section of the three-dimensional structure of human ferroportin (Fpn; green ribbon) in complex with hepcidin (Hepcidin; gold ribbon) and cobalt (pink sphere) showing the internal vestibule of the protein in the outward open conformation (PDB: 6WBV). The residues coordinating the cobalt ion and those mutated (shown in red) and/or discussed in this study are shown in stick representation. The image was generated with Chimera.

4.2.1 Results

Representative fluorescence spectra of wild type FPN titrated with cobalt 2-3000 μM are shown in Figure 16 (upper panel). The $(F_0\text{-}F)/F_0$ *vs* $[CoCl_2]$ curve was fit to a two-site binding model; the fit to a one-site model was very poor (Figure 16, bottom panel) indicating that the two-site model was indeed a better model. Wild type FPN exhibits a high-affinity metal-binding site with K_{D1}

close to 5 μM and a low affinity site with K_{D2} about 300 μM (Table 1), which contribute about 50% each to the binding signal.

The $(F_0\text{-}F)/F_0$ *vs* $[CoCl_2]$ curves of the mutants are displayed in Figure 17 with the corresponding fit to the two-site model. All K_D values are presented in Figure 18 and Table 1. For all the Fpn mutants the K_{D1} values show no statistically significant change; D39A, D325A and the double mutant D39A-D181V present larger variation compared to wild type and other mutants. The K_D values clearly evidence that the low affinity site is compromised in Fpn D39A, D181V and the double mutant D39A-D181V, with a statistically significant, almost 3-fold increase of K_{D2}. The K_{D2} of Fpn D325A is increased over two-fold, while K_D values of Fpn G80S, D157G, N174I and C326S are not significantly affected. The triple mutant G80S-D157G-N174I presents an increase in K_{D1}, although not significant compared to wild type, and K_{D2} similar to D157G.

The effect of hepcidin has been evaluated by cobalt titration of FPN in the presence of the peptide (Fig. 17C). The results obtained show that hepcidin causes a marked increase of both K_{D1} and K_{D2}, drastically reducing the ability of wild type Fpn to bind the metal (Table 1). When the peptide is added to the protein saturated with cobalt, the fluorescence signal is essentially unchanged, suggesting that hepcidin does not displace cobalt (Fig. 17C). Preincubation with hepcidin has no significant impact on both K_D values for cobalt of the FPN C326S mutant (Fig. 18 and Table 1).

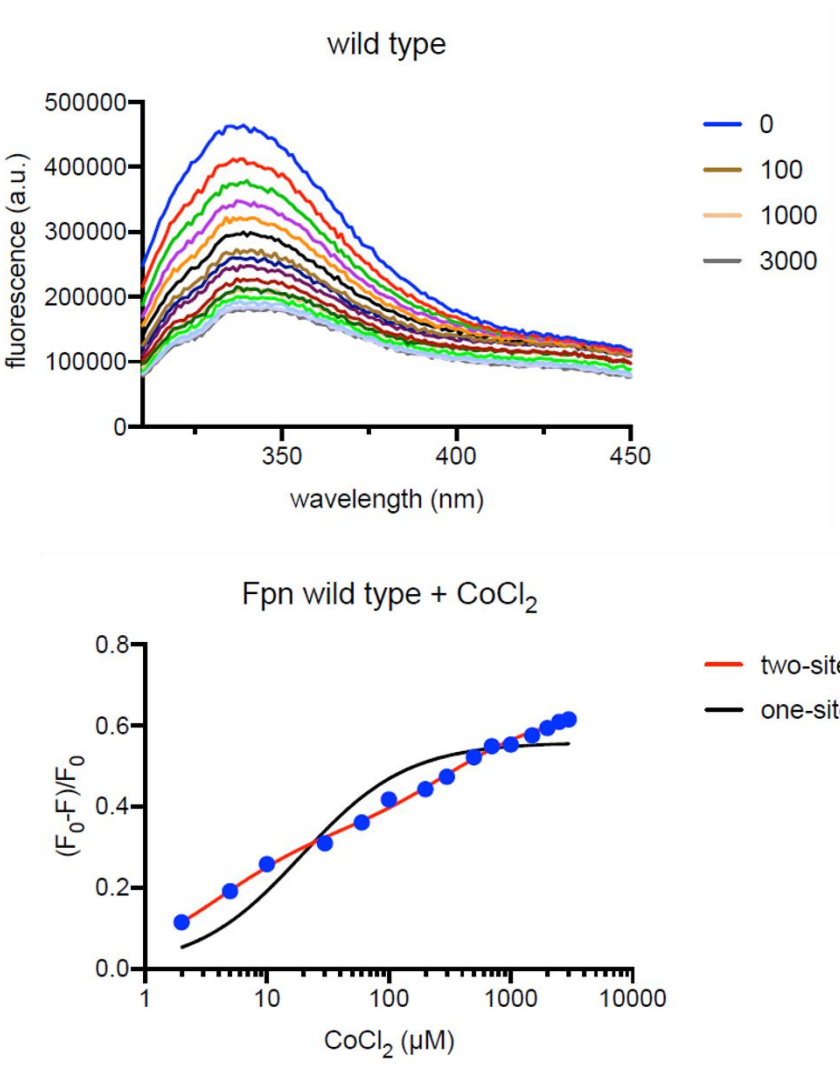

Figure 16. Cobalt titration of FPN. Wild type Fpn (500 nM) in MOPS 25 mM, NaCl 150 mM, DDM 0.01% pH 7.0 was titrated with cobalt chloride (2-3000 µM) and emission spectra were recorded with excitation at 295 nm. Plot $(F_0\text{-}F)/F_0$ vs $[CoCl_2]$ of wild type FPN fit to a one-site ($R^2 = 0.92$) or two-site ($R^2 = 0.99$) binding equation.

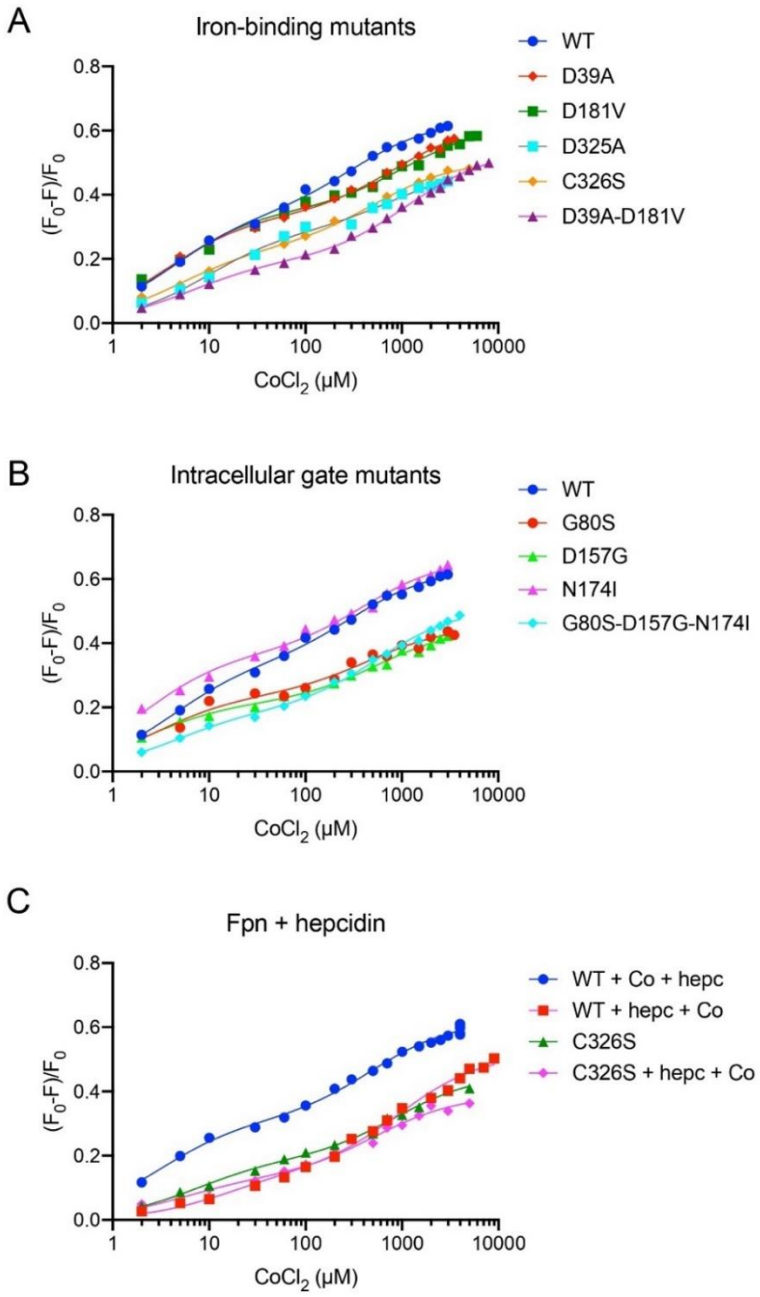

Figure 17. Binding of cobalt to FPN and effect of hepcidin**.** Plot $(F_0\text{-}F)/F_0$ vs $[CoCl_2]$ of wild type and mutant Fpn (panels A, B). Panel C: plot $(F_0\text{-}F)/F_0$ vs $[CoCl_2]$ of FPN (500 nM) with

hepcidin (900 nM) added either before or at the end of metal titration. The data were fit to a two-site binding equation.

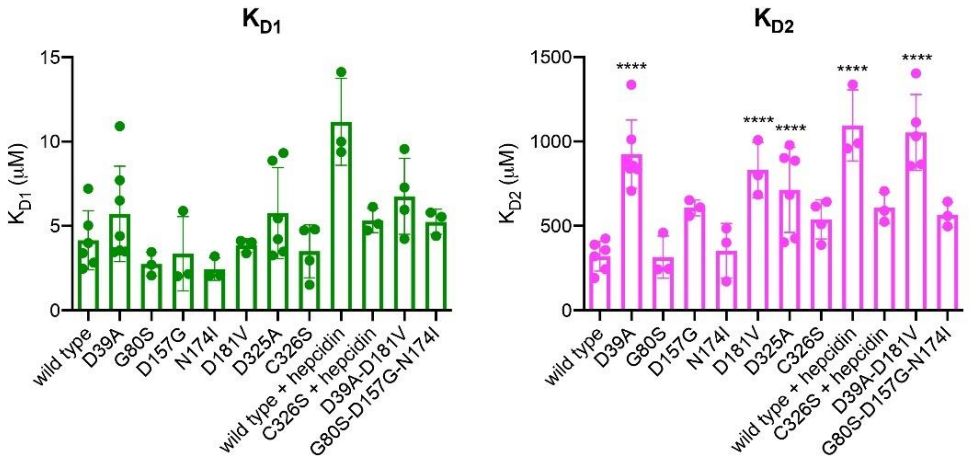

Figure 18. K_D values of FPN for cobalt. Scatter plot with individual K_D values obtained for biological replicates. Error bars indicate the SD of the mean. P values were calculated by two-way ANOVA with Dunnett's post hoc test; **** $p < 0.0001$ *vs* wild type.

FPN	**K_{D1} (μM)**	(SEM)	**K_{D2} (μM)**	(SEM)
Wild type	4.16	0.71	320	36.20
D39A	5.72	1.07	924	76.38
G80S	2.74	0.40	315	72.12
D157G	3.36	1.27	607	26.97
N174I	2.44	0.38	352	93.96
D181V	3.84	0.23	831	94.78
D325A	5.77	1.10	713	102.73
C326S	3.50	0.79	538	58.13
D39A-D181V	6.76	1.12	1053	100.42
G80S-D157G-N174I	5.25	0.43	567	42.35
Wild type + hepcidin	11.17	1.49	1095	121.38
C326S + hepcidin	5.33	0.42	607	53.08

Table 1. K_D values of human FPN for cobalt.

4.2.2 Discussion

Titration with much higher concentrations of the metal uncovered the existence of a second, low-affinity binding site for cobalt in FPN. This wasn't detected in the previous analyses presented in Section 4.1, as the cobalt concentrations employed were in the low micromolar range. Indeed, repeating the titration of Y54Da under the same conditions used in this section yielded two K_D values consistent with those of non-dansylated FPN WT (data not shown). The finding that two different K_D values are observed for the metal-binding sites of FPN is novel and it allows to reconcile contrasting data reported in the literature. As a matter of fact, if assays are carried out with a metal concentration of 100 μM or lower, essentially only the high-affinity site will contribute. In fact, the high affinity K_{D1} is fully in line with the value obtained for dansylated FPN, that was determined by titration with cobalt 2-50 μM (Amadei et al., 2023; Section 4.1), and with the affinity estimation obtained in a *Xenopus* oocyte expression system (Mitchell et al., 2014). ITC analyses reported by different groups observed a single K_D of the same order of magnitude of the low affinity K_{D2} (Shen et al., 2023; Pan et al., 2020; Deshpande et al., 2018)

The large increase in K_{D2} obtained with FPN D39A (S1 mutant) and D181V suggests that S1 is the low affinity site. The report that the D39A mutant was found to be similar to wild type FPN in a liposome-based transport assay performed with Fe^{2+} 10 μM (Li et al., 2020) supports our suggestion that S1 is the low-affinity site because at this low concentration of metal only the behavior of the high-affinity site can be observed. The naturally occurring mutation D181V causes 'ferroportin disease' due to failure of FPN to efficiently export iron, and decreased iron-binding capacity (Fernandes et al.,

2009; Bonaccorsi Di Patti et al., 2014). Residue D181 is located on TM5 closer to the cytosolic side and about 8.5 Å away from D39 in the outward-open structure of Fpn (PDB: 6W4S), but its side chain moves nearer to D39 in the occluded form (PDB: 8C03). This suggests that D181 may take part in the intracellular entrance path of iron to site S1. The double mutant D39A-D181V is similar to D39A, suggesting that this aspartate residue plays a more prominent role in iron binding.

Somewhat unexpectedly, the S2 site mutant C326S appears to maintain full metal binding capacity. However, this result is consistent with the observation that the C326S mutant exports iron as efficiently as the wild type protein (Praschberger et al., 2014; Aschemeyer et al., 2018). A possible explanation is that coordination of the metal at the S2 site is more complex, with other residues (D325 and T320) participating and compensating for the absence of C326, as suggested by the structure of the complex of FPN with cobalt and hepcidin (Billesbølle et al., 2020). The definite importance of C326 for hepcidin binding is confirmed by the lack of effect on K_D by preincubation of the C326S mutant with the peptide, at variance with the result obtained with wild type FPN.

Further support for the hypothesis that S2 is the high affinity site comes from MD simulations that indicated that ferrous iron, initially positioned randomly in bulk solvent, bound spontaneously to the S2 site, only occasionally contacting D39 of S1 (Billesbølle et al., 2020).

Pathogenic substitutions G80S, D157G and N174I are all hypothesized to alter the TM5-TM10 intracellular gate that stabilizes the outward-open conformation of Fpn (Guellec et al., 2019; Tortosa et al., 2017), presumably impairing the inward-open to outward-open transition, and leading to

decreased ability to translocate iron. However, the G80S, D157G and N174I mutants retain iron-binding capacity similar to the wild type protein. Intriguingly, in all cases K_{D1} appears to decrease slightly, although not significantly, suggesting that these mutants may share a similar conformation. The triple mutant G80S-D157G-N174I shows a K_{D1} comparable to wild type Fpn and a K_{D2} value similar to the D157G mutant, possibly pointing to a more critical role for this latter residue in maintaining the integrity of the intracellular gate.

Fpn D325A exhibits K_D values similar to the S1 site mutant D39A, with somewhat lower K_{D2}. In the presence of hepcidin, residue D325 contributes to binding of iron at S2 through a water-mediated contact, while in the absence of metal the side-chain of D325 is much more mobile (Billesbølle et al., 2020). Interestingly, modeling of the inward-open conformation of human FPN predicts that D325 participates also in binding of the metal at the S1 site (Tortosa et al., 2017; Bonaccorsi Di Patti et al., 2014), suggesting that this aspartate residue may act as a bridge between the two metal-binding sites.

Since the two aspartate residues are embedded deeply in the central cavity of FPN, the higher variability in both K_{D1} and K_{D2} values observed for the D39A and D325A mutants (and the D39A-D181V double mutant) could be due to local instabilities that create a conformationally heterogeneous protein with subtle changes in metal affinity.

FPN partners with a ferroxidase that safely oxidizes ferrous iron to generate the ferric ion that is bound by transferrin for distribution to all tissues. Depending on the cell type, the ferroxidase activity is provided by ceruloplasmin or hephaestin, enzymes belonging to the multicopper oxidase family (Helman et al., 2023). Based on our data, we propose a working model

of the process of iron export by FPN driven by the different affinity of the two metal binding sites: S1 would capture iron when intracellular levels are high and translocate it to site S2 driving outward directionality of transport. In support of this model, the tarsier FPN S2 mutant C326A-H508A had a significantly slower rate of metal transport in a liposome-based assay, while the S1 mutant D39A-H43A showed only a modest decrease (Pan et al., 2020). Once bound to S2 the metal would be held strongly enough to require a ferroxidase for release, avoiding escape of potentially toxic ferrous iron. The ferroxidases ceruloplasmin and hephaestin exhibit two K_m values for ferrous iron, which differ by approximately two orders of magnitude (ceruloplasmin: K_{m1} 0.6 μM and K_{m2} 50 μM, (Osaki, 1966); hephaestin: K_{m1} 3.5 μM and K_{m2} 107 μM (Vashchenko et al., 2012)), with the low K_{m1} consistent with the proposed transfer of the metal from S2 of Fpn. Therefore, the ferroxidase would create an iron gradient from FPN to the final recipient, transferrin, coupling oxidation and dissociation, and providing a further driver of outward flow of iron. In line with this prediction, inclusion of ceruloplasmin and apo-transferrin in the efflux medium of *Xenopus* oocytes expressing FPN increased the efflux rate constant for iron (Mitchell et al., 2014).

The higher affinity of S2 would also hold iron in place facilitating hepcidin binding to FPN. This would provide a molecular explanation as to why if a ferroxidase activity is lacking, such as in aceruloplasminemia, iron is trapped on Fpn and the transporter is bound by hepcidin, internalized and degraded (De Domenico et al., 2007). We show here that hepcidin binding to cobalt-free Fpn remarkably increases K_D values for both metal-binding sites. Thus, when hepcidin levels are high, the peptide can bind also in the absence of iron and it drastically reduces the capacity of Fpn to capture the metal. It would be

interesting to test if the synthetic inhibitor vamifeport, which binds to the central cavity of Fpn overlapping with hepcidin (E Lehmann et al., 2023), produces analogous effects on K_D values.

The low affinity of the S1 site poses a question concerning the efficiency of FPN-mediated export of iron in a physiologic cellular context, where very low levels of free iron are found in the cytosol. The iron chaperone PCBP2 has been demonstrated to act as the intracellular donor of iron to Fpn (Yanatori et al., 2016). No quantitative estimates of the iron-dependent interaction of PCBP2 with Fpn are available, and it is currently unknown if the interaction with the chaperone may modulate/increase the affinity of S1 for ferrous iron. We predict that this might be the case because in the absence of PCBP2 FPN-mediated efflux of iron was suppressed in cells (Yanatori et al., 2016). Moreover, it was shown that Fe-PCBP1 and Fe-PCBP2 bound to ferritin with over ten-fold higher affinity than ferrous iron alone (Leidgens et al., 2013). Therefore, iron-loaded PCBP2 would likely increase the low affinity of S1 that would otherwise make FPN inefficient in the free-iron-poor cytosol. When intracellular iron levels are inappropriately high, efflux through FPN may take place also independent of PCBP2. Anyhow, even in the presence of PCBP2, S1 is still expected to display a much lower affinity than S2 thus making the proposed mechanism still feasible.

Attempts to directly measure K_D for iron proved to be unfeasible: it was possible to titrate FPN with $Fe(NH_4)_2(SO_4)_2$ only up to 100 μM due to the large inner filter effect of ascorbate, that was required to keep iron in the reduced state and avoid precipitation of ferric iron during titration (data not shown). In these conditions, only K_{D1} could be estimated with a value close to 4 μM, similar to the K_{D1} for cobalt, further validating the use of cobalt as a substitute

for iron. This means that, even for the high affinity site, K_{D1} for iron is still in the μM range, consistent with the moderately weak binding required for rapid transport of substrates across the membrane. Furthermore, it is possible that our (and others') metal-binding studies reflect the properties of the outward-open conformation of Fpn, as this is likely the resting state of the protein in solution (Jormakka, 2023; Tortosa et al., 2017). In the inward facing form, which is responsible for binding intracellular iron, the status of the metal binding sites may differ. It is tempting to assign the K_D values obtained for the conformationally-restricted G80S, D157G and N174I mutants and the triple mutant to the protein in the inward-open conformation. However, until an experimental three-dimensional structure of human FPN in the inward-open state becomes available, this proposal should be viewed with caution and the hypothesis that the inward-open conformation may possess higher affinity for iron and possibly additional amino acid residues might be involved in metal coordination should not be disregarded.

FPN is the central component of a multiprotein pipeline that includes an intracellular donor (PCBP2), an extracellular or membrane-bound ferroxidase (CP or HEPH) and an iron transporter (transferrin) that collaborate to safely escort iron out of the cell. Aspects of how the different partners may physically interact are beginning to be unveiled (Leidgens et al., 2013; Tortosa et al., 2017), but disclosure of molecular details awaits further studies to reveal the full picture of the journey of iron from inside the cell to the extracellular milieu.

4.3 Production and Characterization of CP mutants

Despite being known for decades, the ferroxidase ceruloplasmin (CP) remains a challenging target for recombinant expression and purification. This has limited the ability to further characterize the protein, hindering biochemical investigations of key residues whose mutations are associated with pathological conditions (such as aceruloplasminemia). Moreover, it has restricted the exploration of the roles of specific residues through structure-based mutagenesis approaches. To date, only our laboratory has successfully reported the purification of high-quality recombinant CP produced in *Pichia pastoris* (Bonaccorsi di Patti et al., 2021). Building on this protocol, this section presents, for the first time, the purification and functional characterization of CP mutants. Two of these mutants are associated with pathological conditions, while the other two were specifically designed based on the protein structure to investigate a potential iron entry pathway.

4.3.1 Characterization of CP mutants N244S and G876A

The CP mutant N244S has been associated with pathological conditions in a pediatric patient (S. Galosi, personal communication). Mutation G876A has been described in various patients (Cuenca et al., 2020)). Thanks to the ability to successfully express and purify recombinant CP, these two mutants and CP wt were produced in *Pichia pastoris*. Despite a relatively low yield of 0.1 mg per 1 L of culture, this allowed us to perform assays aimed at characterizing the functionality of the two pathological variants. Although the residues N244 and G876 are located relatively far from the catalytic centers of the protein,

their involvement in pathological states may suggest a reduced oxidase activity toward Fe^{2+} or an altered ability to oxidize aromatic amines (such as hormones and neurotransmitters).

Ferroxidase activity was monitored using $Fe(NH_4)_2(SO_4)_2$ as a substrate, while oxidase activity toward aromatic amines was assessed using the non-natural aromatic amine substrate ortho-dianisidine (oDA), which is routinely used in laboratories as a non-physiological substrate for CP.

CP wild type and mutants were tested, together with human plasma-purified CP (CP reference, CP ref) used as a control.

After adding 200 µM $Fe(NH_4)_2(SO_4)_2$ to 250 nM CP, ferroxidase activity was measured by monitoring the increase in absorbance at 315 nm over time. The linear phase of the absorbance curve was analyzed, and the activity was expressed as a percentage relative to wild-type CP. Oxidase activity toward oDA was evaluated using a discontinuous assay, where the substrate (0.1 mg/mL) was incubated with 250 nM CP for 1 hour at 37°C. The reaction was then stopped with H_2SO_4, and the oxidized substrate was quantified by measuring absorbance at 540 nm, results were expressed as a percentage relative to wild-type CP.

As shown in Figure 19, CP wt expressed in *Pichia pastoris* fully retained activity compared to CP ref, confirming that this expression system is suitable for the functional characterization of CP mutants. CP N244S and CP G876A fully retained both ferroxidase activity while displaying a slightly reduced oDA oxidase activity. However, considering the limited number of replicates performed (one for N244S and two for G876A) and the variability typically encountered with this assay, it is likely that the differences detected are not

significant, indicating that both mutations do not affect the catalytic properties of CP.

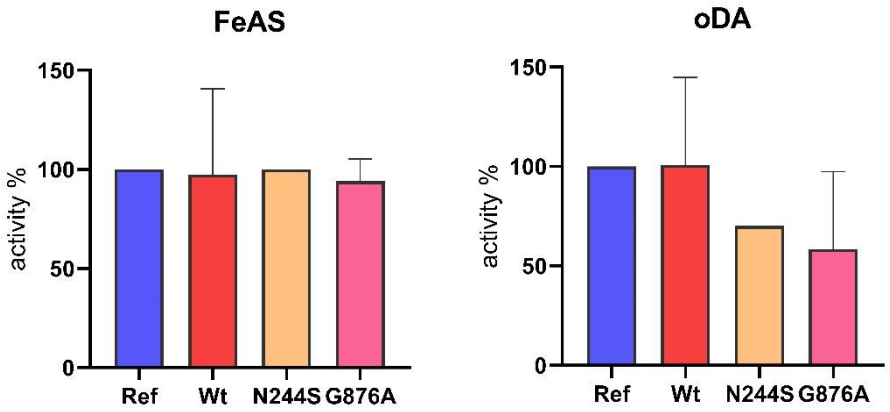

Figure 19. Oxidase activity of CP Wt, N244S and G876A towards Fe^{2+} and oDA reported as a percentage relative to CP Ref, which corresponds to 100% for each independent measurement. Data represent the mean ± SEM, with n=5 for Wt, n=1 for N224S, and n=2 for G876A.

4.3.2 Characterization of CP residues potentially involved in iron channelling

As mentioned, an interaction between FPN and CP is believed to occur. This would not only generate a gradient facilitating rapid removal of iron from FPN, thereby preventing hepcidin binding but would also provide a secure pathway for Fe^{2+} to be oxidized by CP without being released into the extracellular environment. Once oxidized by CP, Fe^{3+} could then be bound by transferrin for safe transport. Upon inspecting the CP structure and considering its predicted

orientation relative to the plasma membrane and to FPN (also supported by the AlphaFold-generated model of the FPN-CP complex, presented below), two clusters of residues drew our attention due to their spatial arrangement. At the bottom of the protein (on the side that should represent the interface with FPN), four residues (Y290, Y992, E651, and E851) are arranged in an almost planar configuration. Tyrosine and glutamate are commonly involved in metal coordination, particularly iron, and these residues are situated at the entrance of a pseudo-channel that extends from the base of the protein toward its core. These observations suggest that these four residues might constitute the iron entry site, receiving Fe^{2+} released from the S2 site of FPN. Directly above this site, approximately 20 Å away, lies another group of residues, three Phe (F298, F659, F1000), arranged in a planar formation, potentially acting as a gate that controls the access of iron to the catalytic sites, which are positioned just above. Based on this hypothesis, these two clusters may mediate the entering and gating mechanisms that regulate iron flow from FPN to the catalytic centers of CP.

To investigate the functional roles of these residues, two CP mutants were designed. The first was a quadruple mutant (Y290F, Y992F, E651A, E851A), aimed at abolishing any coordinating properties of the putative iron entry site, hereafter referred to as 4EY. The second was a triple mutant (termed Triple), where the three Phe were replaced by Ile (F298I, F659I, F1000I), maintaining hydrophobicity while eliminating aromatic interactions. As previously described, CP has several substrates, and its functionality is typically assessed by measuring its ability to oxidize Fe^{2+} and the non-natural aromatic amine substrate ortho-dianisidine (oDA). According to our hypothesis, both the 4EY

and Triple mutants should exhibit impaired Fe^{2+} oxidation, while maintaining unaltered catalytic activity toward oDA.

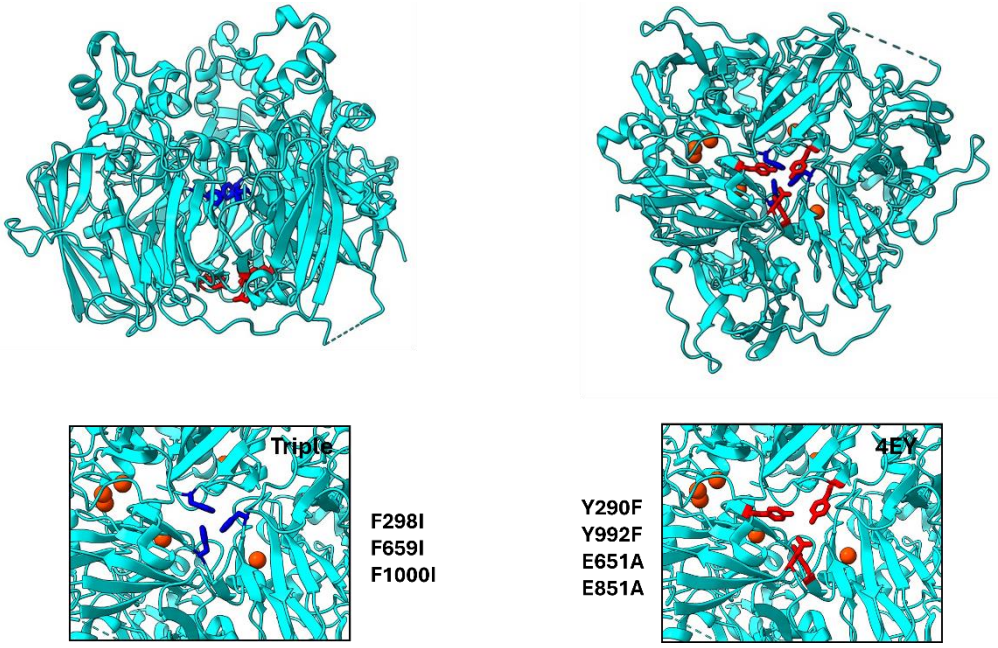

Figure 20. Structure of CP highlighting the mutated residues in the Triple mutant (blue) and 4EY mutant (red). Top left: side view. Top right: bottom view. Bottom panels: close-up details of the mutated residues. Images were generated with ChimeraX.

To test this hypothesis, the two mutants and wild-type CP were expressed recombinantly in *Pichia pastoris*, following a protocol developed in our lab. CP WT, 4EY, and Triple were then assayed for their oxidase activity towards Fe^{2+} and oDA, alongside human plasma-purified CP (CP reference, CP ref) used as a control. Assays were performed as described above in section 4.3.1. As shown in Figure 21, the 4EY mutant displayed unaltered oxidase activity towards oDA, as well as preserved ferroxidase activity, indicating that the Y290, Y992, E651, and E851 residues do not play a significant role in

promoting iron entry into the catalytic core of CP under these conditions. In contrast, the Triple mutant showed a significant reduction (~70%) in ferroxidase activity, with a similarly reduced oxidase activity towards oDA. These results suggest that the F298, F659, and F1000 residues are not primarily involved in the iron entry pathway but instead play a crucial role in catalysis for both substrates.

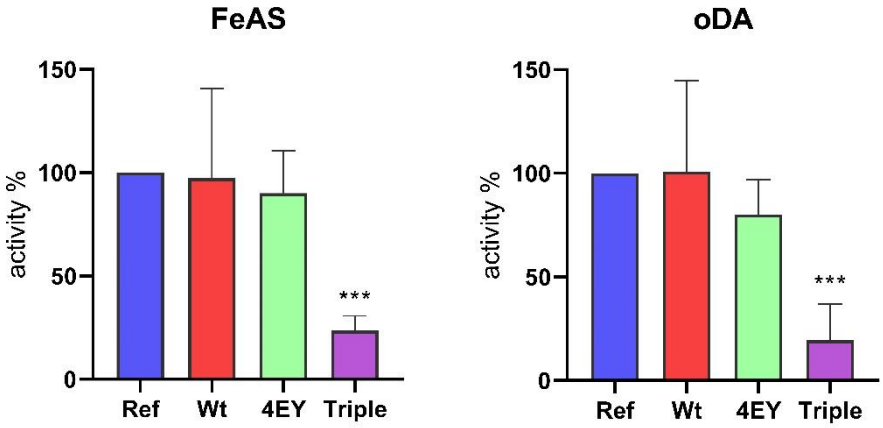

Figure 21. Oxidase activity of CP Wt, 4EY and Triple towards Fe^{2+} and oDA reported as a percentage relative to CP Ref, which corresponds to 100% for each independent measurement. Data represent the mean ± SEM, with n=5 for WT, n=3 for 4EY, and n=4 for Triple. P-values were calculated by one-way ANOVA mixed model;*** p <0.0001.

Given the severe impact of the introduced mutations in the Triple mutant on both CP activities and their potential to disrupt the aromatic interactions of three Phe residues at the core of CP, it was important to determine whether these mutations affect protein folding and copper content. Due to the low yield,

obtaining enough sample to measure copper content using the bi-quinoline assay was not feasible. Nevertheless, protein folding was assessed by circular dichroism (CD) and compared to the wt. The CD spectra (Fig. 22, left panel), indicating a predominantly β-sheet structure, were fully superimposable, confirming the correct folding of the Triple mutant. Additionally, the visible absorption spectrum showed a peak around 600 nm, typical of T1 copper centers, for both proteins (Fig. 22, right panel), with the A_{600}/A_{280} ratio at 0.03 for both. This suggests that the mutations did not affect the folding or copper loading, and the affected residues are crucial for CP function. The higher absorbance below 500 nm for the Triple mutant may be due to differences in copper content. However, the limited amount of protein prevented determination of copper stoichiometry.

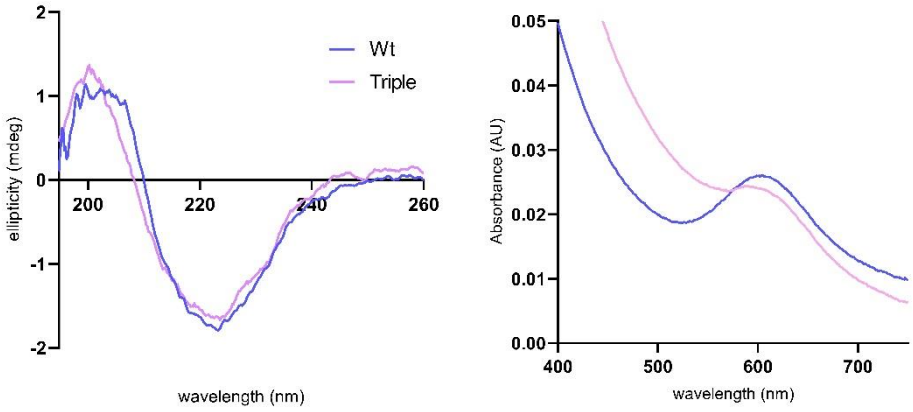

Figure 22. CD (left panel) and Absorbance (right panel) spectra of CP wt and Triple.

4.3.3 Discussion

For the first time, thanks to recombinant expression in *Pichia pastoris*, CP mutants were successfully purified and functionally characterized. This represents a significant advancement in CP biology, enabling the analysis of pathological mutants without relying on blood samples from patients (in those cases where some CP is detected). Additionally, this now allows for structure-based mutagenesis, which can be used to investigate the role of specific residues not only in a cellular context but also through a thorough biochemical analysis. Specifically, the analyzed mutations, N244S and G876A, despite being associated with pathological conditions, do not appear to significantly impact the catalytic activity of the protein. This observation aligns with the fact that the N244 and G876 residues are not located near CP's catalytic centers.

This result is interesting in the context of aceruloplasminemia, where CP mutations are often associated with a loss of ferroxidase activity and/or reduced enzyme secretion. The retention of activity in these two mutants suggests that these residues may not be directly involved in enzymatic function, but rather could play a role, for example, in interactions with other molecules.

We also employed mutagenesis to explore the functional roles of residues proposed to be involved in iron channeling in CP, this study gave us unexpected results. The quadruple mutant (4EY), which targeted key residues hypothesized to mediate iron entry into CP, exhibited unaltered ferroxidase activity, suggesting that these residues do not play a significant role in the iron entry under these conditions. It is important to consider that the experimental conditions employed to characterize these mutations differ significantly from

the physiological context. *In vivo*, CP would receive iron exiting the cell with specific directionality, pulling it from the S2 site of FPN as proposed in section 4.2. However, in an *in vitro* setup, the protein is surrounded by iron in the solution, which would not require a preferential pathway to reach the catalytic sites, as they are fully accessible in this condition. Further studies using a system that mimics iron export from the cell (e.g., in *Xenopus* oocytes) will be necessary to clarify the potential role of the investigated residues in iron channeling.

In contrast, the triple mutant (Triple), targeting three Phe residues thought to function as an iron gate, showed a substantial reduction in both ferroxidase activity and oDA oxidation. Triple retained a folded structure and similar copper content compared to the recombinant WT. This indicates that these residues are critical for broader catalytic functions rather than specifically regulating iron entry. Interestingly the three mutated Phe (F298, F659, F1000) in CP are completely conserved in HEPH where they correspond to positions 326, 678, and 1025, further evidence indicating the importance of these residues in human ferroxidases functionality.

4.4 Hephaestin expression and purification

Similarly to CP, obtaining pure recombinant HEPH is quite challenging. Only a few studies have described the purification of recombinant soluble HEPH, achieved by deleting its C-terminal transmembrane domain (Vashchenko et al., 2012). However, no studies have yet reported the successful purification of full-length HEPH. The complexity of purifying HEPH is largely due to its structural difference from CP. Unlike CP, HEPH contains a C-terminal transmembrane helix, which anchors it to the plasma membrane of enterocytes. This membrane association makes full-length HEPH more challenging to purify and study, as the presence of the transmembrane domain complicates both its expression and its extraction and purification. This has limited detailed functional and structural studies on both the HEPH protein itself and its interaction with FPN.

4.3.1 Hephaestin production and purification screening in different expression systems

As for CP, eukaryotic expression is required for proper HEPH biosynthesis and copper loading. Given the high similarity of CP and HEPH ectodomain, the first attempts to express and purify HEPH employed a strategy similar to that of its homolog CP (Bonaccorsi di Patti et al., 2021). HEPH cDNA has been cloned in different vectors for expression in *Pichia pastoris* SuperMan5, and various expression and purification tests were made.

Several attempts to purify full-length HEPH didn't bring successful results. Different plasmids for constitutive (pIB2) or inducible (pIB4) expression,

changing signal peptide to promote secretion to the right compartment, addition of purification tag, and the employment of a range of detergents and conditions only bring small improvements. Even in the best extraction and purification condition (employing 0.5% OG as solubilization agent), protein yield was found to be low, with only a small fraction bound to FLAG resin, as appreciable by the relative band intensity between input, flow-through, and elution lanes (Fig. 23, OG 0.5%). The aromatic amine ortho-dianisidine (oDA), a well-known non-physiological substrate of CP and HEPH, has been employed to screen HEPH fractions during purification. oDA screening assay revealed that the elution HEPH fraction wasn't active, while input and flowthrough fractions displayed some activity.

All these unsuccessful attempts led us to change the expression system for HEPH production. Therefore, an expression screening has been performed in human (Expi 293F) and insect (*Spodoptera frugiperda*, Sf9) cells, entering the Membrane Protein Lab (Research Complex Harwell, UK) well-established workflow for membrane protein expression and purification. First, HEPH full-length cDNA has been cloned by ligation-independent cloning, in different vectors from pOPINE plasmid family (pOPINEneo-3C-TGP-His; pOPINEneo-TEV-TGP-His; pOPINEneo-TGP-2Strep-His; pOPINEneo-link3C-TGP-His) for the expression in Expi293 and two pFastBac plasmids (pFB-CT-His-FLAG and pFB-CT-His-2Strep) for Sf9 cells. The different vectors harbouring the HEPH coding sequence were employed to transfect 2 ml of Expi293 or Sf9 cells, and protein expression was boosted with the supplementation of cell media with CuSO4 50 μM to promote copper incorporation during HEPH biosynthesis.

A

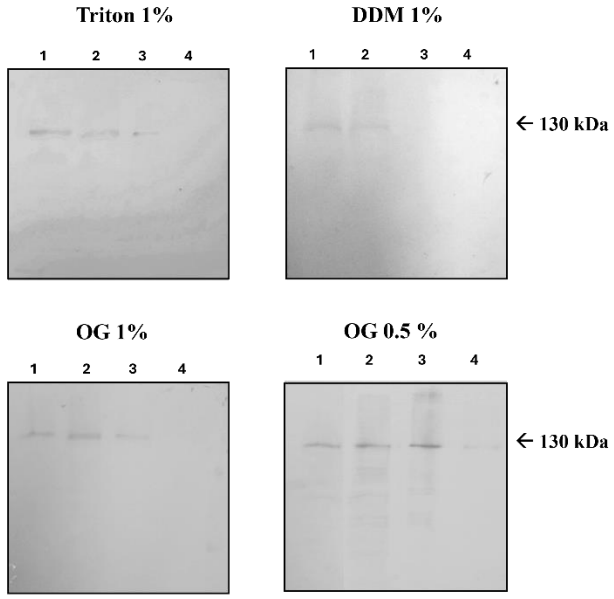

B

fraction	oDA assay
1	positive
2	positive
3	negative
4	N.D.

Figure 23. Analysis of HEPH fractions from purification tests, producing the protein in *P. pastoris.* The different detergents employed are specified. A) Western blots. Lane 1: Input, lane 2: flowthrough, lane 3: FLAG peptide elution, lane 4: acidic buffer elution. B) Summary of oDA activity screening, numbers of fractions correspond to Western blot lane numbering, all the tests gave the same results.

72 h post-transfection cells were harvested and disrupted by sonication. After cell lysis, membrane proteins were extracted by adding 1% dodecylmaltoside (DDM) and 1% fos-choline 12 (FC12), and a small-scale purification with TALON resin was performed. Samples were analyzed by SDS-PAGE, the

quality and yield of eluted samples were evaluated by in-gel fluorescence (where applicable, for constructs with GFP or TGP tag) and Coomassie staining. Test expression in Sf9 cells didn't give protein production (data not shown). Instead, all the different constructs for Expi293 gave a relatively good and comparable expression of HEPH, with a detectable band for both in-gel fluorescence and Coomassie staining of an expected size of 150 kDa (Fig. 24).

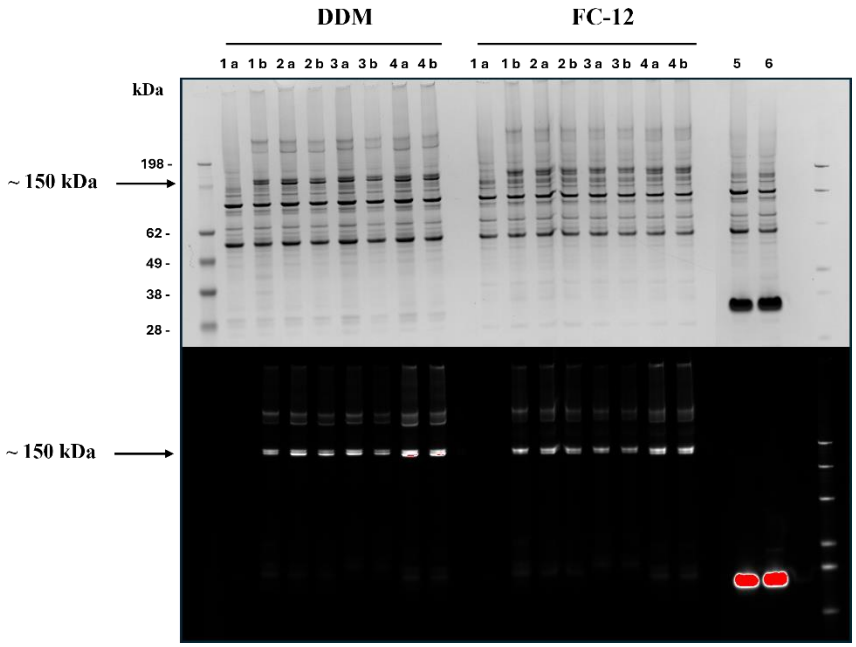

Figure 24. SDS-PAGE analysis of HEPH expression tests in Expi293 cells, stained by Coomassie staining (top gel) and in-gel fluorescence (bottom gel). Lanes numbering: numbers correspond to the different plasmids 1) pOPINEneo-TEV-TGP-His 2) pOPINEneo-3C-TGP-His 3) pOPINEneo-TGP-2Strep-His 4) pOPINEneo-link3C-TGP-His; letters (a-b) refer to two different clones of the same construct. 5-6) GFP positive controls. Detergents employed are specified on top.

Thus, all the pOPINEneo constructs have been employed to scale up cell culture and to perform a detergent screen. Pellets from small-scale cultures (30 ml) were lysed using a cell disruptor and cell membranes were collected by ultracentrifugation. Membrane proteins were extracted with 12 different detergents (Table 2) and a small-scale purification was performed for all the conditions. Eluted samples were analyzed by SDS-PAGE, F-SEC, and nano-Differential Scanning Fluorimetry (nanoDSF), to evaluate protein yield, monodispersion, and thermal stability. Best detergents were identified in DDM + cholesterol (CHS) and lauryl maltose neopentyl glycol (LMNG) which gave higher melting temperature (Tm) (about 39°C and 41°C respectively, for all conditions) and increased mono dispersion, compared to the other detergents (Fig. 25 and 26) The best constructs were also identified in vectors pOPINEneo-3C-TGP-His and pOPINEneo-TEV-TGP-His which showed increased protein yield and lower aggregation propensity, as evaluated by band intensity and quality on SDS-PAGE (Fig. 25).

Detergents
1) DDM
2) DDM + CHS
3) DM
4) DM + CHS
5) OG
6) LMNG
7) OGNG + CHS
8) LDAO
9) C12E8
10) C12E9
11) Cymal-5
12) Fos choline-12 (FC-12)

Table 2. Detergents employed in the HEPH detergent screen. All detergents were used at a concentration of 1% during the extraction. For wash and elution buffers, detergents were diluted to 3 x critical micelle concentration (CMC).

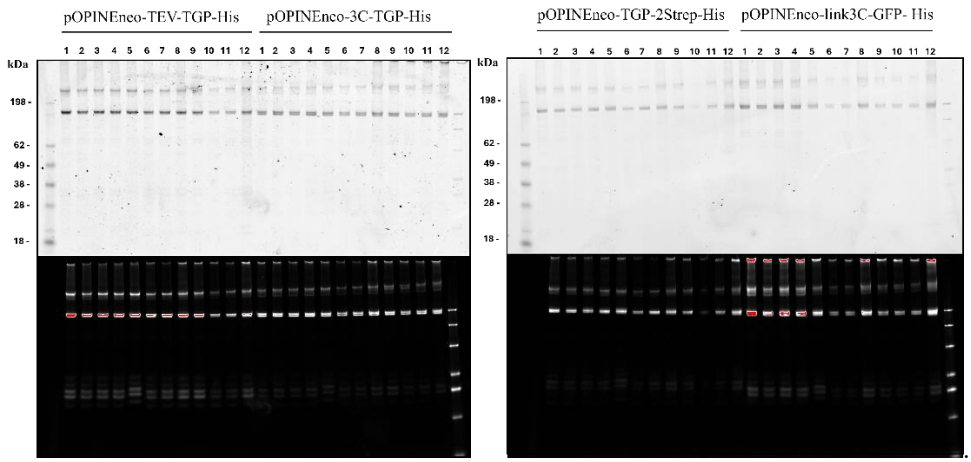

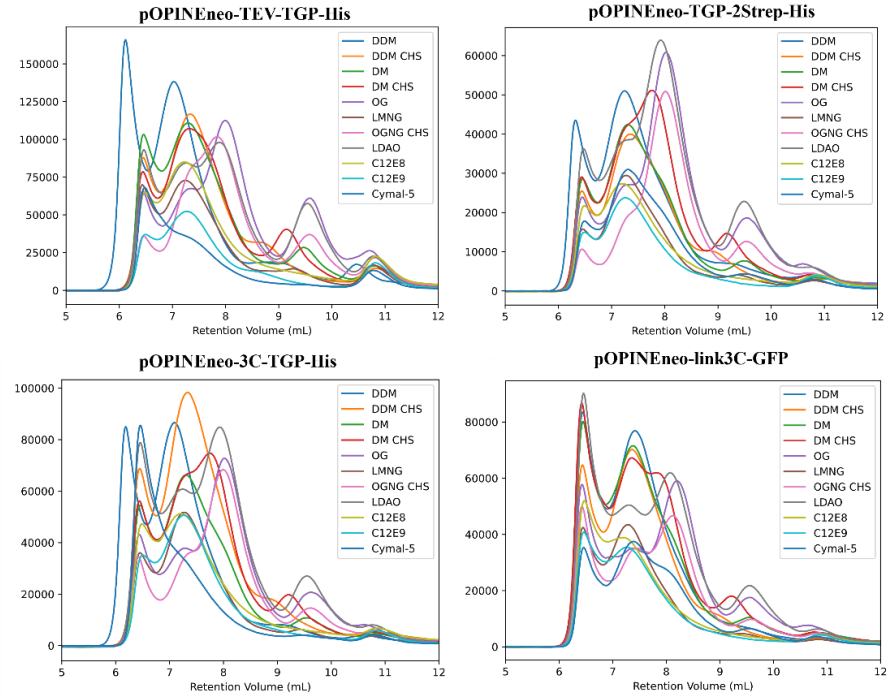

Figure 25. Detergent screen. Upper panels: SDS-PAGE analysis of HEPH constructs. The numbers correspond to the detergents in Table 2. The different constructs are specified on top. Lower panels: F-SEC profiles for each HEPH construct as measured by GFP or TGP fluorescence.

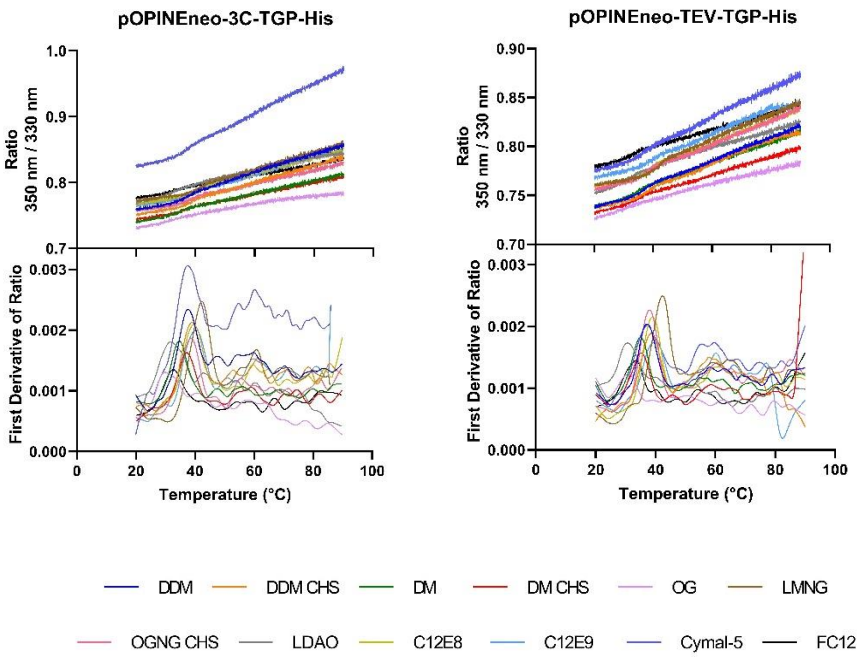

Figure 26. Detergent screen, nano-DSF of pOPINEneo-3C-TGP-His and pOPINEneo-TEV-TGP-His constructs, as an example. Top panels: ratio of intensities at 350 nm and 330 nm as measured by Trp fluorescence. Bottom panels: first derivative of 350 nm / 330 nm ratios.

At this point, HEPH production in Expi293 was scaled up to 300 ml of culture, for both pOPINEneo-3C-TGP-His and pOPINEneo-TEV-TGP-His constructs, to have enough material to set up a purification protocol. Cell culture and lysis were performed as before, and membranes were collected by ultracentrifugation. Membrane proteins were extracted from pellets with 1 % DDM+ 0.1 % CHS or 1% LMNG and after clarification, samples were incubated with TALON resin. After incubation samples were loaded into gravity columns to proceed with extensive wash step and elution. Imidazole was removed from eluted proteins with PD10 columns and samples were

incubated overnight with HRV-3C protease to remove tags. After further incubation with TALON resin to remove tags, uncleaved proteins, and protease (reverse-TALON), HEPH was collected in the flow-through fraction. Purified samples were analyzed by SDS-PAGE to assess protein yield (which was found to be increased in the DDM CHS condition) and tag removal efficiency for the different conditions, nano-DSF, and F-SEC for thermal stability and mono dispersion of the cleaved products. analysis. Given the substantial comparability of the other parameters, we have chosen to select the construct and the detergent that provided the highest yield: pOPINEneo-3C-TGP-His and DDM CHS, respectively.

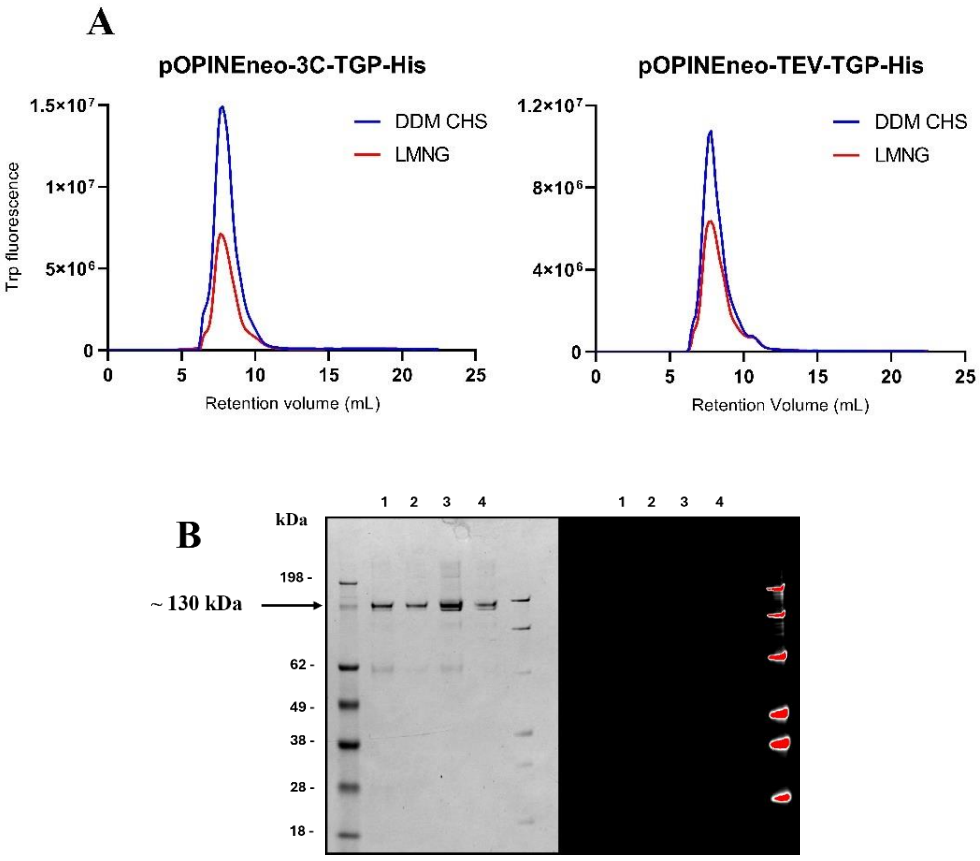

Figure 27. A) F-SEC profiles of HEPH purification test employing DDM CHS and LMNG as selected detergents and pOPINEneo-3C-TGP-His and pOPINEneo-TEV-TGP-His as selected constructs. B) SDS-PAGE analysis of F-SEC sample, stained by Coomassie staining (left gel) and in-gel fluorescence (right gel). Lane 1: pOPINEneo-TEV-TGP-His contruct, DDM CHS extracted, lane 2: pOPINEneo-TEV-TGP-His construct LMNG extracted, lane 3: pOPINEneo-3C-TGP-His construct DDM CHS extracted, lane 4: pOPINEneo-3C-TGP-His LMNG extracted.

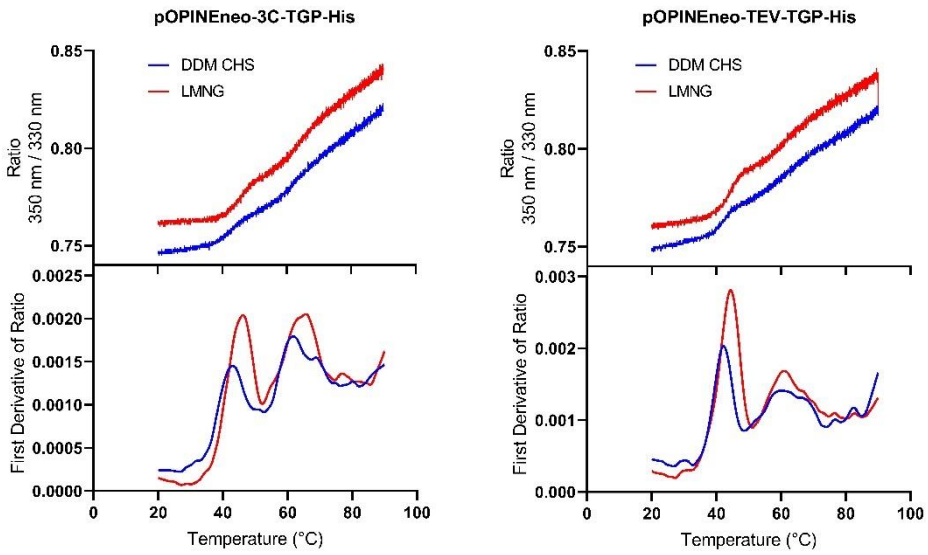

Figure 28. Nano-DSF of HEPH purification test employing DDM CHS and LMNG as selected detergents and pOPINEneo-3C-TGP-His and pOPINEneo-TEV-TGP-His as selected constructs. Top panels: ratio of intensities at 350 nm and 330 nm as measured by Trp fluorescence. Bottom panels: first derivative of 350 nm / 330 nm ratios.

Tag removal was efficient for both constructs and detergent conditions (Fig 27B). Nano-DSF analysis showed two different Tm, around 43°C and 61°C (Fig. 28). Both Tm were slightly increased in LMNG for both constructs. F-SEC profiles showed a similar size and dispersion of protein-detergent micelles. At the same time, the fluorescence signal was significantly increased in the DDM CHS conditions, suggesting an increased protein yield, as confirmed by SDS-PAGE.

Expi293 culture was scaled up (1 L) and transfected with pOPINEneo-3C-TGP-His plasmid. Cell pellets were collected and processed as above, and membrane proteins extracted with DDM CHS and HEPH was purified by

TALON resin. After cleavage, tag and protease were removed by reverse-TALON purification, the flow-through sample was concentrated and loaded on Superdex 200 SEC column for further purification. SEC fractions (200 µL) were analyzed by SDS-PAGE (Fig. 29)

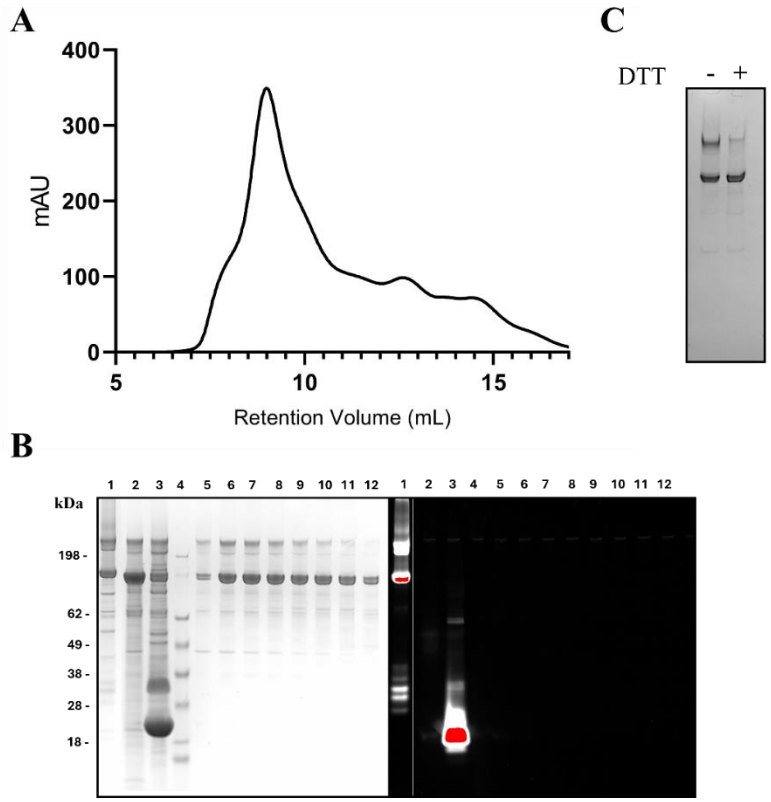

Figure 29. A) SEC chromatogram of purified HEPH expressed in pOPINEneo-3C-TGP-His vector. B) SDS-PAGE analysis of selected fractions from the HEPH purification process, stained by Coomassie staining (left gel) and in-gel fluorescence (right gel). Lane 1: elution of TALON chromatography, lane 2: flowthrough of reverse-TALON chromatography, lane 3: elution of reverse-TALON chromatography, lane 4: molecular weight marker, lanes 5-12: different fractions from SEC chromatography. C) SDS-PAGE analysis of purified HEPH with or without DTT in the loading buffer.

SEC profile (Fig. 29A) revealed the existence of different multimeric conformational states of HEPH. As for previous gels, an additional high molecular weight band was present along with the main band of 130 kDa (Fig 29B). Even after SEC purification, fractions corresponding to the peak of the chromatogram showed the second upper band, which thanks to in-gel fluorescence staining was clearly attributable to a multimeric form of HEPH, and which could not be completely separated from the monomeric form by SEC. Pre-treatment of the SDS-PAGE sample with dithiothreitol (DTT) revealed that this multimerization is mainly stabilized by a disulfide bridge(s) (Fig. 29C).

A new batch of protein was purified in the presence of 0.5 mM TCEP to try to improve the sample uniformity of monomeric HEPH. SEC profile showed an increased sample uniformity and monodispersion (Fig. 30A). But SDS-PAGE still revealed the presence of the high molecular weight band. Anyway, the use of Expi293 cells (compared to the yeast *Pichia pastoris* and insect cells Sf9) as an expression system, along with extensive screening of various constructs and detergents, allowed us to develop a protocol to obtain pure, high-quality, full-length HEPH.

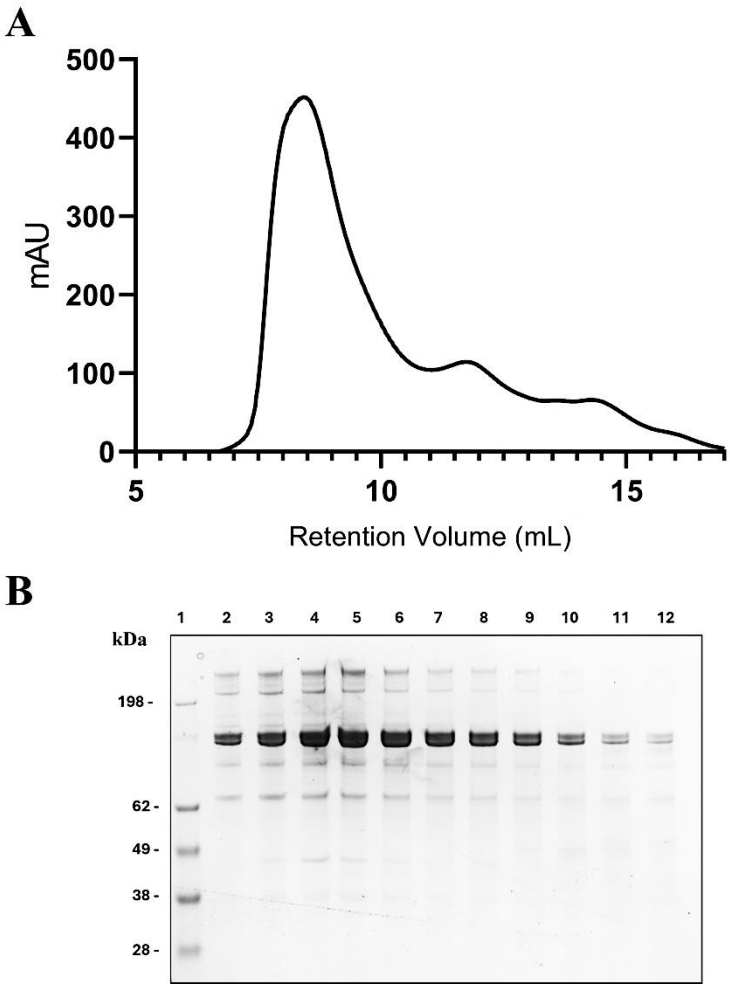

Figure 30. Analysis of HEPH purified in the presence of 0.5 mM TCEP. A) SEC chromatogram. B) SDS-PAGE of different fractions from SEC chromatography.

4.3.2 Discussion

Obtaining pure full-length HEPH is challenging for the complex biosynthetic pathway and its membrane protein feature. Our results demonstrate that switching from yeast and insect cell expression systems to human Expi293 cells, combined with an extensive screening of constructs and detergents, enabled the production of high-quality full-length HEPH.

By systematically testing various detergents, we identified DDM+CHS and LMNG as the most effective for extracting and stabilizing the full-length HEPH, achieving increased thermal stability and monodispersion. DDM CHS bring a higher yield, also. The construct pOPINEneo-3C-TGP-His provided the highest yield, allowing for the successful purification of HEPH.

Despite these advancements, multimerization of HEPH remained an issue, likely due to disulfide bridge formation, as indicated by the persistent presence of high molecular weight bands. Although treatment with reducing agents like TCEP improved sample uniformity, complete elimination of multimeric forms was not achieved. Nevertheless, our protocol represents a significant step forward in obtaining pure full-length HEPH for further structural and functional studies, overcoming limitations in the recombinant production of this membrane-bound ferroxidase.

4.5 Functional Characterization of HEPH Cancer-Related Variants

Only few data are available on HEPH single nucleotide polymorphisms (SNPs) linked to diseases. HEPH polymorphisms have been found associated with migraine pathogenesis (Maher et al., 2012; Albury et al., 2017). Then, in the context of neoplasm and in particular in asbestos-related cancers, the prototype of an iron-dependent oxidative stress-induced type of cancers, a SNP in the coding sequence of HEPH was identified (Crovella et al., 2016; Celsi et al., 2019). This SNP introduces a glutamic acid substitution by histidine at position 568 (D568H) and was shown to confer protection against cancer development in exposed subjects through still uncharacterized molecular mechanisms. Another SNP in the *HEPH* gene, leading to alanine substitution by threonine at position 595 (A595T), has been identified in association with the most aggressive form of ovarian cancer, the high-grade serous subtype (Chornokur et al., 2015), whose complex pathogenesis has also been linked to persistent oxidative stress mediated by iron overload generated by a retrograde menstruation mechanism (Vercellini et al., 2011). In this context it is worth mentioning that ovarian cancer has also been included into the list of malignant diseases associated with asbestos exposure [2014 update on Asbestos in Helsinki (Henrik Wolff et al., 2015)]. The fact that two Heph mutants emerged in association with iron-overload dependent carcinogenesis is indicative that alterations in the iron export route may play a paramount role in the oncogenic process. Recently, HEPH distribution in the context of asbestos-independent lung cancer was addressed and the protein was found to be mainly expressed by endothelial cells, a distribution reminiscent of what has been observed at neuro-vascular unit but whose functional significance has yet to be elucidated

(Zacchi et al., 2021). These findings prompted us to hypothesize that HEPH, expressed by cells of the vascular compartment in different tissue contexts, such as lung, pleura, and ovary, may play a role in sensing local iron demand, thus extending the paradigm uncovered at the blood-brain barrier (BBB). At this location, HEPH variants could exert a fine control on tissue iron supply, either by favouring or hampering its procurement and therefore facilitating or impeding the establishment of a harmful iron-overload environment, a fertile soil for cancer development.

In this section, a functional characterization of the HEPH D568H and A595T is presented, as part of a wider and comprehensive study of HEPH variants exploited along with collaborators of us (that is not being discussed here), that aims to build up a mechanistic framework to correlate alterations in iron sensing/supply with the risk of neoplastic transformation.

4.5.1 Results and Discussion

Since both cancer-promoting versus cancer-protective HEPH variants are similarly enriched at the plasma membrane as compared to the WT form when expressed in HEK293T cells (P. Zacchi, unpublished observation), we asked whether their opposite phenotypes may rely on differences in the ferroxidase activity. The position of residues D568 and A595 is predicted to be at the surface on the same side of the protein, with D568 located in a loop in the basal region of HEPH and A595 closer to the top, in a short helix following a beta-strand (Fig. 31A). Both target amino acids are not predicted to participate in copper coordination/binding, suggesting a mild impact, if any, on ferroxidase activity. Recombinant full-length Heph WT, D568H and A595T were produced

in Expi293F cells and purified as above. Both WT and mutant HEPH were enzymatically active, as shown by ferroxidase activity measurement at 315 nm with 60 μM ferrous iron (Fig. 31C). Time course measurements can be employed to extract the kinetic parameters K_m and V_{max} based on an integrated form of the Michaelis-Menten equation (Schnell & Mendoza, 1997). The time course of iron oxidation by WT and mutant HEPH was analyzed with iFIT (Petrič et al., 2022) and the kinetic parameters are reported in Table 3.

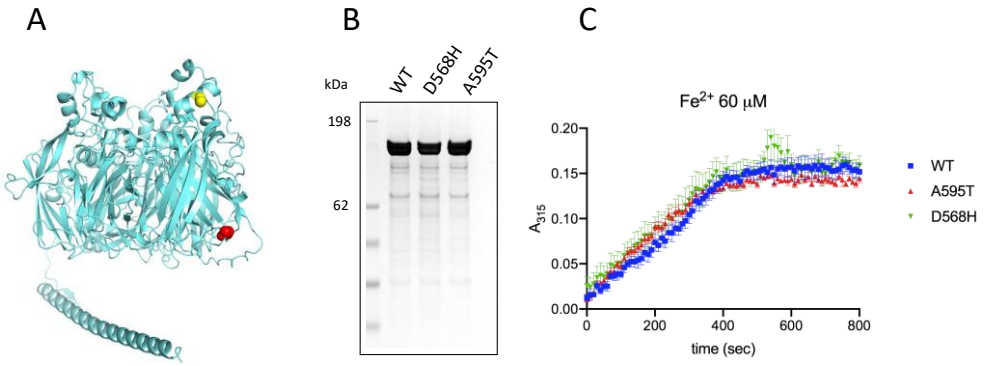

Figure 31. A) Alphafold structural model of human HEPH, residues D568 and A595 are colored in red and yellow, respectively. B) SDS-PAGE analysis of purified human HEPH WT and mutants. The gel was stained with Coomassie Blue. C) time-course of ferroxidase activity measured at 315 nm with 60 μM $Fe(NH_4)_2(SO_4)_2$ and 0.3 μM HEPH.

Hephaestin	K_m (mM)	(SEM)	V_{max} (mM/min)	(SEM)
Wild type	7.71	1.55	10.60	0.80
D568H	5.38	0.97	10.30	0.60
A595T	14.88	0.84	13.46	0.56

Table 3. Kinetic parameters for HEPH ferroxidase activity

The K_m and V_{max} for WT HEPH are in line with the values at low iron concentration reported for the protein expressed in BHK cells (Vashchenko et al., 2012). The results obtained indicate that both mutations appear to have limited impact on V_{max}. Interestingly, the K_m value for HEPH D568H is slightly decreased respect to WT, while HEPH A595T exhibits a significantly increased K_m (p 0.0044, calculated by two-way ANOVA with Dunnett's post hoc test). Residue A595 is located relatively close to a predicted iron binding site formed by D616 and H621 in domain 4; however, this site was shown to be dispensable for ferroxidase activity (Vashchenko et al., 2012) leaving open the question of how the replacement of alanine with threonine may cause the increase in K_m. It is tempting to relate these differences in K_m to some aspect of the cancer-protective (D568H) *vs* promoting (A595T) action of the HEPH variants. On the other hand, these changes in the kinetic parameters appear to be too subtle to be the main cause of the cancer-protective *vs* promoting effect of HEPH. They may be favouring factors together with alteration of the ability of the HEPH variants to interact with apo- and holo-Tfn.

4.6 Ferroportin-Ferroxidase Interaction

4.6.1 Proximity Ligation Assay enables FPN-CP complex *in situ* detection

Given the challenges in obtaining direct evidence of the FPN-CP interaction using classical methods such as co-immunoprecipitation (Co-IP), the proximity ligation assay (PLA) was selected as a more sensitive alternative. PLA is a technique that enables the detection of protein-protein interactions by using two antibodies specific to the target proteins. When the proteins are in close proximity (typically less than 40 nm), secondary antibodies conjugated with oligonucleotides come into contact, forming a circular DNA template that is amplified by PCR. The resulting concatemer can be detected via fluorescent probe hybridization. This method is particularly well-suited for detecting interactions that are difficult to observe by traditional means.

To ensure sufficient expression of both CP and FPN, we decided to perform an initial interaction assay on HEK293T cells, this cell line does not express endogenous FPN and CP but can be easily transfected. HEK293T cells were co-transfected with constructs encoding FPN tagged at the C-terminus with either FLAG (pCMV-FPN-FLAG) or GFP (pCMV-FPN-GFP), along with a construct for the GPI-anchored version of CP (pCMV-CP-GPI). The choice of CP-GPI was made to enhance CP localization at the plasma membrane, facilitating the detection of the complex. Moreover, previous studies have shown that CP-GPI stabilizes FPN, further justifying its use in this study.

Before performing the PLA, co-expression of FPN and CP-GPI was confirmed via immunofluorescence. Forty-eight hours post-transfection, the cells were incubated with α-FPN and α-CP antibodies at 4°C for 1 h to label proteins

exposed on the plasma membrane. The cells were then fixed with 2% PFA to preserve the surface-labeled proteins. Following incubation with secondary antibodies, fluorescence microscopy confirmed that FPN and CP-GPI were co-expressed and co-localized at the plasma membrane (Fig. 32).

Various combinations of plasmid DNA concentrations and primary antibody dilutions were tested to optimize the PLA conditions to ensure an appropriate signal. The best results (shown in Figure 33) were obtained with cells transfected with 800 ng of pCMV-FPN-FLAG and 350 ng of pCMV-CP-GPI. The optimal relative antibody signal was achieved using α-CP at 1:1500 and α-FPN at 1:1000. These conditions were subsequently used for the interaction analysis.

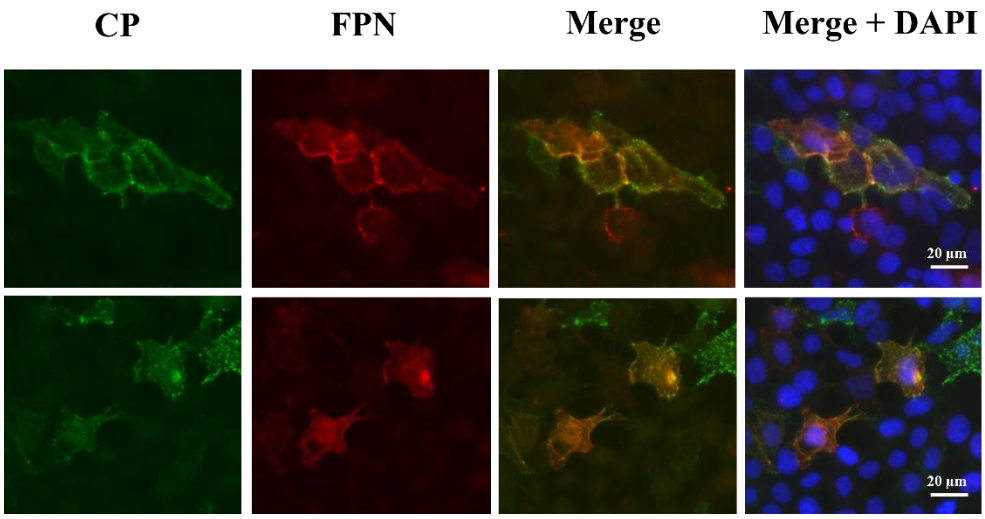

Figure 32. Immunofluorescence analysis of HEK293T cells co-transfected with pCMV-FPN-FLAG and pCMV-CP-GPI. Only cellular surfaces are stained. Nuclei are stained in DAPI. Images were acquired using a Leica DM3000 microscope and Leica DFC320 digital camera.

HEK293T cells co-transfected with plasmids for the expression of FPN-flag/CP-GPI and FPN-GFP/CP-GPI were then analyzed using the PLA assay. Initially, a surface labeling step was performed with primary antibodies to ensure that only FPN-CP complexes present on the plasma membrane were detected. Before applying the PLA kit, the cells adhered to coverslips were incubated with α-FPN and α-CP (at the selected dilutions) at 4°C for 1 h. Following fixation in 4% PFA, the PLA kit was applied.

For each condition, control coverslips were prepared by incubating with only one of the two primary antibodies to assess the specificity of the PLA under the given conditions. As shown in (Fig. 33), a strong PLA signal was observed only when both primary antibodies were used, while a small number of red puncta were detected as background in the single-antibody controls. Figure 33 shows the results obtained with FPN-FLAG and CP-GPI, same results were obtained using FPN-GFP (not shown for convenience). Additionally, the PLA puncta co-localized with the FPN-GFP signal on the plasma membrane (Fig. 34A). These results clearly demonstrate that FPN and CP-GPI physically associate at the cell surface, when overexpressed in HEK293T cells. The experiment was subsequently repeated on the human glioblastoma cell line U373MG, which endogenously expresses both CP-GPI and FPN, to investigate complex formation at endogenous protein concentrations. The results were consistent with those obtained previously, although the number of PLA spots per cell was lower, in line with the lower endogenous expression levels of the proteins (Fig. 34B). These findings confirm that FPN and CP can interact even at low concentrations, supporting the relevance of this interaction under more physiological cellular conditions.

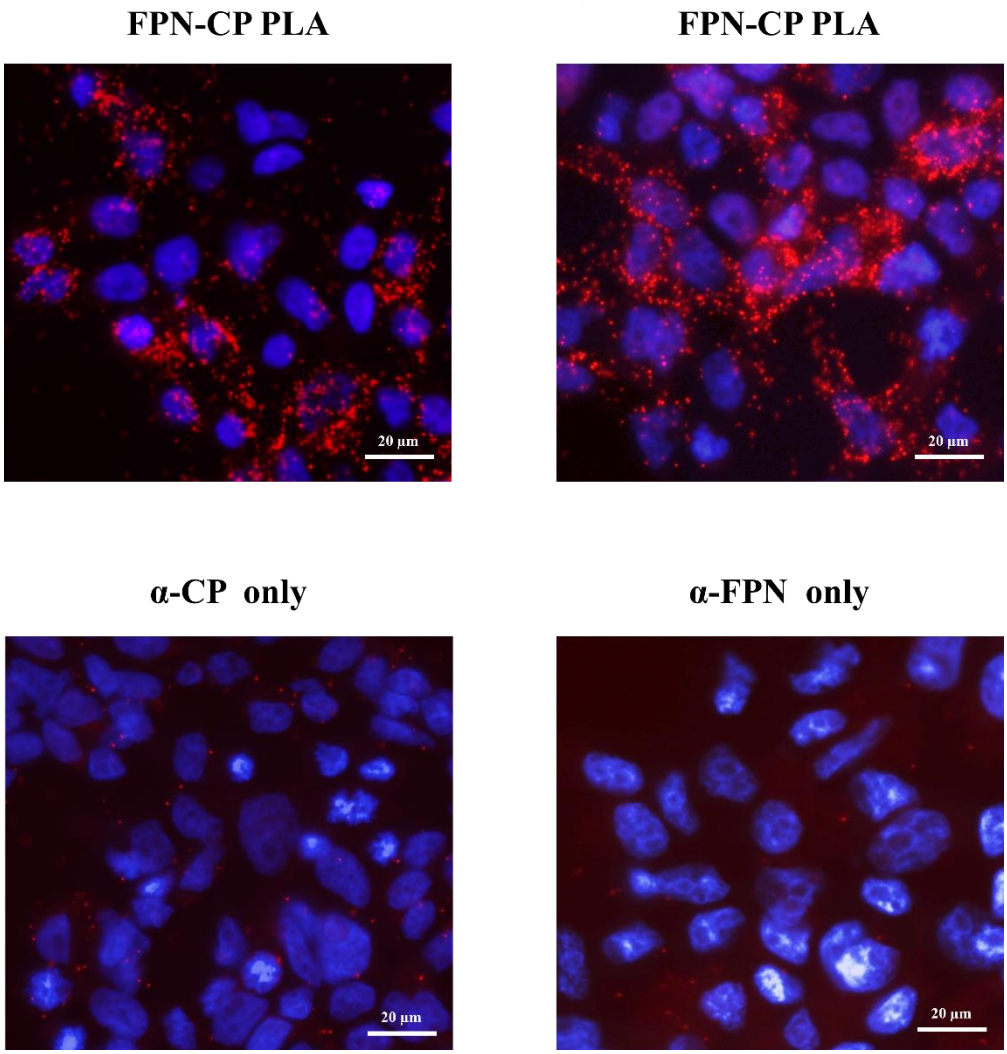

Figure 33. Detection by PLA of CP-GPI/FPN-FLAG complex in HEK293T (upper panels). For negative controls only the primary antibody for CP or for FPN was used (lower panels). Nuclei are stained with DAPI. Images were acquired using a Leica DM3000 microscope and Leica DFC320 digital camera.

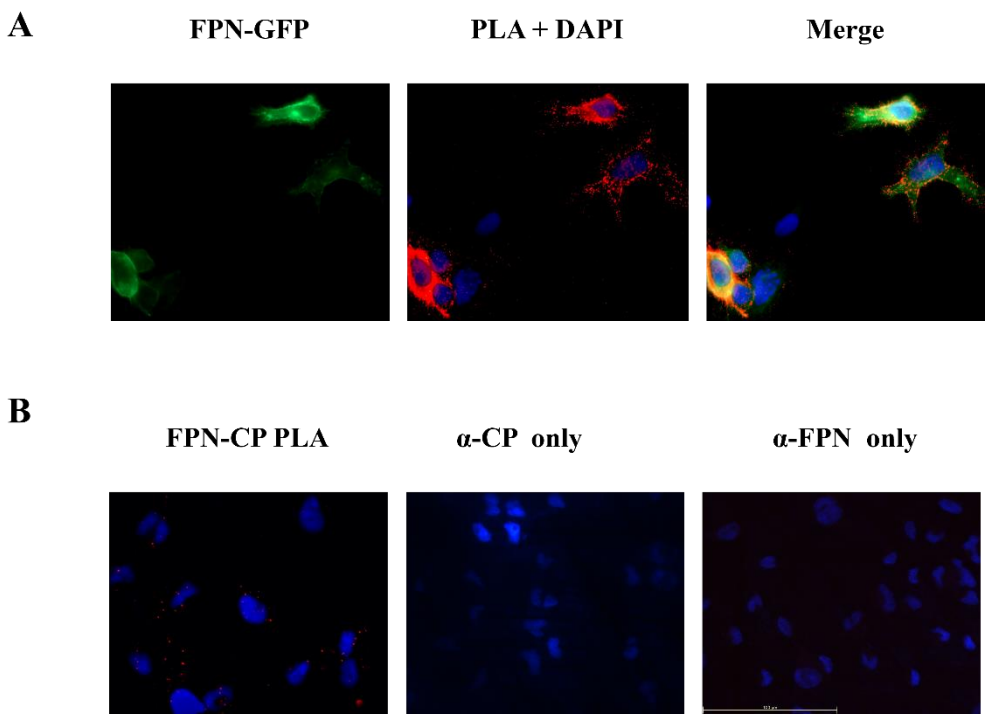

Figure 34. Detection by PLA of CP-GPI/FPN-GFP complex in HEK293T cells and superimposition of PLA and FPN-GFP signals (A). CP-GPI/FPN complex in U373MG cells (B). Nuclei are stained with DAPI. Images were acquired using a Leica DM3000 microscope and Leica DFC320 digital camera.

4.6.2 FPN-CP interaction assays on purified proteins

In addition to the *in situ* identification of the FPN-CP complex, investigating the interaction of the two purified proteins *in vitro* would allow for a more detailed biophysical and structural characterization, providing deeper insights into the specific regions and residues involved in the interaction. To pursue this, both proteins were purified: FPN-flag was produced recombinantly in *Pichia pastoris*, while CP was purified from human plasma. A pull-down assay

was performed to assess the interaction between FPN and CP. FPN-flag and CP were mixed at a 1:1 ratio at a concentration of 4 μM and incubated for 30 minutes at 4°C in the presence of 10 μM FeAS to facilitate the formation and stabilization of the complex. Following incubation, FPN was purified from the mixture using 20 μL of alpha-flag resin. After extensive washing, the bound proteins were eluted using an acidic buffer. As a negative control, a sample containing only 4 μM CP was processed under the same conditions. The fractions from the pull-down assay were analyzed by Western blot using α-FPN and α-CP antibodies. Western blot analysis demonstrated the presence of a CP band in the eluate when incubated with FPN, whereas no CP band was detectable in the absence of FPN (Figure 35 shows the same result, repeated in the experiments conducted in the presence or absence of hepcidin). This result provides clear evidence of an interaction between CP and FPN *in vitro*, although only a small fraction of CP remained bound to the resin. This finding is consistent with the transient or weak nature of the interaction, which has historically impeded the definitive identification of the complex.

Previous studies showed how CP can aid and stabilize FPN, protecting it from hepcidin-mediated degradation (McCarthy et al., 2013; 2014; Kono et al., 2010; De Domenico et al., 2007). These findings suggest a potential competitive interaction between CP and hepcidin for binding to FPN. To explore whether hepcidin inhibits the formation of the FPN-CP complex, pull-down assays were performed both in the presence and absence of the hormone. In these experiments, 4 μM FPN was treated with hepcidin at two different stoichiometric ratios (1:1 and 1:5 FPN:Hepcidin) in the presence of 10 μM FeAS, followed by incubation with CP and processed as described above. Western blot analysis suggested that hepcidin pre-treatment reduced the

amount of CP bound to FPN by 60% and 70% for the 1:1 and 1:5 FPN:Hepcidin conditions, respectively (Fig. 35A and 35B).

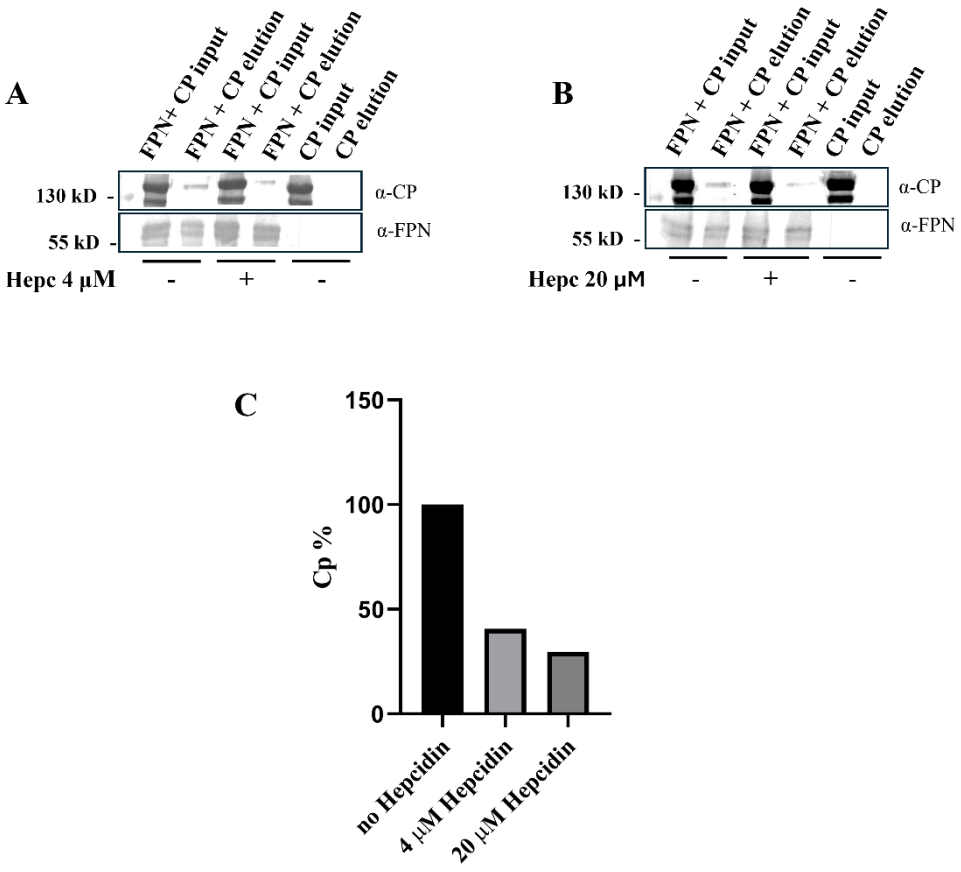

Figure 35. Western-blot analysis of the FPN-CP pull-down assays in the presence of Hepcidin 4 uM (A) and 20 uM (B). C) Histograms representing densitometry analysis performed with ImageJ.

The formation of a stable FPN-CP complex is a critical prerequisite for pursuing structural characterization. Considering the low proportion of CP bound to FPN observed in the pull-down assays, the stability of the complex

was further examined by size-exclusion chromatography (SEC). To promote FPN-CP complex stabilization, the proteins were incubated together in the presence of 1 mM CoCl2. Cobalt was selected over iron due to its greater stability and its ability to effectively mimic FPN's natural substrate, including its role in mediating interaction with hepcidin (Billesbølle et al., 2020). Following a 30-minute incubation at 4°C, the sample was loaded on a Superdex 200 column, and the resulting SEC profile was compared to those of the individual proteins under identical conditions. As shown by the overlaid chromatograms (Fig. 36), no shift in the elution times of either protein was observed, the SEC profiles of the combined and individual protein runs being entirely superimposable. Western blot analysis of the fractions further corroborated the absence of co-elution between the two proteins (data not shown).

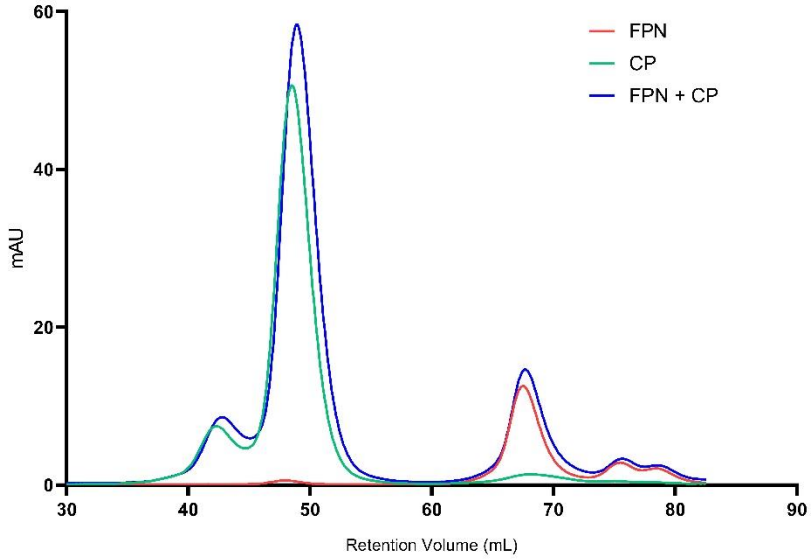

Figure 36. Superimposition of SEC chromatography of FPN, CP and FPN + CP on Superdex 200 column.

Given the inability to further characterize the FPN-CP complex via SEC, we opted to use the dansylated version of FPN at position 54 (FPN Y54Da), previously employed in cobalt-binding assays. Considering that the DA54 residue is located on the extracellular side of FPN, an interaction with CP, predicted to occur in this same region, may perturb the microenvironment surrounding the dansyl group, potentially resulting in detectable changes in the fluorophore emission spectrum. Based on this rationale, 0.5 μM FPN Y54Da was titrated with increasing concentrations of CP, up to 3.8 μM. After each addition of CP, the proteins were incubated for 5 minutes before recording fluorescence emission spectra between 400 and 650 nm, upon excitation at 340 nm. The experiment was repeated at different concentrations of CoCl2 (0, 100, and 4000 μM) to assess the potential impact of the metal on complex formation. As shown by the fluorescence spectra (Fig 37), the change in the dansyl emission signal during titration with CP was not significant across all concentrations of CoCl2 tested. The plot of the detected signal intensities also resulted in poor fitting, further indicating that no significant interaction between CP and FPN Y54Da was detectable under these experimental conditions.

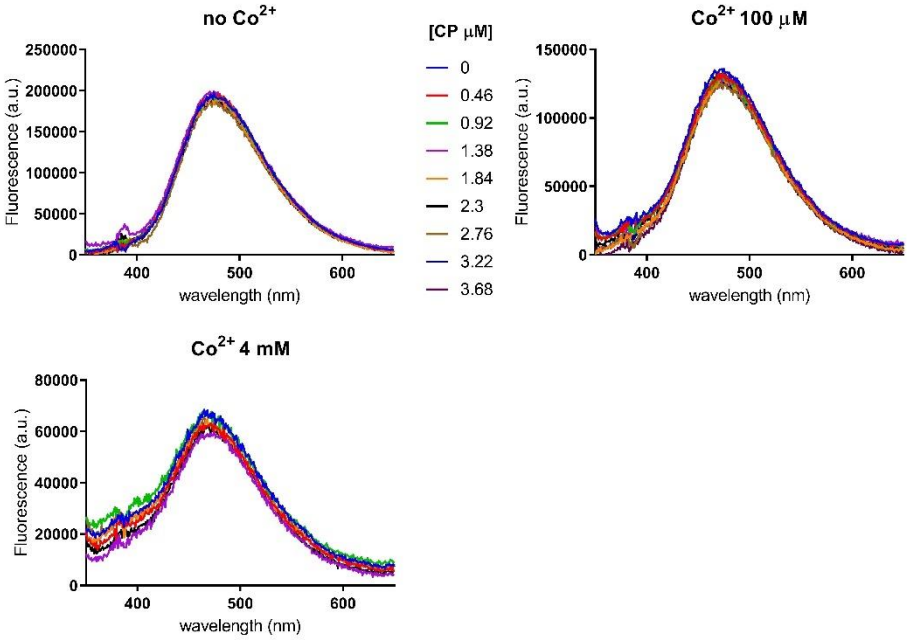

Figure 37. Fluorescence spectra recorded during titration of FPN Y54DA with CP in MOPS 25 mM pH 7.0, NaCl 150 mM, DDM 0.01%. Excitation was at 340 nm.

4.6.3 AlphaFold prediction of FPN-CP complex

The difficulty in obtaining a stable FPN-CP complex limits the potential for structural characterization. To gain some insights into the interaction, the AlphaFold2 algorithm was employed to predict the 3D model of the complex, using ColabFold, an open-source software that leverage AlphaFold2's homology search with the implementation of the 40–60-fold faster MMseqs2 (Many-against-Many sequence searching) (Mirdita et al., 2022). Thanks to the collaboration with Dr. F. Polticelli (Università Roma Tre) ColabFold

successfully generated an FPN-CP complex model (Fig. 38), with FPN in an outward-facing conformation. Although the pLDDT confidence scores indicate lower reliability at the interface region, this prediction offers several interesting insights.

In this model, FPN adopts an outward-open conformation, which is consistent with its role during iron release when interacting with a ferroxidase. This is the same conformation adopted by the transporter when binding hepcidin, reinforcing the idea that adding a substrate is a rational strategy for experimentally stabilizing the complex. The loops at the interface between FPN and CP appear to play a crucial role in the interaction, suggesting that targeted mutagenesis or deletions in these regions could help identify the residues mediating the interaction without altering the overall structure of the two proteins. Of particular note, despite the low confidence in this region, one of the loops of FPN is predicted to fold into a configuration that inserts itself into the cavity of the transporter, acting like a plug. In this conformation, hepcidin binding would be obstructed, providing a potential structural explanation for the protective effect of the ferroxidase against hepcidin-mediated degradation of FPN. Furthermore, upon inspecting the residues at the interface, it becomes evident that Y54, although located on the extracellular side, is not positioned within the region that interacts with CP. This could explain why no interaction was observed in the fluorescence assays using the FPN Y54DA mutant, as this residue would not be directly involved in CP binding.

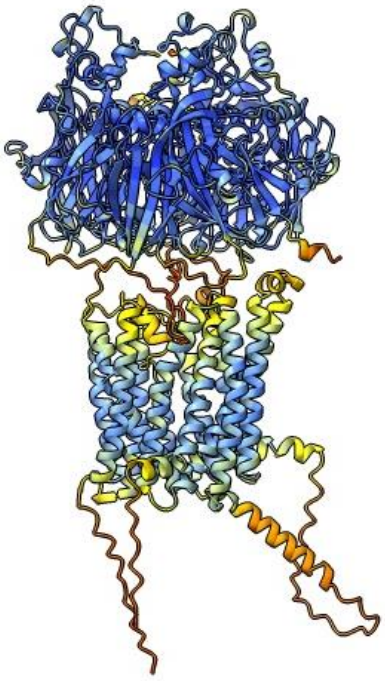

Figure 38. Model of the CP/FPN complex generated by AlphaFold 3. The model is colored by pLDDT score where blue indicates higher and red lower score.

4.6.4 FPN-HEPH interaction assays on purified proteins

Unlike the interaction with CP, the interaction between FPN and HEPH has already been described (Baringer et al., 2023; Han et al., 2007). Clarifying the molecular architecture of the HEPH/FPN complex would be crucial for gaining a deeper understanding of the iron export mechanism. Given that, for the first time, full-length HEPH has been successfully purified, as described above, experiments were conducted at the Membrane Protein Lab to assess whether

and how stably the complex could form *in vitro*, with the ultimate goal of solving the complex 3D structure by cryo-EM.

In parallel with HEPH purification, FPN was produced in insect Sf9 cells using an established construct and protocol from the lab, and both proteins were employed in interaction assays. Since both proteins have the His-tag, the pull-down strategy used for the CP/FPN complex could not be applied. Instead, a crosslinker (BS3) was employed to covalently stabilize any potential complex formation, allowing its visualization by SDS-PAGE. FPN and HEPH were mixed at a 1:1 ratio in the presence or absence of 1 mM CoCl2 and incubated with the crosslinker at room temperature for 30 minutes, following the manufacturer's instructions. Appropriate controls with each protein alone were included, and all experimental conditions were repeated without BS3. The samples were then analyzed by SDS-PAGE. Despite BS3 not containing disulfide bonds, no reducing agents were added to the loading buffer during sample preparation for electrophoresis. This was done to avoid confounding effects from the higher molecular weight band typically observed in HEPH samples (see above). As shown in Figure 39A, the interaction between FPN and HEPH was not stabilized by the crosslinker, as no high molecular weight bands corresponding to covalently crosslinked polypeptides were observed. The only visible effect, as expected, was the stabilization of the HEPH upper band, which appeared more intense in all BS3-treated samples. BS3 is an amine-reactive crosslinker, and the low abundance of lysine residues on the extracellular surface of FPN (the region where the interaction with HEPH is predicted to occur) could explain why no covalent stabilization of the complex was observed.

To further investigate this, SEC was employed as an alternative approach. As before, HEPH and FPN (1:2 ratio) were incubated in the presence of $CoCl_2$, both individually and in combination, and the samples were loaded onto a Superose 6 column. As the SEC runs with CP and FPN, superimposition of the chromatograms showed no evidence of complex formation (Fig. 39B). FPN and HEPH, even when incubated together, eluted according to their respective molecular weights, with no shift indicating the formation of a stable complex.

Given that SEC can fail in the detection of weak or highly transient interaction, there was still a possibility that purified FPN and HEPH are capable of interacting *in vitro.* Given the opportunity to use cryo-electron microscopy (cryo-EM) during the experience at the Membrane Protein Lab (which is interconnected with the eBIC EM center), a final attempt was made using this technique. FPN and HEPH were mixed as before, at a 1:2 ratio, and applied to glow-discharged UltrAufoil 300 grids. The sample was vitrified using the Vitrobot Mark IV system. After an initial screening that appeared promising, a mini-data collection was carried out using the Talos Arctica Cryo-TEM.

Figure 40 shows the 2D average analysis of the particles, where no evidence of a complex between HEPH and FPN was found. Additionally, the poor quality of the sample prevented further analysis to investigate the structure of HEPH alone.

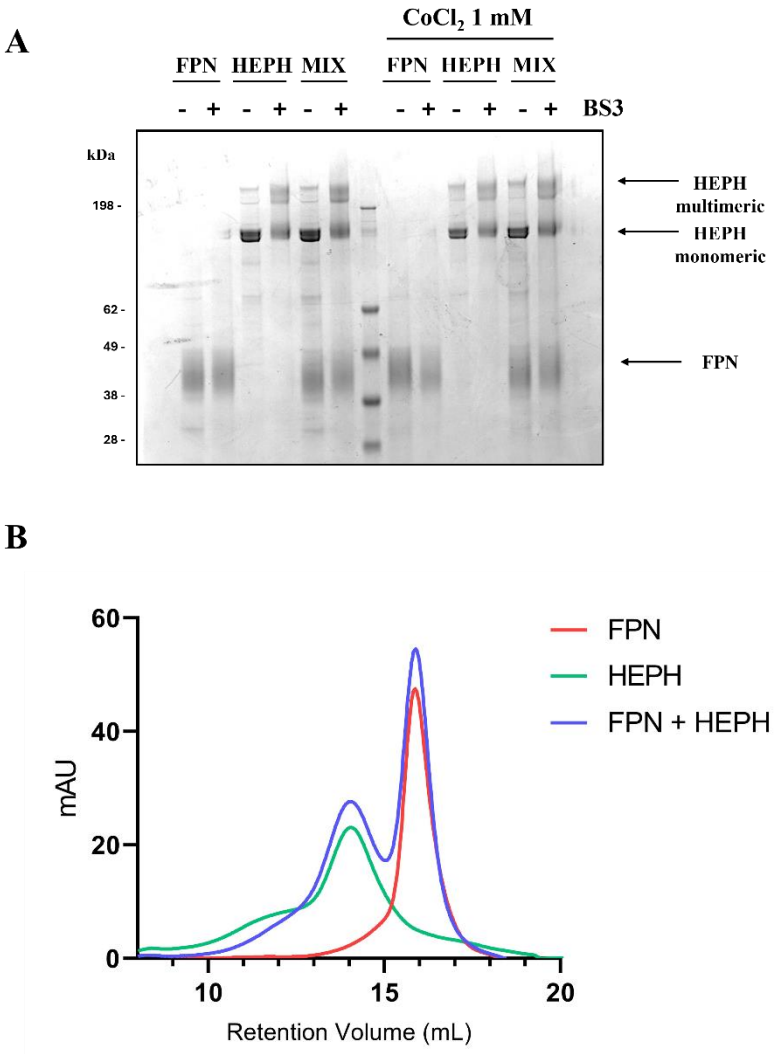

Figure 39. FPN-HEPH interaction assays. A) SDS-PAGE analysis of BS3-crosslink experiment. B) Superimposition of SEC chromatography of FPN, HEPH and FPN + HEPH on Superose 6 column.

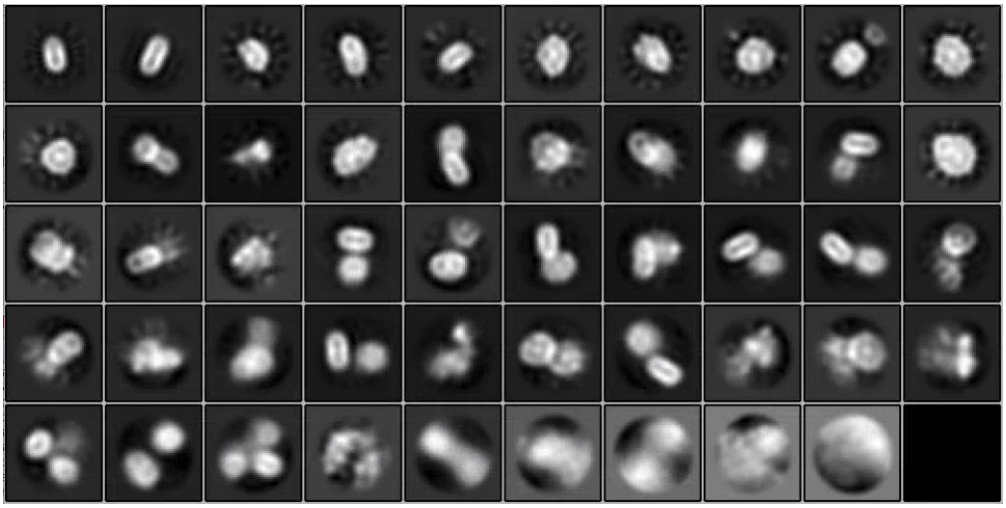

Figure 40. 2D class averages of the cryo-EM FPN-HEPH grids showed no evidence of complex formation. The low quality of the sample did not allow for further processing.

4.6.5 Discussion

The interplay between FPN and CP is pivotal in cellular iron homeostasis, facilitating iron export, oxidation, and loading on TF. Despite the physical association between these two proteins was proposed several years ago, only indirect proofs supported this hypothesis, recently reinforced by the finding that the other ferroxidase HEPH associates with FPN in cells. While any effort to demonstrate FPN-CP interaction failed.

PLA provided the first clear evidence of the interaction between these two proteins, allowing the FPN-CP complex detection at the plasma membrane of HEK 293. The reproducibility of this assay in the U373MG glioblastoma cell line supports the physiological relevance of the FPN-CP interaction even under lower endogenous protein expression levels.

In vitro, pull-down assays on purified proteins further validated the FPN-CP interaction, although the binding appeared transient and weak as a small fraction of CP remained bound to FPN during the experiment and no complex formation was observed by SEC. This observation aligns with previous difficulties in obtaining clear proof of this interaction. Highly transient interaction between CP and FPN can possibly be explained by the high dynamicity of the iron export system which is regulated by different factors such as fluctuations in iron levels or the presence of hepcidin. Notably, our findings suggest a competitive dynamic between CP and hepcidin, where hepcidin pre-treatment of FPN drastically reduced its interaction with CP. This suggests that CP competes with hepcidin for binding to FPN, offering a mechanistic insight into how CP may protect FPN from hepcidin-mediated degradation.

The AlphaFold model of the FPN-CP complex provided intriguing structural insights, proposing that FPN adopts an outward-open conformation during its interaction with CP, consistent with its iron export mechanism and CP/hepcidin competition for FPN binding. The model also suggests that specific loops at the FPN-CP interface may play crucial roles in mediating the interaction, offering targets for future mutagenesis studies. Interestingly, the model predicts (with low confidence) that one of the FPN loops may insert into its cavity. The hepcidin binding site would be obstructed in this conformation, offering a structural explanation for CP's protective role against hepcidin-mediated degradation of FPN.

Experiments with HEPH highlighted additional complexities. Despite the FPN-HEPH interaction has been recently proved, our experiments using crosslinking and SEC failed to detect a stable FPN-HEPH complex. Also, an

ambitious attempt to bypass interaction assays and directly visualize complex formation by cryo-EM failed as well. These results suggest that the interaction may be highly transient (as for CP) or dependent on specific conditions that were not replicated in vitro, such as a specific lipid bilayer composition, or (more unlikely) the presence of a third unknown component that could stabilize the interaction. It is also important to emphasize that characterizing interactions between two membrane proteins presents significant challenges, as the presence of detergents could hinder the interaction by masking the regions involved in complex formation on both proteins. An alternative strategy to capture and purify the complex could be co-expressing the two proteins and stabilizing the interaction through crosslinking or extracting the complex from the membrane using encapsulating agents such as styrene-maleic acid-lipid particles (SMALPs).

5. CONCLUSIONS

The ferroportin-ferroxidase system is central to human iron metabolism, yet several unresolved questions have hindered a complete understanding of the molecular mechanisms governing this crucial process. This thesis has explored several aspects of iron export that remain poorly understood, focusing on all the three proteins involved: FPN, CP, and HEPH.

The first section of the research focused on the FPN transporter. There has been significant debate among research groups about the mechanism by which iron translocation occurs, leading to the proposal of various, often conflicting, models. By analogy with the Major Facilitator Superfamily (MFS) of transporters, it is believed that FPN adopts an alternating access mechanism during the translocation of its substrate(s). This mechanism has been primarily proposed based on studies conducted on the bacterial transporter LacY, which used fluorescence-based techniques to probe conformational transitions during substrate transport. One of the key limitations in studying FPN's translocation mechanism has been the lack of a robust experimental system capable of providing such detailed information. Techniques used with LacY exploit the fluorescence of specific tryptophan residues or cysteine modifications for fluorescent probe attachment, but these methods are not applicable to FPN, as they require the generation of a tryptophan- or cysteine-free background to achieve single-site labeling.

This work focused on developing an experimental system suitable for studying FPN's alternating access mechanism through the genetic incorporation of

unnatural amino acids. This approach bypasses the issues associated with an excess of tryptophan or cysteine residues by allowing the site-specific introduction of amino acids with unique properties at various positions in the protein. Four different dansyl-labeled FPN variants were successfully produced using this technique. Equilibrium binding assays demonstrated that the dansyl probe could effectively detect conformational changes induced by cobalt binding, with specific responses based on the probe's position within the FPN structure. This experimental system offers a promising platform for future studies aimed at elucidating the alternating access mechanism of FPN, particularly through kinetic studies using stopped-flow techniques.

Another unresolved issue in understanding FPN's mechanism is that all proposed models to date fail to account for the presence of two iron-binding sites within the protein. This unique feature within the MFS family complicates our understanding of FPN-mediated iron translocation but also offers a new avenue for investigation. This thesis has provided a comprehensive characterization of these two binding sites. Through mutagenesis, the contribution of different residues to metal binding and the relative affinities of the two sites have been clarified, leading to the proposal of a new model of translocation that reconciles conflicting data from the literature. According to this model, the directionality of transport is ensured (at least in part) by the differing affinities of the two iron-binding sites, offering a molecular explanation for the interactions between FPN, its inhibitor hepcidin, and its ferroxidase partners.

Although the two parts of this section differ in their reported affinities of FPN for cobalt, as discussed in Section 4.2.2, this discrepancy is solely due to different cobalt concentration ranges employed in the experiments. The cobalt

titrations in Section 4.1 were conducted specifically to demonstrate the effectiveness of the dansylated-FPN system in detecting conformational changes induced by metal binding. Conversely, Section 4.2 presents a more comprehensive analysis of FPN's affinity for cobalt, which enabled a refinement of its mechanism.

The second part of this work focused on the ferroxidases CP and HEPH. For CP, the lack of an adequate protocol for recombinant expression and purification, due to the complex biosynthesis of the protein, has severely limited the characterization of mutants involved in pathological conditions. It has also hindered an in-depth study of the protein via structure-based mutagenesis. In this thesis, for the first time, the biochemical study of two pathological CP mutants (N244S and G876A) and two specifically designed mutants aimed at investigating previously unexplored characteristics of the protein is presented. This approach opens the door to the functional characterization of a wide variety of CP mutants, facilitating the detailed study of residues that have not yet been characterized. Additionally, this study led to the identification of three phenylalanine residues that had not previously been considered, but were found to be essential for the correct catalytic activity of the protein. Although this finding is not sufficient to fully clarify the functional implication of these residues, it paves the way for further investigations into the catalytic mechanism of the protein.

Similarly, HEPH presents numerous challenges due to its additional complexity as a membrane-bound protein. To date, only a few studies have explored the production and characterization of HEPH mutants, and these have primarily relied on solubilized forms of the protein. However, this approach limits studies to the ectodomain of the protein, excluding the transmembrane

region, which is crucial for a comprehensive understanding of the protein's function. This is especially important when comparing HEPH to its soluble homolog, CP. For the first time, a protocol is presented here that ensures the production and purification of high-quality, full-length HEPH - a necessary condition for its complete structural characterization. This work paves the way for the resolution of HEPH's structure, which will allow for a detailed comparison with ceruloplasmin, highlighting both similarities and differences. Such comparisons will aid in defining the unique roles of HEPH, particularly regarding its transmembrane domain.

Furthermore, similar to CP, the functional characterization of HEPH mutants involved in pathological conditions remains limited. This thesis presents a study on the ferroxidase activity of two HEPH variants that are implicated in either protective or aggravating roles in different types of cancer. For both CP and HEPH, the analyses conducted revealed that the mutants examined did not exhibit significant impacts on the enzymatic functionality of the two ferroxidases. This suggests that other features of the proteins, unrelated to their ferroxidase activity, may play a substantial role in their physiological function. Understanding these features could be key to uncovering the broader biological roles of these ferroxidases in human health and disease.

The third and final section of this thesis focuses on the connection between FPN and the ferroxidases CP and HEPH. While their functional relationship has long been recognized, demonstrating a physical interaction between these components has remained a challenge. Using a highly sensitive technique such as PLA, the existence of the FPN-CP complex has been identified for the first time. This discovery not only reconciles and strengthens previous indirect evidence of this interaction but also provides a pathway to explore the

molecular details of the association, including the identification of regions and residues involved in the interaction.

In vitro experiments with purified proteins confirmed the existence of the FPN-CP interaction and its regulation by the inhibitory hormone hepcidin. However, the data also highlighted several challenges related to the biochemical characterization of the FPN-CP complex. Specifically, the weakness of this interaction was confirmed, indicating that significant future work will be required to stabilize and structurally characterize the complex. This challenge is even more pertinent in the case of the FPN-HEPH complex, where it was not possible to confirm its existence in vitro.

Future research aimed at stabilizing these complexes will be crucial for finally solving their structures. This will allow a deeper understanding of the molecular details behind the iron export mechanism from cells and ultimately uncover the intricate processes of this essential system, addressing the remaining questions regarding iron homeostasis regulation and its dysregulation in disease contexts.

6. PUBLICATIONS

1. Longo C, Lepri A, Paciolla A, Messore A, De Vita D, Bonaccorsi di Patti MC, Amadei M, Madia VN, Ialongo D, Di Santo R, Costi R, Vittorioso P. New Inhibitors of the Human p300/CBP Acetyltransferase Are Selectively Active against the Arabidopsis HAC Proteins. Int J Mol Sci. 2022 Sep 9;23(18):10446. doi: 10.3390/ijms231810446. PMID: 36142359; PMCID: PMC9499386.

2. Amadei M, Niro A, Fullone MR, Miele R, Polticelli F, Musci G, Bonaccorsi di Patti MC. Genetic Incorporation of Dansylalanine in Human Ferroportin to Probe the Alternating Access Mechanism of Iron Transport. Int J Mol Sci. 2023 Jul 25;24(15):11919. doi: 10.3390/ijms241511919. PMID: 37569293; PMCID: PMC10418311.

3. Amadei M, De Lauro A, Polticelli F, Musci G, Bonaccorsi di Patti MC. The different affinity of the two metal-binding sites of human ferroportin drives outward directionality of transport. Submitted.

4. Longo F, Marconato A, Amadei M, Bonaccorsi di Patti MC, Li P, Fan H, Zacchi P, Violetta B. Characterization of Hephaestin variants provides novel mechanistic insights on iron overload-dependent cancer risk. In preparation.

5. Amadei M, Polticelli F, Musci G, Bonaccorsi di Patti MC. The ferroxidase-permease system for translocation of iron across membranes: from yeast to man. In preparation.

7. BIBLIOGRAPHY

Abbaspour, N., Hurrell, R., and Kelishadi, R., Review on Iron and Its Importance for Human Health, *Journal of Research in Medical Sciences*, 2014.

Abboud, S. and Haile, D. J., A Novel Mammalian Iron-Regulated Protein Involved in Intracellular Iron Metabolism, *Journal of Biological Chemistry*, vol. **275**, no. 26, 2000. DOI: 10.1074/jbc.M000713200

Aisen, P., Transferrin Receptor 1, *International Journal of Biochemistry and Cell Biology*, 2004.

Albury, C. L., Stuart, S., Haupt, L. M., and Griffiths, L. R., Ion Channelopathies and Migraine Pathogenesis, *Molecular Genetics and Genomics*, 2017.

Amadei, M., Niro, A., Fullone, M. R., Miele, R., Polticelli, F., Musci, G. and Bonaccorsi di Patti, M. C., Genetic Incorporation of Dansylalanine in Human Ferroportin to Probe the Alternating Access Mechanism of Iron Transport, *International Journal of Molecular Sciences*, vol. **24**, no. 15, 2023. DOI: 10.3390/ijms241511919

Aronova, M. A., Noh, S. J., Zhang, G., Byrnes, C., Meier, E. R., Kim, Y. C. and Leapman, R. D., Use of Dual-Electron Probes Reveals the Role of Ferritin as an Iron Depot in Ex Vivo Erythropoiesis, *IScience*, vol. **24**, no. 8, 2021. DOI: 10.1016/j.isci.2021.102901

Arosio, P., Carmona, F., Gozzelino, R., Maccarinelli, F. and Poli, M., The Importance of Eukaryotic Ferritins in Iron Handling and Cytoprotection, *Biochemical Journal*, vol. **472**, no. 1, 2015. DOI: 10.1042/BJ20150787

Aschemeyer, S., Qiao, B., Stefanova, D., Valore, E. V., Sek, A. C., Alex Ruwe, T., Vieth, K. R., et al., Structure-Function Analysis of Ferroportin Defines the Binding Site and an Alternative Mechanism of Action of Hepcidin, *Blood*, vol. **131**, no. 8, 2018. DOI: 10.1182/blood-2017-05-786590

Back, D. Z. de, Kostova, E. B., Kraaij, M. van, Berg, T. K. van den, and Bruggen, R. van, Of Macrophages and Red Blood Cells; A Complex Love Story, *Frontiers in Physiology*, 2014.

Baerenfaenger, M., Moritz, M. and Meyer, B., Quantitation of Glycopeptides by ESI/MS - Size of the Peptide Part Strongly Affects the Relative Proportions and Allows Discovery of New Glycan Compositions of Ceruloplasmin, *Glycoconjugate Journal*, vol. **36**, no. 1, 2019. DOI: 10.1007/s10719-018-9852-5

Baringer, S. L., Palsa, K., Spiegelman, V. S., Simpson, I. A. and Connor, J. R., Apo- and Holo-Transferrin Differentially Interact with Hephaestin and Ferroportin in a Novel Mechanism of Cellular Iron Release Regulation, *Journal of Biomedical Science*, vol. **30**, no. 1, 2023. DOI: 10.1186/s12929-023-00934-2

Bielli, P., and Calabrese, L., Structure to Function Relationships in Ceruloplasmin: A "moonlighting" Protein, *Cellular and Molecular Life Sciences*, 2002.

Billesbølle, C. B., Azumaya, C. M., Kretsch, R. C., Powers, A. S., Gonen, S., Schneider, S., Arvedson, T., Dror, R. O., Cheng, Y. and Manglik, A., Structure of Hepcidin-Bound Ferroportin Reveals Iron Homeostatic Mechanisms, *Nature*, vol. **586**, no. 7831, 2020. DOI: 10.1038/s41586-020-2668-z

Bonaccorsi Di Patti, Maria C., Polticelli, F., Cece, G., Cutone, A., Felici, F., Persichini, T. and Musci, G., A Structural Model of Human Ferroportin and of Its Iron Binding Site, *FEBS Journal*, vol. **281**, no. 12, 2014. DOI: 10.1111/febs.12825

Bonaccorsi Di Patti, Maria Carmela, Cutone, A., Nemčovič, M., Pakanová, Z., Baráth, P. and Musci, G., Production of Recombinant Human Ceruloplasmin: Improvements and Perspectives, *International Journal of Molecular Sciences*, vol. **22**, no. 15, 2021. DOI: 10.3390/ijms22158228

Bonaccorsi di Patti, M. C., Cutone, A., Polticelli, F., Rosa, L., Lepanto, M. S., Valenti, P. and Musci, G., The Ferroportin-Ceruloplasmin System and the Mammalian Iron Homeostasis Machine: Regulatory Pathways and

the Role of Lactoferrin, *BioMetals*, vol. **31**, no. 3, 2018. DOI: 10.1007/s10534-018-0087-5

Celsi, F., Crovella, S., Moura, R. R., Schneider, M., Vita, F., Finotto, L., Zabucchi, G., Zacchi, P. and Borelli, V., Pleural Mesothelioma and Lung Cancer: The Role of Asbestos Exposure and Genetic Variants in Selected Iron Metabolism and Inflammation Genes, *Journal of Toxicology and Environmental Health - Part A: Current Issues*, vol. **82**, no. 20, 2019. DOI: 10.1080/15287394.2019.1694612

Chen, H., Attieh, Z. K., Syed, B. A., Kuo, Y. M., Stevens, V., Fuqua, B. K., Andersen, H. S., et al., Identification of Zyklopen, a New Member of the Vertebrate Multicopper Ferroxidase Family, and Characterization in Rodents and Human Cells, *Journal of Nutrition*, vol. **140**, no. 10, 2010. DOI: 10.3945/jn.109.117531

Chen, H., Huang, G., Su, T., Gao, H., Attieh, Z. K., McKie, A. T., Anderson, G. J. and Vulpe, C. D., Decreased Hephaestin Activity in the Intestine of Copper-Deficient Mice Causes Systemic Iron Deficiency, *Journal of Nutrition*, vol. **136**, no. 5, 2006. DOI: 10.1093/jn/136.5.1236

Cheng, Y., Zak, O., Aisen, P., Harrison, S. C. and Walz, T., Structure of the Human Transferrin Receptor-Transferrin Complex, *Cell*, vol. **116**, no. 4, 2004. DOI: 10.1016/S0092-8674(04)00130-8

Chornokur, G., Lin, H. Y., Tyrer, J. P., Lawrenson, K., Dennis, J., Amankwah, E. K., Qu, X., et al., Common Genetic Variation in Cellular Transport Genes and Epithelial Ovarian Cancer (EOC) Risk, *PLoS ONE*, vol. **10**, no. 6, 2015. DOI: 10.1371/journal.pone.0128106

Crovella, S., Bianco, A. M., Vuch, J., Zupin, L., Moura, R. R., Trevisan, E., Schneider, M., et al., Iron Signature in Asbestos-Induced Malignant Pleural Mesothelioma: A Population-Based Autopsy Study, *Journal of Toxicology and Environmental Health - Part A: Current Issues*, vol. **79**, no. 3, 2016. DOI: 10.1080/15287394.2015.1123452

Cuadrado, A., Rojo, A. I., Wells, G., Hayes, J. D., Cousin, S. P., Rumsey, W. L., Attucks, O. C., et al., Therapeutic Targeting of the NRF2 and KEAP1 Partnership in Chronic Diseases, *Nature Reviews Drug Discovery*, 2019.

Cuenca, M. V., Marchi, G., Barqué, A., Esteban-Jurado, C., Marchetto, A., Giorgetti, A., Chelban, V., et al., Genetic and Clinical Heterogeneity in Thirteen New Cases with Aceruloplasminemia. Atypical Anemia as a Clue for an Early Diagnosis, *International Journal of Molecular Sciences*, vol. **21**, no. 7, 2020. DOI: 10.3390/ijms21072374

Deshpande, C. N., Ruwe, T. A., Shawki, A., Xin, V., Vieth, K. R., Valore, E. V., Qiao, B., et al., Calcium Is an Essential Cofactor for Metal Efflux by the Ferroportin Transporter Family, *Nature Communications*, vol. **9**, no. 1, 2018. DOI: 10.1038/s41467-018-05446-4

Dlouhy, A. C., Bailey, D. K., Steimle, B. L., Parker, H. V. and Kosman, D. J., Fluorescence Resonance Energy Transfer Links Membrane Ferroportin, Hephaestin but Not Ferroportin, Amyloid Precursor Protein Complex with Iron Efflux, *Journal of Biological Chemistry*, vol. **294**, no. 11, 2019. DOI: 10.1074/jbc.RA118.005142

Domenico, I. De, Ward, D. M. V., Patti, M. C. B. Di, Jeong, S. Y., David, S., Musci, G. and Kaplan, J., Ferroxidase Activity Is Required for the Stability of Cell Surface Ferroportin in Cells Expressing GPI-Ceruloplasmin, *EMBO Journal*, vol. **26**, no. 12, 2007. DOI: 10.1038/sj.emboj.7601735

Donovan, A., Brownlie, A., Zhou, Y., Shepard, J., Pratt, S. J., Moynihan, J., Paw, B. H., et al., Positional Cloning of Zebrafish Ferroportin1 Identifies a Conserved Vertebrate Iron Exporter, *Nature*, vol. **403**, no. 6771, 2000. DOI: 10.1038/35001596

Donovan, A., Lima, C. A., Pinkus, J. L., Pinkus, G. S., Zon, L. I., Robine, S. and Andrews, N. C., The Iron Exporter Ferroportin/Slc40a1 Is Essential for Iron Homeostasis, *Cell Metabolism*, vol. **1**, no. 3, pp. 191–200, March 2005. DOI: 10.1016/j.cmet.2005.01.003

Drakesmith, H., Nemeth, E., and Ganz, T., Ironing out Ferroportin, *Cell Metabolism*, 2015.

Drew, D., North, R. A., Nagarathinam, K., and Tanabe, M., Structures and General Transport Mechanisms by the Major Facilitator Superfamily (MFS), *Chemical Reviews*, 2021.

Fernandes, A., Preza, G. C., Phung, Y., Domenico, I. De, Kaplan, J., Ganz, T. and Nemeth, E., The Molecular Basis of Hepcidin-Resistant Hereditary Hemochromatosis, *Blood*, vol. **114**, no. 2, 2009. DOI: 10.1182/blood-2008-03-146134

Fuqua, B. K., Lu, Y., Frazer, D. M., Darshan, D., Wilkins, S. J., Dunn, L., Loguinov, A. V., et al., Severe Iron Metabolism Defects in Mice With Double Knockout of the Multicopper Ferroxidases Hephaestin and Ceruloplasmin, *CMGH*, vol. **6**, no. 4, 2018. DOI: 10.1016/j.jcmgh.2018.06.006

Gac, G. Le, Ka, C., Joubrel, R., Gourlaouen, I., Lehn, P., Mornon, J. P., Férec, C. and Callebaut, I., Structure-Function Analysis of the Human Ferroportin Iron Exporter (SLC40A1): Effect of Hemochromatosis Type 4 Disease Mutations and Identification of Critical Residues, *Human Mutation*, vol. **34**, no. 10, 2013. DOI: 10.1002/humu.22369

Galy, B., Conrad, M., and Muckenthaler, M., Mechanisms Controlling Cellular and Systemic Iron Homeostasis, *Nature Reviews Molecular Cell Biology*, 2024.

Gassmann, M., and Muckenthaler, M. U., Adaptation of Iron Requirement to Hypoxic Conditions at High Altitude, *Journal of Applied Physiology*, 2015.

Gkouvatsos, K., Papanikolaou, G., and Pantopoulos, K., Regulation of Iron Transport and the Role of Transferrin, *Biochimica et Biophysica Acta - General Subjects*, 2012.

Guellec, J., Elbahnsi, A., Tertre, M. Le, Uguen, K., Gourlaouen, I., Férec, C., Ka, C., Callebaut, I. and Gac, G. Le, Molecular Model of the Ferroportin Intracellular Gate and Implications for the Human Iron Transport Cycle and Hemochromatosis Type 4A, *FASEB Journal*, vol. **33**, no. 12, 2019. DOI: 10.1096/fj.201901857R

Gulec, S., Anderson, G. J., and Collins, J. F., Mechanistic and Regulatory Aspects of Intestinal Iron Absorption, *American Journal of Physiology - Gastrointestinal and Liver Physiology*, 2014.

Haase, V. H., HIF-Prolyl Hydroxylases as Therapeutic Targets in Erythropoiesis and Iron Metabolism, *Hemodialysis International*, 2017.

Hamdi, A., Roshan, T. M., Kahawita, T. M., Mason, A. B., Sheftel, A. D. and Ponka, P., Erythroid Cell Mitochondria Receive Endosomal Iron by a "Kiss-and-Run" Mechanism, *Biochimica et Biophysica Acta - Molecular Cell Research*, vol. **1863**, no. 12, 2016. DOI: 10.1016/j.bbamcr.2016.09.008

Han, O. and Kim, E. Y., Colocalization of Ferroportin-1 with Hephaestin on the Basolateral Membrane of Human Intestinal Absorptive Cells, *Journal of Cellular Biochemistry*, vol. **101**, no. 4, 2007. DOI: 10.1002/jcb.21392

Hellman, N. E., and Gitlin, J. D., Ceruloplasmin Metabolism and Function, *Annual Review of Nutrition*, 2002.

Helman, S. L., Wilkins, S. J., McKeating, D. R., Perkins, A. V., Whibley, P. E., Cuffe, J. S. M., Simmons, D. G., et al., The Placental Ferroxidase Zyklopen Is Not Essential for Iron Transport to the Fetus in Mice, *Journal of Nutrition*, vol. **151**, no. 9, 2021. DOI: 10.1093/jn/nxab174

Helman, S. L., Zhou, J., Fuqua, B. K., Lu, Y., Collins, J. F., Chen, H., Vulpe, C. D., Anderson, G. J., and Frazer, D. M., The Biology of Mammalian Multi-Copper Ferroxidases, *BioMetals*, 2023.

Hentze, M. W., Muckenthaler, M. U., Galy, B., and Camaschella, C., Two to Tango: Regulation of Mammalian Iron Metabolism, *Cell*, 2010.

Hognon, C., Bignon, E., Harle, G., Touche, N., Grandemange, S. and Monari, A., The Iron Maiden. Cytosolic Aconitase/Irp1 Conformational Transition in the Regulation of Ferritin Translation and Iron Hemostasis, *Biomolecules*, vol. **11**, no. 9, 2021. DOI: 10.3390/biom11091329

Hooda, J., Shah, A., and Zhang, L., Heme, an Essential Nutrient from Dietary Proteins, Critically Impacts Diverse Physiological and Pathological Processes, *Nutrients*, 2014.

Ji, C., Steimle, B. L., Bailey, D. K. and Kosman, D. J., The Ferroxidase Hephaestin But Not Amyloid Precursor Protein Is Required for Ferroportin-Supported Iron Efflux in Primary Hippocampal Neurons, *Cellular and Molecular Neurobiology*, vol. **38**, no. 4, 2018. DOI: 10.1007/s10571-017-0568-z

Jiang, L., Wang, J., Wang, K., Wang, H., Wu, Q., Yang, C., Yu, Y., et al., RNF217 Regulates Iron Homeostasis through Its E3 Ubiquitin Ligase Activity by Modulating Ferroportin Degradation, *Blood*, vol. **138**, no. 8, 2021. DOI: 10.1182/blood.2020008986

Jiang, S., Fang, X., Liu, M., Ni, Y., Ma, W. and Zhao, R., MiR-20b down-Regulates Intestinal Ferroportin Expression in Vitro and in Vivo, *Cells*, vol. **8**, no. 10, 2019. DOI: 10.3390/cells8101135

Jormakka, M., Structural Insights into Ferroportin Mediated Iron Transport, *Biochemical Society Transactions*, 2023.

Katsarou, A., and Pantopoulos, K., Basics and Principles of Cellular and Systemic Iron Homeostasis, *Molecular Aspects of Medicine*, 2020.

Kong, Y., Hu, L., Lu, K., Wang, Y., Xie, Y., Gao, L., Yang, G., et al., Ferroportin Downregulation Promotes Cell Proliferation by Modulating the Nrf2–MiR-17-5p Axis in Multiple Myeloma, *Cell Death and Disease*, vol. **10**, no. 9, 2019. DOI: 10.1038/s41419-019-1854-0

Kono, S., Aceruloplasminemia. An Update, in *International Review of Neurobiology*, 2013.

Kono, S., Yoshida, K., Tomosugi, N., Terada, T., Hamaya, Y., Kanaoka, S. and Miyajima, H., Biological Effects of Mutant Ceruloplasmin on Hepcidin-Mediated Internalization of Ferroportin, *Biochimica et Biophysica Acta - Molecular Basis of Disease*, vol. **1802**, no. 11, 2010. DOI: 10.1016/j.bbadis.2010.07.011

Koorts, A. M. and Viljoen, M., Ferritin and Ferritin Isoforms I: Structure-Function Relationships, Synthesis, Degradation and Secretion, *Archives of Physiology and Biochemistry*, vol. **113**, no. 1, 2007. DOI: 10.1080/13813450701318583

Lakowicz, J. R., *Principles of Fluorescence Spectroscopy*, *Principles of Fluorescence Spectroscopy*, 2006.

Lane, D. J. R., Bae, D. H., Merlot, A. M., Sahni, S., and Richardson, D. R., Duodenal Cytochrome b (DCYTB) in Iron Metabolism: An Update on Function and Regulation, *Nutrients*, 2015.

Lehmann, E. F., Liziczai, M., Drożdżyk, K., Altermatt, P., Langini, C., Manolova, V., Sundstrom, H., Dürrenberger, F., Dutzler, R. and Manatschal, C., Structures of Ferroportin in Complex with Its Specific Inhibitor Vamifeport, *ELife*, vol. **12**, 2023. DOI: 10.7554/elife.83053

Lehmann, H. P., Schosinsky, K. H. and Beeler, M. F., Standardization of Serum Ceruloplasmin Concentrations in International Enzyme Units with o Dianisidine Dihydrochloride as Substrate, *Clinical Chemistry*, vol. **20**, no. 12, 1974. DOI: 10.1093/clinchem/20.12.1564

Leidgens, S., Bullough, K. Z., Shi, H., Li, F., Shakoury-Elizeh, M., Yabe, T., Subramanian, P., et al., Each Member of the Poly-r(C)-Binding Protein 1 (PCBP) Family Exhibits Iron Chaperone Activity toward Ferritin, *Journal of Biological Chemistry*, vol. **288**, no. 24, 2013. DOI: 10.1074/jbc.M113.460253

Li, S., Yang, Y. and Li, W., Human Ferroportin Mediates Proton-Coupled Active Transport of Iron, *Blood Advances*, vol. **4**, no. 19, 2020. DOI: 10.1182/bloodadvances.2020001864

Lin Cereghino, G. P., Lin Cereghino, J., Jay Sunga, A., Johnson, M. A., Lim, M., Gleeson, M. A. G. and Cregg, J. M., New Selectable Marker/Auxotrophic Host Strain Combinations for Molecular Genetic Manipulation of Pichia Pastoris, *Gene*, vol. **263**, no. 1–2, 2001. DOI: 10.1016/S0378-1119(00)00576-X

Lindley, P. F., Card, G., Zaitseva, I., Zaitsev, V., Reinhammar, B., Selin-Lindgren, E. and Yoshida, K., An X-Ray Structural Study of Human Ceruloplasmin in Relation to Ferroxidase Activity, *Journal of Biological Inorganic Chemistry*, vol. **2**, no. 4, 1997. DOI: 10.1007/s007750050156

Liu, C. C., and Schultz, P. G., Adding New Chemistries to the Genetic Code, *Annual Review of Biochemistry*, 2010.

Liu, X. B., Yang, F. and Haile, D. J., Functional Consequences of Ferroportin 1 Mutations, *Blood Cells, Molecules, and Diseases*, vol. **35**, no. 1, 2005. DOI: 10.1016/j.bcmd.2005.04.005

Machonkin, T. E., Zhang, H. H., Hedman, B., Hodgson, K. O. and Solomon, E. I., Spectroscopic and Magnetic Studies of Human Ceruloplasmin:

Identification of a Redox-Inactive Reduced Type 1 Copper Site, *Biochemistry*, vol. **37**, no. 26, 1998. DOI: 10.1021/bi980434v

Maher, B. H., Lea, R. A., Benton, M., Cox, H. C., Bellis, C., Carless, M., Dyer, T. D., et al., An x Chromosome Association Scan of the Norfolk Island Genetic Isolate Provides Evidence for a Novel Migraine Susceptibility Locus at Xq12, *PLoS ONE*, vol. **7**, no. 5, 2012. DOI: 10.1371/journal.pone.0037903

Maio, N., Polticelli, F., Francesco, G. De, Rizzo, G., Patti, M. C. B. Di and Musci, G., Role of External Loops of Human Ceruloplasmin in Copper Loading by ATP7B and Ccc2p, *Journal of Biological Chemistry*, vol. **285**, no. 27, 2010. DOI: 10.1074/jbc.M109.090027

Manolova, V., Nyffenegger, N., Flace, A., Altermatt, P., Varol, A., Doucerain, C., Sundstrom, H. and Dürrenberger, F., Oral Ferroportin Inhibitor Ameliorates Ineffective Erythropoiesis in a Model of β-Thalassemia, *Journal of Clinical Investigation*, vol. **130**, no. 1, 2020. DOI: 10.1172/JCI129382

Mao, J., McKean, D. M., Warrier, S., Corbin, J. G., Niswander, L. and Zohn, I. E., The Iron Exporter Ferroportin 1 Is Essential for Development of the Mouse Embryo, Forebrain Patterning and Neural Tube Closure, *Development*, vol. **137**, no. 18, 2010. DOI: 10.1242/dev.048744

Marro, S., Chiabrando, D., Messana, E., Stolte, J., Turco, E., Tolosano, E. and Muckenthaler, M. U., Heme Controls Ferroportin1 (FPN1) Transcription Involving Bach1, Nrf2 and a MARE/ARE Sequence Motif at Position -7007 of the FPN1 Promoter, *Haematologica*, vol. **95**, no. 8, 2010. DOI: 10.3324/haematol.2009.020123

McCarthy, R. C. and Kosman, D. J., Ferroportin and Exocytoplasmic Ferroxidase Activity Are Required for Brain Microvascular Endothelial Cell Iron Efflux, *Journal of Biological Chemistry*, vol. **288**, no. 24, 2013. DOI: 10.1074/jbc.M113.455428

McCarthy, R. C. and Kosman, D. J., Glial Cell Ceruloplasmin and Hepcidin Differentially Regulate Iron Efflux from Brain Microvascular Endothelial Cells, *PLoS ONE*, vol. **9**, no. 2, 2014. DOI: 10.1371/journal.pone.0089003

McKie, A. T., Marciani, P., Rolfs, A., Brennan, K., Wehr, K., Barrow, D., Miret, S., et al., A Novel Duodenal Iron-Regulated Transporter, IREG1, Implicated in the Basolateral Transfer of Iron to the Circulation, *Molecular Cell*, vol. **5**, no. 2, 2000. DOI: 10.1016/S1097-2765(00)80425-6

Mirdita, M., Schütze, K., Moriwaki, Y., Heo, L., Ovchinnikov, S. and Steinegger, M., ColabFold: Making Protein Folding Accessible to All, *Nature Methods*, vol. **19**, no. 6, 2022. DOI: 10.1038/s41592-022-01488-1

Mitchell, C. J., Shawki, A., Ganz, T., Nemeth, E. and Mackenzie, B., Functional Properties of Human Ferroportin, a Cellular Iron Exporter Reactive Also with Cobalt and Zinc, *American Journal of Physiology - Cell Physiology*, vol. **306**, no. 5, 2014. DOI: 10.1152/ajpcell.00348.2013

Miyajima, H., Aceruloplasminemia, *Neuropathology*, vol. **35**, no. 1, 2015. DOI: 10.1111/neup.12149

Montosi, G., Donovan, A., Totaro, A., Garuti, C., Pignatti, E., Cassanelli, S., Trenor, C. C., Gasparini, P., Andrews, N. C. and Pietrangelo, A., Autosomal-Dominant Hemochromatosis Is Associated with a Mutation in the Ferroportin (SLC11A3) Gene, *Journal of Clinical Investigation*, vol. **108**, no. 4, 2001. DOI: 10.1172/JCI200113468

Montosi, Giuliana, Donovan, A., Totaro, A., Garuti, C., Pignatti, E., Cassanelli, S., Trenor, C. C., Gasparini, P., Andrews, N. C. and Pietrangelo, A., Autosomal-Dominant Hemochrom-Atosis Is Associated with a Mutation in the Ferroportin (SLC11A3) Gene, *Journal of Clinical Investigation*, vol. **108**, no. 4, 2001. DOI: 10.1172/jci13468

Muckenthaler, M., Gray, N. K. and Hentze, M. W., IRP-1 Binding to Ferritin MRNA Prevents the Recruitment of the Small Ribosomal Subunit by the Cap-Binding Complex ElF4F, *Molecular Cell*, vol. **2**, no. 3, 1998. DOI: 10.1016/S1097-2765(00)80282-8

Muckenthaler, M. U., Rivella, S., Hentze, M. W., and Galy, B., A Red Carpet for Iron Metabolism, *Cell*, 2017.

Musci, M. C., Ceruloplasmin-Ferroportin System of Iron Traffic in Vertebrates, *World Journal of Biological Chemistry*, vol. **5**, no. 2, 2014. DOI: 10.4331/wjbc.v5.i2.204

Nemeth, E., and Ganz, T., Regulation of Iron Metabolism by Hepcidin., *Annual Review of Nutrition*, 2006.

Nemeth, E., Tuttle, M. S., Powelson, J., Vaughn, M. D., Donovan, A., Ward, D. M. V., Ganz, T. and Kaplan, J., Hepcidin Regulates Cellular Iron Efflux by Binding to Ferroportin and Inducing Its Internalization, *Science*, vol. **306**, no. 5704, 2004. DOI: 10.1126/science.1104742

Osaki, S., Kinetic Studies of Ferrous Ion Oxidation with Crystalline Human Ferroxidase (Ceruloplasmin)., *Journal of Biological Chemistry*, vol. **241**, no. 21, 1966. DOI: 10.1016/s0021-9258(18)99669-9

Pan, Y., Ren, Z., Gao, S., Shen, J., Wang, L., Xu, Z., Yu, Y., et al., Structural Basis of Ion Transport and Inhibition in Ferroportin, *Nature Communications*, vol. **11**, no. 1, 2020. DOI: 10.1038/s41467-020-19458-6

Pasquadibisceglie, A., Bonaccorsi di Patti, M. C., Musci, G., and Polticelli, F., Membrane Transporters Involved in Iron Trafficking: Physiological and Pathological Aspects, *Biomolecules*, 2023.

Patel, B. N., Dunn, R. J. and David, S., Alternative Rna Splicing Generates a Glycosylphosphatidylinositol- Anchored Form of Ceruloplasmin in Mammalian Brain, *Journal of Biological Chemistry*, vol. **275**, no. 6, 2000. DOI: 10.1074/jbc.275.6.4305

Petrič, B., Goličnik, M. and Bavec, A., The Removal of Time–Concentration Data Points from Progress Curves Improves the Determination of Km: The Example of Paraoxonase 1, *Molecules*, vol. **27**, no. 4, 2022. DOI: 10.3390/molecules27041306

Philpott, C. C., Patel, S. J., and Protchenko, O., Management versus Miscues in the Cytosolic Labile Iron Pool: The Varied Functions of Iron Chaperones, *Biochimica et Biophysica Acta - Molecular Cell Research*, 2020.

Piperno, A., and Alessio, M., Aceruloplasminemia: Waiting for an Efficient Therapy, *Frontiers in Neuroscience*, 2018.

Pospíšil, P., Luxem, K. E., Ener, M., Sýkora, J., Kocábová, J., Gray, H. B., Vlček, A. and Hof, M., Fluorescence Quenching of (Dimethylamino)Naphthalene Dyes Badan and Prodan by Tryptophan in Cytochromes P450 and Micelles, *Journal of Physical Chemistry B*, vol. **118**, no. 34, 2014. DOI: 10.1021/jp504625d

Praschberger, R., Schranz, M., Griffiths, W. J. H., Baumgartner, N., Hermann, M., Lomas, D. J., Pietrangelo, A., Cox, T. M., Vogel, W. and Zoller, H., Impact of D181V and A69T on the Function of Ferroportin as an Iron Export Pump and Hepcidin Receptor, *Biochimica et Biophysica Acta - Molecular Basis of Disease*, vol. **1842**, no. 9, 2014. DOI: 10.1016/j.bbadis.2014.05.011

Qiao, B., Sugianto, P., Fung, E., Del-Castillo-Rueda, A., Moran-Jimenez, M. J., Ganz, T. and Nemeth, E., Hepcidin-Induced Endocytosis of Ferroportin Is Dependent on Ferroportin Ubiquitination, *Cell Metabolism*, vol. **15**, no. 6, 2012. DOI: 10.1016/j.cmet.2012.03.018

Quintanar, L., Stoj, C., Taylor, A. B., Hart, P. J., Kosman, D. J. and Solomon, E. I., Shall We Dance? How a Multicopper Oxidase Chooses Its Electron Transfer Partner, *Accounts of Chemical Research*, vol. **40**, no. 6, 2007. DOI: 10.1021/ar600051a

Quistgaard, E. M., Löw, C., Guettou, F., and Nordlund, P., Understanding Transport by the Major Facilitator Superfamily (MFS): Structures Pave the Way, *Nature Reviews Molecular Cell Biology*, 2016.

Rishi, G., Secondes, E. S., Wallace, D. F. and Nathan Subramaniam, V., Evidence for Dimerization of Ferroportin in a Human Hepatic Cell Line Using Proximity Ligation Assays, *Bioscience Reports*, vol. **40**, no. 5, 2020. DOI: 10.1042/BSR20191499

Sangokoya, C., Doss, J. F. and Chi, J. T., Iron-Responsive MiR-485-3p Regulates Cellular Iron Homeostasis by Targeting Ferroportin, *PLoS Genetics*, vol. **9**, no. 4, 2013. DOI: 10.1371/journal.pgen.1003408

Schnell, S. and Mendoza, C., Closed Form Solution for Time-Dependent Enzyme Kinetics, *Journal of Theoretical Biology*, vol. **187**, no. 2, 1997. DOI: 10.1006/jtbi.1997.0425

Sendamarai, A. K., Ohgami, R. S., Fleming, M. D. and Lawrence, C. M., Structure of the Membrane Proximal Oxidoreductase Domain of Human Steap3, the Dominant Ferrireductase of the Erythroid Transferrin Cycle, *Proceedings of the National Academy of Sciences of the United States of America*, vol. **105**, no. 21, 2008. DOI: 10.1073/pnas.0801318105

Shah, Y. M., Matsubara, T., Ito, S., Yim, S. H. and Gonzalez, F. J., Intestinal Hypoxia-Inducible Transcription Factors Are Essential for Iron Absorption Following Iron Deficiency, *Cell Metabolism*, vol. **9**, no. 2, 2009. DOI: 10.1016/j.cmet.2008.12.012

Shawki, A., Anthony, S. R., Nose, Y., Engevik, M. A., Niespodzany, E. J., Barrientos, T., Öhrvik, H., Worrell, R. T., Thiele, D. J. and Mackenzie, B., Intestinal DMT1 Is Critical for Iron Absorption in the Mouse but Is Not Required for the Absorption of Copper or Manganese, *American Journal of Physiology - Gastrointestinal and Liver Physiology*, vol. **309**, no. 8, 2015. DOI: 10.1152/ajpgi.00160.2015

Shawki, A., Engevik, M. A., Kim, R. S., Knight, P. B., Baik, R. A., Anthony, S. R., Worrell, R. T., Shull, G. E. and Mackenzie, B., Intestinal Brush-Border Na+/H+ Exchanger-3 Drives H+-Coupled Iron Absorption in the Mouse, *American Journal of Physiology - Gastrointestinal and Liver Physiology*, vol. **311**, no. 3, 2016. DOI: 10.1152/ajpgi.00167.2016

Shen, J., Wilbon, A. S., Zhou, M. and Pan, Y., Mechanism of Ca2+ Transport by Ferroportin, *ELife*, vol. **12**, 2023. DOI: 10.7554/eLife.82947

Suh, Y. J. and David, S., Age-Related Changes in Iron Homeostasis and Cell Death in the Cerebellum of Ceruloplasmin-Deficient Mice, *Journal of Neuroscience*, vol. **26**, no. 38, 2006. DOI: 10.1523/JNEUROSCI.2922-06.2006

Summerer, D., Chen, S., Wu, N., Deiters, A., Chin, J. W. and Schultz, P. G., A Genetically Encoded Fluorescent Amino Acid, *Proceedings of the National Academy of Sciences of the United States of America*, vol. **103**, no. 26, 2006. DOI: 10.1073/pnas.0603965103

Syed, B. A., Beaumont, N. J., Patel, A., Naylor, C. E., Bayele, H. K., Joannou, C. L., Rowe, P. S. N., Evans, R. W. and Srai, S. K. S., Analysis of the Human Hephaestin Gene and Protein: Comparative Modelling of the N-Terminus Ecto-Domain Based upon Ceruloplasmin, *Protein Engineering*, vol. **15**, no. 3, 2002. DOI: 10.1093/protein/15.3.205

Takahashi, N., Ortel, T. L. and Putnam, F. W., Single-Chain Structure of Human Ceruloplasmin: The Complete Amino Acid Sequence of the Whole Molecule, *Proceedings of the National Academy of Sciences of the United States of America*, vol. **81**, no. 2 I, 1984. DOI: 10.1073/pnas.81.2.390

Taniguchi, R., Kato, H. E., Font, J., Deshpande, C. N., Wada, M., Ito, K., Ishitani, R., Jormakka, M. and Nureki, O., Outward-and Inward-Facing Structures of a Putative Bacterial Transition-Metal Transporter with Homology to Ferroportin, *Nature Communications*, vol. **6**, 2015. DOI: 10.1038/ncomms9545

Taylor, M., Qu, A., Anderson, E. R., Matsubara, T., Martin, A., Gonzalez, F. J. and Shah, Y. M., Hypoxia-Inducible Factor-2α Mediates the Adaptive Increase of Intestinal Ferroportin during Iron Deficiency in Mice, *Gastroenterology*, vol. **140**, no. 7, 2011. DOI: 10.1053/j.gastro.2011.03.007

Tortosa, V., Bonaccorsi Di Patti, M. C., Brandi, V., Musci, G. and Polticelli, F., An Improved Structural Model of the Human Iron Exporter Ferroportin. Insight into the Role of Pathogenic Mutations in Hereditary Hemochromatosis Type 4, *Bio-Algorithms and Med-Systems*, vol. **13**, no. 4, 2017. DOI: 10.1515/bams-2017-0029

Vashchenko, G. and MacGillivray, R. T. A., Functional Role of the Putative Iron Ligands in the Ferroxidase Activity of Recombinant Human Hephaestin, *Journal of Biological Inorganic Chemistry*, vol. **17**, no. 8, 2012. DOI: 10.1007/s00775-012-0932-x

Vashchenko, G., and MacGillivray, R. T. A., Multi-Copper Oxidases and Human Iron Metabolism, *Nutrients*, 2013.

Vasilyev, V. B., Looking for a Partner: Ceruloplasmin in Protein–Protein Interactions, *BioMetals*, 2019.

Vercellini, P., Crosignani, P., Somigliana, E., Viganò, P., Buggio, L., Bolis, G., and Fedele, L., The “incessant Menstruation” Hypothesis: A Mechanistic Ovarian Cancer Model with Implications for Prevention, *Human Reproduction*, 2011.

Vlasveld, L. T., Janssen, R., Bardou-Jacquet, E., Venselaar, H., Hamdi-Roze, H., Drakesmith, H., and Swinkels, D. W., Twenty Years of Ferroportin Disease: A Review or an Update of Published Clinical, Biochemical, Molecular, and Functional Features, *Pharmaceuticals*, 2019.

Vulpe, C. D., Kuo, Y. M., Murphy, T. L., Cowley, L., Askwith, C., Libina, N., Gitschier, J. and Anderson, G. I., Hephaestin, a Ceruloplasmin Homologue Implicated in Intestinal Iron Transport, Is Defective in the Sla Mouse, *Nature Genetics*, vol. **21**, no. 2, 1999. DOI: 10.1038/5979

Wallace, D. F., Harris, J. M. and Subramaniam, V. N., Functional Analysis and Theoretical Modeling of Ferroportin Reveals Clustering of Mutations According to Phenotype, *American Journal of Physiology - Cell Physiology*, vol. **298**, no. 1, 2010. DOI: 10.1152/ajpcell.00621.2008

Wang, H., Shi, H., Rajan, M., Canarie, E. R., Hong, S., Simoneschi, D., Pagano, M., et al., FBXL5 Regulates IRP2 Stability in Iron Homeostasis via an Oxygen-Responsive [2Fe2S] Cluster, *Molecular Cell*, vol. **78**, no. 1, 2020. DOI: 10.1016/j.molcel.2020.02.011

Wang, J., Xie, J. and Schultz, P. G., A Genetically Encoded Fluorescent Amino Acid, *Journal of the American Chemical Society*, vol. **128**, no. 27, 2006. DOI: 10.1021/ja062666k

Wang, L., Engineering the Genetic Code in Cells and Animals: Biological Considerations and Impacts, *Accounts of Chemical Research*, vol. **50**, no. 11, 2017. DOI: 10.1021/acs.accounts.7b00376

White, C., Yuan, X., Schmidt, P. J., Bresciani, E., Samuel, T. K., Campagna, D., Hall, C., et al., HRG1 Is Essential for Heme Transport from the Phagolysosome of Macrophages during Erythrophagocytosis, *Cell Metabolism*, vol. **17**, no. 2, 2013. DOI: 10.1016/j.cmet.2013.01.005

Wilbon, A. S., Shen, J., Ruchala, P., Zhou, M. and Pan, Y., Structural Basis of Ferroportin Inhibition by Minihepcidin PR73, *PLoS Biology*, vol. **21**, no. 1, 2023. DOI: 10.1371/journal.pbio.3001936

Wolff, H., Vehmas, T., Oksa, P., Rantanen, J. and Vainio, H., Asbestos, Asbestosis, and Cancer, the Helsinki Criteria for Diagnosis and Attribution 2014: Recommendations, *Scandinavian Journal of Work, Environment and Health*, vol. **41**, no. 1, 2015. DOI: 10.5271/sjweh.3462

Wolff, N. A., Garrick, M. D., Zhao, L., Garrick, L. M., Ghio, A. J. and Thévenod, F., A Role for Divalent Metal Transporter (DMT1) in Mitochondrial Uptake of Iron and Manganese, *Scientific Reports*, vol. **8**, no. 1, 2018. DOI: 10.1038/s41598-017-18584-4

Wong, B. X., Ayton, S., Lam, L. Q., Lei, P., Adlard, P. A., Bush, A. I. and Duce, J. A., A Comparison of Ceruloplasmin to Biological Polyanions in Promoting the Oxidation of Fe2 +under Physiologically Relevant Conditions, *Biochimica et Biophysica Acta - General Subjects*, vol. **1840**, no. 12, 2014. DOI: 10.1016/j.bbagen.2014.08.006

Yanatori, I., Richardson, D. R., Imada, K. and Kishi, F., Iron Export through the Transporter Ferroportin 1 Is Modulated by the Iron Chaperone PCBP2, *Journal of Biological Chemistry*, vol. **291**, no. 33, 2016. DOI: 10.1074/jbc.M116.721936

Yanatori, I., Yasui, Y., Tabuchi, M. and Kishi, F., Chaperone Protein Involved in Transmembrane Transport of Iron, *Biochemical Journal*, vol. **462**, no. 1, 2014. DOI: 10.1042/BJ20140225

Yoshinaga, M., Nakatsuka, Y., Vandenbon, A., Ori, D., Uehata, T., Tsujimura, T., Suzuki, Y., Mino, T. and Takeuchi, O., Regnase-1 Maintains Iron Homeostasis via the Degradation of Transferrin Receptor 1 and Prolyl-Hydroxylase-Domain-Containing Protein 3 MRNAs, *Cell Reports*, vol. **19**, no. 8, 2017. DOI: 10.1016/j.celrep.2017.05.009

Young, T. S., Ahmad, I., Brock, A. and Schultz, P. G., Expanding the Genetic Repertoire of the Methylotrophic Yeast Pichia Pastoris, *Biochemistry*, vol. **48**, no. 12, 2009. DOI: 10.1021/bi802178k

Yu, Y., Jiang, L., Wang, H., Shen, Z., Cheng, Q., Zhang, P., Wang, J., et al., Hepatic Transferrin Plays a Role in Systemic Iron Homeostasis and Liver Ferroptosis, *Blood*, vol. **136**, no. 6, 2020. DOI: 10.1182/BLOOD.2019002907

Zacchi, P., Belmonte, B., Mangogna, A., Morello, G., Scola, L., Martorana, A. and Borelli, V., The Ferroxidase Hephaestin in Lung Cancer: Pathological Significance and Prognostic Value, *Frontiers in Oncology*, vol. **11**, 2021. DOI: 10.3389/fonc.2021.638856

Zaitsev, V. and Lindley, P., Structural Comparison of Two Mammalian Multicopper Oxidases, Hephaestin and Ceruloplasmin, *Acta Crystallographica Section A Foundations and Advances*, vol. **75**, no. a2, 2019. DOI: 10.1107/s2053273319094191

Zaitseva, I., Zaitsev, V., Card, G., Moshkov, K., Bax, B., Ralph, A. and Lindley, P., The X-Ray Structure of Human Serum Ceruloplasmin at 3.1 Å: Nature of the Copper Centres, *Journal of Biological Inorganic Chemistry*, vol. **1**, no. 1, 1996. DOI: 10.1007/s007750050018

Zhang, D. L., Hughes, R. M., Ollivierre-Wilson, H., Ghosh, M. C. and Rouault, T. A., A Ferroportin Transcript That Lacks an Iron-Responsive Element Enables Duodenal and Erythroid Precursor Cells to Evade Translational Repression, *Cell Metabolism*, vol. **9**, no. 5, 2009. DOI: 10.1016/j.cmet.2009.03.006

Zhang, Z., Zhang, F., An, P., Guo, X., Shen, Y., Tao, Y., Wu, Q., et al., Ferroportin1 Deficiency in Mouse Macrophages Impairs Iron Homeostasis and Inflammatory Responses, *Blood*, vol. **118**, no. 7, 2011. DOI: 10.1182/blood-2011-01-330324

Zhang, Z., Zhang, F., Guo, X., An, P., Tao, Y. and Wang, F., Ferroportin1 in Hepatocytes and Macrophages Is Required for the Efficient Mobilization of Body Iron Stores in Mice, *Hepatology*, vol. **56**, no. 3, 2012. DOI: 10.1002/hep.25746